CHAPTER 1

PALEOCLIMATE VARIABILITY IN THE MEDITERRANEAN REGION

Abrantes F[1,2*]., Voelker A[1,2]., Sierro, F[3]., Naughton, F[1,2]., Rodrigues, T[1,2]., Cacho, I[4]., Ariztegui, D[5]., Brayshaw, D[6]., Sicre, M-A[7]. and Batista, L[1].

1 – Laboratório Nacional de Energia e Geologia – LNEG. Unidade de Geologia Marinha, Amadora, Portugal (fatima.abrantes@lneg.pt)
2 – Centro de Investigação Marinha e Ambiental – CIMAR, Porto, Portugal
3 – Department of Geology, University of Salamanca, Spain
4 – GRC Geociències Marines, Dept. Estrat. Paleont. i Geoc. Marines Facultat de Geologia, Universitat de Barcelona, Spain
5 – Section of Earth & Environmental Sciences, University of Geneva. Switzerland
6 – National Centre for Atmospheric Sciences, Department of Meteorology, University of Reading, UK
7 – CNRS, Laboratoire des Sciences du Climat et de l'Environnement, Gif-sur-Yvette, France

Paleo-climatic and -oceanographic studies are essentially motivated by elementary societal and scientific needs for understanding our planet, in particular the amplitude of natural variability with the purpose of discriminating between natural and human-made change and predicting the effect of anthropogenic impacts on the future global climatic system.

By collecting and compiling quantitative paleoclimatic information of the principal parameters from the Mediterranean region, both on land and in the ocean, in various climate periods: (i) warm climate intervals of the Pleistocene including the Holocene (our current interglacial period) and (ii) times of abrupt climate shift, in particular from cold to warming periods, such as deglaciation(s) and the glacial millennial-scale variations, we hope to contribute to a better understanding of the forcing mechanisms behind the temporal and spatial patterns observed, provide information useful for model improvement and validation and hopefully help to predict how future climate may affect the Mediterranean area.

1. Introduction on Paleoclimate Reconstruction Methods

The climatic system, as we know it today, is complex and variability is caused both by external forcing and by internal processes. A quick look into the global record of ice volume for the past 65 million years (My) (Fig. 1[1]) is enough to give us the idea that Earth's history has been marked by climatic variation of a more abrupt than gradual nature. Major climatic variations can be detected at four different time scales (Fig. 2[2]):

1. Tectonic (> 0.5 million years - My) - caused by changes in atmospheric and oceanic circulation in response to changes in the relative position of continents and oceans, and, the opening and closing of gateways, (i.e. plate tectonics). At this scale the effects on the biological evolution and biogeochemical cycles are of particular importance.

2. Orbital (20 to 400 thousand years - ky) - originated by variations in the earth's position relative to the sun, that is, variations in the orbital parameters, eccentricity, obliquity and precession[3; 4]. This scale is recorded back to 34 My mainly through expansions and retractions of the global ice volume that occur with periodicities of 400, 100, 40 and 19-23 ky.

3. Millennial (few ky) - corresponds to climatic variations generated by interactions between slowly evolving components of the climate system (*e.g.*, the ocean and the cryosphere) resulting, for example, in the instability of the oceanic thermohaline circulation[5]. The effects of such changes over the land surface are generally mediated by changes in the atmospheric circulation.

4. Historic (centuries to seasons) – includes the climatic variations on shorter periods (best observed in historical times) and the more recent anthropogenic climate change at global scales.

In spite of the intrinsic importance of paleoclimate studies, recent interest in climate reconstructions has evolved from the perception that understanding the dynamics of past climatic

events and their impact is fundamental in modelling and understanding future climate changes.

The main geophysical properties that paleoclimatologists attempt to reconstruct are the same as physical, chemical or biological climatologist grapple with in the present day. However, past climate reconstructions have to be done through the study of "climate-archives" such as tree-rings, speleothems, ice-cores, corals or sedimentary sequences (lakes and marine). Being like multi-channel recorders, all of them contain multiple climatic information, but of different nature and resolution (Fig. 3[2]).

Past climatic reconstructions typically take one of two forms: time series or time slices. Time series provide information through time at one or more specific location(s), time-slice reconstructions attempt the spatial distribution of a property at a specific time. Independent of the selected approach, their interpretation has to follow the general geology principle of Lyell[6] "the present is the key to the past" to later allow a turn around of that principle into "the past as the key to the future"! Besides, given the impossibility of directly measuring past oceanic properties in any archive, it is necessary to use indicators or proxies.

A proxy is an archive property or component that can be related to an environmental parameter or process. There are a multitude of proxies in use, from methods based on biological, physical and chemical sciences to modern statistical techniques that allow the use of extensive and complex databases. Proxies can be classified on the basis of their type (physical, chemical, biological, isotopic, *etc*) or grouped by the type of parameter that they attempt to reconstruct [7].

Paleoclimate proxies can be subtle and complex. This is the reason why most studies use a multi proxy approach. In this chapter we will be using a combination of proxies described elsewhere, for oceanic surface temperature (SST), primary production, bottom / intermediate waters ventilation and flow strength, and for continental climate atmospheric temperature, precipitation, wind strength and direction. For SST reconstruction we will incorporate records from foraminiferal $\delta^{18}O$, C_{37} alkenone unsaturation index ($U^{K'}_{37}$), TEX_{86}, Mg/Ca ratio, and microfossil assemblages transfer functions that relate species distributions to modern hydrographic conditions. Primary production conditions at any time will be estimated from the organic carbon, Ba contents, as well as from microfossil abundance and assemblages. Bottom / intermediate waters ventilation will be determined via benthic foraminifera $\delta^{13}C$ and sediments geochemical composition. For bottom water strength, grain size is the main used proxy. Continental temperature reconstructions are based primarily on palinological data preserved in sedimentary archives, supplemented by other lake data where available. On land precipitation is also derived from pollen data, continental plants' biomarkers data, $\delta^{18}O$ in speleothem carbonate, and Fe, Ti and clay minerals' abundance and type. Location of all the records used in this compilation is presented in Fig. 4 and their position information and original references to all the works used are listed in Table 1. Sites numbers mentioned in the following text refer to the Fig. 4's number of the respective site.

Given the nature of climate reconstructions there are several uncertainties related to any data point. Age uncertainties are the most important, since the chronology of the archive constitutes the base for accurate environmental or climatic reconstructions. A good age control is fundamental to estimate rates of change for any one parameter or process in one location, as well as to establish relationships between sites. The process or property / proxy relation can also be a source of uncertainty given that there is no form of verifying if the modern relations hold through geologic time. Furthermore, the numeric relationships defined from the proxies to modern conditions may also incur into problems by assuming them as good analogs when in reality modern conditions may result from a combination of natural and anthropogenic forcing. Error can also derive from the methodologies and equipment used to do the proxy measurements. Typically, however, a final error can be estimated, as the sum of its different components (dating, sampling, counting, etc…).

Values obtained by reconstructions should not be seen as an exact value. However, when calibration is done and replicate estimations give a good accuracy, they constitute the best source of

information on the reaction of the different components of the earth's climatic system to past external forcing or internal reorganization, on the range of natural variability as well as on the rate of change of any process through time.

Regional reconstructions of environmental and climatic variability have been recognized by the IPCC[8] as essential for better understanding specific local reactions to global climatic trends. The Mediterranean Basin is particularly suitable to provide information on the climatic connection between high and low latitudes in the Northern Hemisphere, because of its mid latitude location. Furthermore as a semienclosed sea it has the potential to amplify global paleoenvironmental and paleoceanographic changes[9]. In this chapter we attempt to compile the currently available quantitative data for the Mediterranean region for selected time intervals and investigate regional scale change during specific climatic conditions through spatial patterns of natural variability. Furthermore, results from some recent climate modelling studies of the Holocene are discussed in the context of our well-constrained datasets. Although climate models have their own limitations (for example, spatial resolution, temporal coverage, missing physical processes and model uncertainty), these comparisons offer the potential for identifying flaws in the models, weaknesses in the data, critical geographic regions at key time slices, as well as independent means of validating the climate model's response to applied "forcings" (*e.g.*[10]). It should, however, be noted that climate models only simulate "responses" (outputs) that are consistent with prescribed "forcings" (inputs): if the forcing is not well understood, then the response may not be informative. The nature of the forcing is somewhat dependent on the components included in the model (for example some models include ocean dynamics or dynamic vegetation while others do not[11]) but they will generally include at least some of the following: changes in orbital parameters, greenhouse gas concentrations, sea-surface height, ice sheet extent, land-surface properties and ocean circulation. Clearly then, some of these forcings are better constrained than others. The reponses produced by climate models are therefore subject to interpretation, based on a physical understanding of the forcings applied and an understanding of the physical processes of the climate system (and their representation in the model). It is therefore in this more nuanced context that a model-data comparison is undertaken within this chapter, rather than contrasting the two datasets on a site-by-site basis.

Reconstruction Approach

After summarizing the birth and early evolution of the modern Mediterranean Sea we discuss a selection of specific time intervals that experienced different climate forcings. For the latter we consider marine records with radiocarbon chronologies for defining the time-slices' patterns for Marine Isotope Stage (MIS) 3 and younger. For continental records, we include both lake and speleothems. In lakes ages are derived both from varve chronology, ^{14}C ages or $\delta^{18}O$ stratigraphy while U-Th dates are the base for speleothems' age models. However, given our intent to focus on the main features, any property or process reconstruction aims to include mainly records that have estimations from different proxies but values based on a single proxy will be considered, given that a multiple approach has only been applied on a very small number of sites. Age models and records were adopted as published by the authors, making no attempt to harmonize the data towards any particular calibration or method. Absolute chronology is usually based on radiocarbon measurements of carbonaceous (mainly marine) and organic matter (continental) samples, but given the radiocarbon-based age constraints, the (usually small) analytical error of the ^{14}C dates as well as errors and uncertainties in the paleo-reservoir ages[12; 13], a tolerance on the order of several centuries to one millennium, as we move back in time, is used for the timing of events. Furthermore, the presented data represents a "mean state" calculated as the average value for the considered time-slice at each site.

Note: Ages are referred to as My (million years) and ky (thousand years), but ka is used if referring to a specific age level.

2. The Geologic History of the Mediterranean through the Meso-Cenozoic: From a Global Latitudinal Ocean to an Enclosed Sea

2.1 Origin of the Mediterranean

The Mediterranean history is the result of the complex interaction between plate tectonics, the formation of orogenic belts, global eustatic changes and climate, which have continuously changed its geographic extension, water exchange with the global Ocean and its local hydrologic budget. It originated from the Tethys Ocean, which was a vast ocean located along the eastern coast of Laurasia and Gondwana during the Mesozoic and early Cenozoic. Since the Eocene (circa 38 My) to the Miocene (23 My) the African plate rotated counterclockwise and moved northward into the Eurasian Plate[14], leading to the progressive restriction of the Tethys connection with the Indian Ocean and the formation of the Paratethys and the Mediterranean[15]. At that time the connection between the Mediterranean and Indo-Pacific Ocean was through a wide and deep gateway located between the Arabian and Anatolian plates along Southern Turkey and Irak[14; 16], but this gateway shoaled to subtidal marine environments, leading to a severe restriction of the Indian-Mediterranean connection by the end of the Oligocene (23 My[15; 16]). However, another shallow water gateway may have developed during the middle Miocene in response to the subduction between the Arabian plate and the Asian plate south of the Bitlis massif[16]. This connection, which was located north of the Arabian Peninsula, deepened to at least 300 to 600 m water depth between 13.8 and 11. 8 My. It remained open until 11 My ago during the Early Tortonian when the Gateway emerged and the Mediterranean became finally disconnected from the Indian Ocean[16].

2.2 The Mediterranean and the Paratethys Sea

The history of Mediterranean and Eurasian climate cannot be understood without knowing its relationship with the Paratethys Sea, the large marginal sea that existed along the Southern margin of Eurasia at around 33 My ago, near the Eocene-Oligocene boundary[14; 17; 18]. The tectonic uplift of the Alps and Carphathian orogenic belts led to the formation of a large basin that stretched from the Alps to the Aral Sea with a connection with the Mediterranean towards the south. The isolation of the Paratethys from the Mediterranean since the Oligocene was recorded by a significant change from open marine planktonic floras and faunas to less diverse or monospecific microfossil assemblages usually characteristic of brackish or freshwater environments as well as the development of stagnant conditions at the bottom[17; 19]. Conditions were similar to those of the modern Black Sea, which is in fact, the reminiscent basin of the ancient Paratethys. This marginal sea was characterized by brackish waters due to a positive freshwater budget and a strong stratification of the water column that favoured accumulation of organic carbon in bottom sediments, which consitute the source for hydrocarbons[20]. As European rivers are the main source of freshwater for the Mediterranean today and probably also during the Miocene, the isolation of the Paratethys from the Mediterranean is likely to have generated a strong hydrologic deficit in the Mediterranean as most of the freshwater was collected in the Paratethys.

Over the Oligocene and Miocene, the geographic boundary between the Paratethys and the Mediterranean and therefore water exchange between both basins changed in response to the intense tectonic activity of the orogenic belts of southern Eurasia and global eustatic changes[21; 22; 23]. The first isolation occurred near the Eocene Oligocene boundary (33.9 My) and may have been triggered by the global sea level fall associated to the onset of the Antarctic ice-sheets. During the Late Miocene and especially during the Pliocene and Quaternary, the original size of the Paratethys Sea was largely reduced and various separated basins, such as the actual Black, Caspian and Aral Seas, appeared in consequence of the uplift in the Carphathian mountains and the Caucasus[14; 24].

The presence of this large epicontinental sea, the Paratethys, had a strong effect on Eurasian climate since it was a significant source of water vapour for the atmosphere and its high water heat capacity contributed to reduce the seasonal thermal gradient[25; 26]. The shrinkage of the Paratethys during the Late Miocene and Pliocene changed the Eurasian climate from oceanic to more continental conditions with much colder winter temperatures and a larger seasonal thermal contrast[25].

The progressive closure of the Tethys-Indian connection from the Oligocene to the Miocene also resulted in drier climates in Anatolia and the Arabian Peninsula as well as in NE Africa[25]. Furthermore, the northward drift of the African continent from the Eocene to the present contributed to an expansion of the subtropical desert along North Africa with a strong impact on the Mediterranean hydrologic budget[26].

2.3 Mediterranean Salinity Crisis

After the final closure of the Indian gateway (11 My) the Mediterranean was connected with the Atlantic Ocean through two gateways, the northern Betic strait located in Southern Spain and the south-riffian gateway in Northern Morocco. However, the convergence between the African and Iberian plates progressively restricted those gateways contributing to the Mediterranean "salinity crisis" between 7.25 and 5.96 My.

The term Mediterranean "salinity crisis" was firstly used by Mediterranean geologists to explain the widespread presence of evaporites (gypsum, salts) all over the Mediterranean marginal basins in Spain, Italy, Crete, Turkey, North Africa, etc[27]. However, the deep implications of this crisis were not fully recognized until the discovery of giant evaporite deposits in the deepest basins of the Mediterranean during Deep Sea Drilling Project (DSDP) expedition Leg XIII in 1970[28; 29; 30]. The discovery of huge saline bodies buried by thousands of meters of Plio-Pleistocene pelagic sediments led scientists to recognize that the Mediterranean had to have been completely or partially desiccated during the latest Miocene. This was one of the most exciting scientific discoveries in earth sciences. The Late Miocene Mediterranean desiccation was, since then, the focus of intensive research both on land and in the deep marine basins of the Mediterranean, generating passionate debates in scientific meetings that ended with new ideas about the origin of this dramatic episode of the Mediterranean history.

Up to today, only the top of the evaporites has been drilled and cored in the deep sea, but nothing is yet known about the rest of the evaporites underneath, which can only be interpreted through the study of seismic profiles. The few meters recovered from the uppermost evaporites indicate that they were deposited in a shallow water desiccated Mediterranean[28; 29; 30], in sharp contrast to the pelagic oozes deposited afterwards, during the lowermost Pliocene. Since existing indication on the sediments underlying the evaporites point to material deposited in a deep marine environment, it was concluded that the Mediterranean Sea dessication was an exceptional event situation during the Messinian (5.9 – 5.3 My[28]).

Seismic profiles in the Western Mediterranean deep basins allowed the recognition of three evaporite units, the so-called "Messinian trilogy"[31; 32; 33] with a total thickness of around 1600 m. These three distinct seismic units were defined as the Lower Unit, Mobile Unit and Upper Unit (LU, MU, UU respectively[32; 33] with thicknesses of 500-800 m for the UU, 600 and 1000 m thick for the MU and 500-700 m for the LU.

As we have no record from the deeper Mediterranean Sea evaporites, most of the geological interpretations and the desiccation scenarios proposed so far are based on observations made in marine sediments preserved on the marginal basins, such as in Spain, Italy, Greece, and Morocco. In particular, deposits outcropping today in the Caltanissetta basin in Sicily[34] and the Northern Apennines[35; 36; 37; 38; 39; 40] were probably deposited in deep marine settings and, consequently may be equivalent to the Western Mediterranean trilogy. The LU has usually been related to the Lower Evaporites cropping out in Sicily, Spain and all over the Mediterranean marginal basins, the MU

with the halite unit in Sicily and the UU with the Upper evaporites in Sicily and the Apennines (Fig. 5).

High resolution astrochronological studies on several sections of the pre-evaporitic deposits in Spain, Italy and Greece concluded that the onset of the Messinian salinity crisis, at least in the marginal basins, was isochronous all over the Mediterranean with an astronomical age of 5.96 My [41; 42]. Since the basal age of the Pliocene is 5.33 My[43] the time period of the Messinian salinity crisis is well constrained with a total duration of 630 ky. However, while the age of the onset of evaporites onland is precisely known, there is still a lot of controversy about the synchronous or diachronous onset of the deep Mediterranean evaporites (see[44] for a review). Over the last decades several dessication scenarios have been proposed[44; 45; 46; 47; 48; 49]. Below we will summarize the main phases of the Messinian salinity crisis.

2.3.1 The History of Mediterranean Dessication

Based on land and deep Mediterranean observations the scenario proposed for the Messinian dessication[49] is the following. 7.2 My, the time when compression between North Africa and the Iberian Peninsula restricted the Betic-riffian corridors that severely reduced the Atlantic-Mediterranean water exchange is likely to represent the beginning of the Mediterranean salinity crisis due to severe restriction of the Atlantic-Mediterranean water exchange. A sudden drop in benthic foraminifera $\delta^{13}C$, well below the Atlantic benthic isotope signal, and the onset of sapropel (i.e., a sediment layer rich in organic matter) deposition at times of precession minima are the evidence for this restriction[50; 51; 52; 53]. A second and more severe restriction of the connection with the Atlantic occurred at 6.7 My as evidenced by widespread deposition of laminated sediments all over the Mediterranean and a significant drop in benthic foraminifera diversity as well as an increase in abundance of species typically living in dysoxic waters[50; 51; 53; 54; 55; 56]. An increase in $\delta^{18}O$ of benthic foraminifers in combination with warmer temperatures also indicates higher Mediterranean salinities [53].

Preceding the deposition of evaporites on the marginal basins the first signs of high surface salinities are recorded in Spain and Italy by the cyclical disappearance of planktonic foraminifera during the so called aplanktonic zones that usually occur between 6.3 and 6.2 My and coincide with times of minimum summer insolation[39; 55]. Progressive restriction of the Atlantic-Mediterranean water exchange, in combination with the cyclical oscillations between periods of higher and lower Mediterranean water deficit led to surface salinities exceeding 49 psu, the maximum tolerable limit for most planktonic foraminifer species[57].

2.3.2 The Onset of Gypsum Deposition on the Marginal Basins

In the beginning of the Messinian salinity crisis, huge amounts of gypsum deposited all over the Mediterranean, in the peripheral basins. This unit, usually called the Lower Evaporites contains geochemical evidence for deposits under marine conditions. In consequence, the connection to the Atlantic, though limited, was still open and sea level in the Mediterranean Sea was possibly at the same level as in the Atlantic. The lower evaporites consist of approximately 16/17 sedimentary cycles formed by the alternation of gypsum and marl beds, which based on the tuning of the gypsum beds to cycles of maximum Earth´s precession[42; 58], were deposited between 5.96 and 5.59 My. Alternatively, gypsum deposition may have been triggered by eustatic sea level changes of millennial scale[59]. The onset of gypsum deposition was an isochronous event in all peripheral basins with an astronomical age of 5.96 My[42; 54; 60].

Recent studies suggest that gypsum deposition was restricted to the marginal, shallow basins, whereas black euxinic shales, barren of microfossils, were laid down in the deep sea, suggesting the existence of a completely anoxic deep Mediterranean Sea at the time of gypsum deposition in the margins[49; 61; 62].

Box models, using the present Mediterranean annual freshwater deficit, suggest that with a continuous Atlantic inflow but a restricted outflow the salinity of Mediterranean water progressively increased to reach gypsum saturation at values up to 145 g/l in 6 ky[63].

2.3.3 The Sea Level Drawdown and Salt Precipitation

The deposition of the Lower evaporites in the margins ended with a major sea level drawdown of at least 1500 m in the Mediterranean that took place at around 5.59 My ago and led to the subaerial exposure of the continental margins and to the excavation of profound canyons by the major rivers. Canyons up to 1000 or 2500 m deep were excavated by the Rhone and the Nile respectively in response to this drastic base level lowering that generated the Messinian Erosive Surface (MES) visible in seismic lines all over the Mediterranean[32; 64]. Because of this massive erosion of the Mediterranan continental shelfs and slopes, huge amounts of sediments, including the gypsum of the lower evaporites that were previously deposited in the margins, were transported downslope and redeposited in the deep Mediterranean basins. By comparison with the Northern Apennines outcrops, it has been hypothesized that these redeposited sediments formed the LU recognized in the Mediterranean seismic profiles[32; 49]. The bottom of the LU in the deep basins and the MES on the continental margins consequently mark the first complete disconnection of the Mediterranean from the Atlantic, occurring at around 5.59 My ago. As a result, and immediately overlaying the LU, started the deposition of 600-1000 m of halite in the deep basins. It has been estimated that salt precipitation took place in the deep basins between 5.59 and 5.52 My, during a time interval of only 70 ky that has been correlated with glacial isotope stages TG14-12[65; 66]. In Sicily deposits, considered to be the equivalent of the deep Mediterranean setting, the halite unit is deposited between the lower and upper evaporites[34].

Oceanographic models suggest that halite saturation in the Mediterranean, which takes place at salinities of 350 g/l, could only be reached with a continuous Atlantic inflow and a blocked outflow[63; 67]. These models also indicate that with the present freshwater deficit, after a complete disconnection with the Atlantic, the Mediterrranean water level would drop rapidly to reach an equilibrium level at -2500 m in 10 ky[68].

2.3.4 The Lago-Mare Phase

The last phase of the Messinian salinity crisis, which lasted from 5.55 to 5.33 My, is marked by the deposition of the Upper Evaporites and is usually known as the Lago Mare event[28]. This period is characterized by 7/10 precessional cycles defined by the alternation of gypsum or conglomerates and marl beds, suggesting cyclical fluctuations in salinity[35; 36; 66; 69]. Strontium isotope values and the presence of fresh and brackish water ostracods and mollusks of Paratethyan origin have been interpreted as a proof of Mediterranean flooding with freshwater from the Paratethys[28; 29; 30; 70; 71; 72]. Although a major change in the Mediterranean hydrological budget can also explain this shift from hyperhaline to hypohaline waters at the onset of the Lago-mare event, no significant change in the Mediterranean climate has been detected at this time[73].

In which respects the Mediterranean water level during the Lago-Mare phase, contradictory evidences have been found. Shallow-water deposits were recorded in deep Mediterranean basins immediately below the Pliocene pelagic sediments, documenting a deep almost dessicated Mediterranean during this period[28; 30; 74]. However, a deep-water habitat for these brackish water microfossils cannot be completely ruled out. By contrast, Lago-Mare deposits with mollusks and ostracodes of Paratethys origin have been reported in many marginal basins, such as in Spain, Italy, Cyprus, NE Morocco, Algeria, Turkey, etc.[75; 76; 77; 78; 79; 80; 81], documenting that Mediterranean water level was not below the paleodepth of these maginal basins, which was probably very shallow as suggested by the abundant presence of shallow water ostracodes and foraminifera. The cyclical occurrence of Lago-Mare and fluvial deposits with evidences of paleosoils in some of the marginal

basins[75; 76] suggests that significant oscillations in the water base level may have occurred during this period and that the lake level in the Mediterranean Sea was, at least temporarily, well below that of the Ocean. Alternatively, the existence of various marginal disconnected lacustrine basins with different water levels cannot be completely ruled out.

2.4 The Pliocene Mediterranean Flooding

The Mediterranean salinity crisis abruptly ended at the Miocene-Pliocene boundary, 5.33 My ago, with the opening of the Strait of Gibraltar and the re-establishment of open marine conditions when the Atlantic water discharge flooded into the Mediterranean. The Mediterranean inundation has been related to either a global eustatic sea level rise at the end of the Miocene or to tectonic or erosive processes in the Strait of Gibraltar.

The analysis of benthic foraminifer $\delta^{18}O$ records from the North Atlantic and its detailed correlation with the Mediterranean show that the Mediterranean flooding was not triggered by any major eustatic rise at the beginning of the Pliocene[66; 82; 83]. On the other hand, several studies have revealed that tectonic processes in the Gibraltar Arc, such as the activity of strike-slip faults or subsidence are probably responsible for the opening of the Strait of Gibraltar[84; 85].

Some models suggest that enhanced fluvial regressive erosion may have developed in the Mediterranean side of Gibraltar in response to the sea level drop of more than 1500 m, which eventually capture the Atlantic waters[86; 87]. A recent study suggests that, although the initial opening of the strait may have been caused by river incision, once Atlantic water discharge began it was the huge hydraulic energy of this water generated by the large difference in altitude of sea levels at both sides of the Strait that excavated the long and deep channel existing today across the Strait of Gibraltar[88]. Water discharge, which may have been low at the beginning, exponentially increased as the rate of incision rapidly opened the floodgate to the Mediterranean to finally generate a catastrophic flood that filled the Mediterranean in less than 2 years with a water discharge of more than, 108 m^3 s^{-1} [88]. This study also suggests that at the time of maximum water discharge the Mediterranean may have been filled at a rate of 10 m per day.

2.5 Mediterranean climate during the Pliocene

During the Early Pliocene pollen records indicate that Mediterranean climate was warmer and wetter than today[73; 89; 90; 91]. Based on the quantitative changes of warm-water planktonic foraminifer species a relative SST record was elaborated for the whole Pliocene in sections from Southern Italy[92]. Although SST oscillated at precession scale, warm-water species were dominant during the Early Pliocene, with a special warm interval between 4.1 and 3.7 My. The first evidence of cooling is found at 3.7 My and a second one between 3.5 and 3.2 My (MIS MG5-M2[92; 93]). Pollen records from the Black Sea and Northwest Mediterranean also reflect a sharp change in the Mediterranean vegetation during this later interval. This event is recorded by a decrease of subtropical trees that were partially replaced by herbs, indicating lower temperatures but still relatively humid conditions[89; 94]. This transitional period of cooling was interrupted by the Mid-Pliocene warmth event between 3.2 and 3 My[95]. Pliocene Mediterranean temperatures have been estimated to be 1-2 ºC warmer than at Present[95] and atmospheric carbon dioxide concentrations were about 30% higher than pre-anthropogenic values[96; 97], consequently climate during this time period has been considered a good analog for future climate conditions. On the basis of climate model simulations the climate of western Europe and Mediterranean was warmer and wetter due to the enhanced atmospheric and oceanic transport of heat and moisture to the North Atlantic and Mediterranean from the Equatorial Atlantic, especially during winter[98].

Pollen data found in sediments from the early and mid-Pliocene fit well with these predictions of a warmer and more humid climate in the northern Mediterranean (1-4 ºC warmer and 400-700 mm higher annual rainfall than today[90; 99]. In the Southern Mediterreanean, however, climate was warmer

by 1 to 5 ºC, but present day arid conditions appear to be in place since the beginning of the Pliocene[90].

SST changes during the Late Pliocene reflect the progressive intensification of the Northern Hemisphere glaciation, but the first pronounced glacial cycle is not recorded until the Late Pliocene, cotemporaneous with an intensification of the Northern Hemisphere glaciation at around 2.7 My. In particular very cool planktonic foraminifer assemblages have been found in MIS G6 and MIS 100-98-88[92] coincident with prominent glacial stages in the Equatorial and North Atlantic[100; 101]. Since 2.7 My ago until the Present, pollen records from the NW Mediterranean indicate alternations between steppe and forest that have been associated with the glacial-interglacial climate oscillations[89; 94; 102].

Contourite deposits (*e.g.*, the Faro drift) suggest that the Mediterranean outflow water (MOW) was already flowing along the southern Iberian margin in the early Pliocene, though its onset has not been precisely dated yet[103]. Continuous deposition in the Faro contourite drift seems to indicate that the Atlantic Mediterranean water exchange was anti-estuarine from the early Pliocene to the Present. In consequence, we may conclude that the Mediterranean hydrologic budget has remained negative since then. A MOW intensification between 3.5 and 3.3 My ago, probably in response to enhanced aridification of the Mediterranean climate, was recorded in the Ireland continental margin[104].

Throughout the Pliocene and Pleistocene the Mediterranean experienced numerous anoxic events recorded by the cyclical deposition of organic rich layers or sapropels whose formation are linked to the monsoon influence on the Mediterranean area and subsequent Nile river run-off and/or enhanced annual rainfall in perimediterranean regions[105; 106; 107; 108; 109]. Sapropel formation is linked to summer insolation maxima in the northern hemisphere (see also section 3) and the patterns of sapropel deposition have been used to elaborate the astronomical time scale[92; 110]. 18 sapropels (S63 to S80) were deposited in the eastern Mediterranean Sea between 2.6 and 3.2 My[111]. Around some of those sapropels, alkenone-based SST values reached 23 to 26 °C during the warmer periods and 20 to 21.5 °C during the colder ones[112], in agreement with the warmer than Pleistocene SST estimated by Dowsett *et al.*[95]. Prior to sapropel deposition export productivity was high. Overall, productivity was higher in the eastern than the western basin and higher in the Pliocene than the Pleistocene [113].

3 Sensitivity and Variability at Different Climate States

3.1 Warm Climate Intervals of the Pleistocene: The case of the last Interglacial

The glacial-interglacial cycles that characterize the last 2.6 My of Earth's climate have been shown to be related to changes in the Earth's orbital elements that affect radiation received at the top of the atmosphere ("insolation") and are a function of hemisphere, latitude, and season[114; 115]. On orbital timescales, full glacial and stadial (*i.e.*, less cold) periods were in general associated with colder global temperatures and lower atmospheric greenhouse gas concentrations and interglacial and interstadial (*i.e.*, less warm) intervals with warmer global temperatures and higher greenhouse gas concentrations (*e.g.*[116; 117; 118]). In the marine realm, interglacials are marked by sea level highstands indicated by lower benthic $\delta^{18}O$ values[101; 119]. On land, interglacial climate conditions are often associated with forest expansion (*e.g.*[120; 121; 122]). However, no interglacial of the last 800 ky was exactly like another[123; 124]. The climate of the Holocene, the current interglacial, will be discussed separately.

In this section we concentrate mainly on the last interglacial period called Marine Isotope Stage (MIS) 5e in the marine isotope stratigraphy and referred to as the Eemian period in continental records based on the palynological evidence. As the multi-proxy study of site 5 (core MD95-2042) off southwestern Portugal revealed, the boundaries of both periods are not the same[125; 126]. The base of MIS 5e, defined as the midpoint of the glacial/ interglacial transition, appears to be 6 ky older than the onset of the Eemian forest phase, while the onset of the sea level highstand related benthic $\delta^{18}O$ plateau preceded the Eemian by about 2 ky[125] (Fig. 6b, c). Here we follow Kukla *et al.*[126] and consider the interval from 128 to 116 ka to calculate the mean SST for MIS 5e (Table 1sm -

supplementary material; Fig. 7), while the Eemian lasted from 126 to 110 ka and thus extended into the MIS 5d stadial when continental ice sheets were already growing. MIS 5e global sea level was about 5±2 m higher than today (*e.g.*[59; 127]). Around the Mediterranean Sea, evidence for past eustatic high stands is still sparse and linked to sedimentary gaps on the continental shelf in the Gulf of Lions[128], deltaic deposits of the Tiber river[129] and submerged cave deposits[130; 131].

One interglacial phenomenon particular to the Mediterranean Sea is the deposition of the already above mentioned organic-rich and thus dark colored sapropel layers (Fig. 6h), especially in the eastern basin (*e.g.*[105; 111; 112; 132]). Sapropel deposition followed (by 1-3 ky) the insolation maxima associated with the glacial/ interglacial transitions (*e.g.* Fig. 6g), but also occurred along with glacial insolation maxima (*e.g.*[133; 134]). During MIS 5e a sapropel called S5 formed between 124 to 119 ky (Fig. 6h), but its duration and intensity varied regionally (*e.g.*[133] Fig. 6h), reaching a thickness of 120 cm in the southern Aegean Sea (site 124 - core LC21[135]; Table 1 and Figs. 4 and 6). Although some sapropel layers are laminated, indicating variable hydrographic conditions, most of them, including S5, were associated with anoxic conditions –as indicated by the absence of benthic foraminifera (*e.g.*[134; 136])– in the intermediate and deep waters in the eastern basin. The shallowest sapropels were detected at 120 m in sediment cores from the Aegean Sea[137], while generally present below 300 m in the open eastern Mediterranean (*e.g.*[138]) and below 400 m in the Adriatic Sea[139]. Although benthic foraminifera were absent, planktonic foraminifera can be found in the sapropel sediments and used to establish isotope stratigraphies (*e.g.* Fig. 6g) and reconstruct hydrographic conditions. Pollen and geochemical evidence have revealed that the formation of sapropels is linked to episodes of enhanced freshwater discharge, especially from the Nile river[140; 141; 142], due to an intensification of the African monsoon (by precessional forcing) and the northward migration of the Intertropical Convergence Zone[143; 144]. A mark of the increased rainfall is well preserved in speleothem, travertine and lake records from Israel (Fig. 6i; [144; 145; 146; 147; 148]). Due to the freshwater flux into the eastern Mediterranean basin, δw was depleted at the beginning of S5[149] and evidence from site 124 indicates a salinity drop of > 4psu in the eastern Aegean Sea[150]. The combination with the slightly cooler SST at the onset of S5[135; 143; 149] lead to temperature and salinity stratification, which inhibited convection and sustained the poor ventilation of the deeper water column and thus organic matter (C_{org}) preservation. Marino *et al.*[135] could show that the subsurface ventilation collapsed within 40± 20 yr in the Aegean Sea and 300± 120 yr later throughout the eastern Mediterranean Sea. The euxinic conditions, extending up to about 200 m water depth, persisted for 650 to 900 yr[135; 151] followed by a > 4 ky long period of variable conditions in the winter mixed layer and water column stratification[151]. At site 141 (core GeoTüKL83) off Israel, Schmiedl *et al.*[134] could show that oxygenation had already recovered during the later S5 phase, at 1433 m water depth, indicating at least local convection. Besides reduced ventilation increased productivity (*e.g.*[133; 151]) and hence enhanced carbon flux to the sea floor also played a role in sapropel formation. Different theories are being debated for the nutrient supply sustaining the high productivity: riverine supply[152]; development of a deep chlorophyll maximum and productivity therein[153; 154]; and trapping of nutrients in the eastern basin[155]. At site 73 (core LC07), at the Sardinian-Sicilian sill, plankton productivity was already high prior to the deposition of S5[156].

Mean SST values for MIS 5e, most of them based on alkenone concentrations ($U^{K'}_{37}$ Index) and limited to the S5 interval, are shown in figure 7 and listed with their minimum and maximum values in Table 1sm. Colder mean SST were recorded off western Iberia, reflecting the effect of the upwelling system, and a 2 °C gradient from north to south (Fig. 7) similarly to modern conditions[157]. Within the Mediterranean Sea, both mean and maximum SSTs were similar throughout the Mediterranean, from the western to the eastern basins, with values around 21 °C, which is 1-2 °C warmer than the late Holocene SST (Chapter 0). At site 90 (borehole PRAD1-2) in the central Adriatic Sea a relatively colder mean value is observed and SST cooled rapidly and faster than in other records after the SST peak at 120.7 ky (Fig. 6d *vs*. 6a). The mean value of 19.4 °C at site 95

(core KC01) in the central Ionian Sea, on the other hand, just includes data from the late MIS 5e when SST was already declining[135; 143; 158]. The record from site 98 (core KS205), in the same region[143], reveals that SST was overall more variable in the Ionian Sea and shows a slight cooling during S5 that is even more strongly depicted by the planktonic foraminifer records. Rohling *et al.*[143] interpret this fluctuation with a timing of 122.5 to 121.4 ky as a disruption in the African monsoon – supported by slightly higher $\delta^{18}O$ values in the Corchia and Peqiin speleothem records (Fig. 6f, i)– and link it to the Eemian cold fluctuation identified in pollen records from Greece[159; 160], Italy[161] and a French lake[162]. The timing also fits with a reduction in coccolith diversity at site 73 (core LC07[156]). A second and more pronounced cooling event is recorded in the planktonic foraminifera and benthic $\delta^{18}O$ climate records of site 84 (ODP Site 963) during late MIS 5e[163]. This cooling event is coeval with the C25 cooling event recorded in North Atlantic sediments (*e.g.*[164]) and with the Greenland Stadial (GS) 26 of the NGRIP ice core[165]. However, Incarbona *et al.*[156] point out that the surface water cooling at site 84 might be linked to local changes since the same event is not as well defined in the records of nearby site 73.

On land, the Eemian pollen records around the Mediterranean region clearly show that the major forested period occurred between 126 and 120 ka. However, they also reveal four main climatic phases of low amplitude, in particular, in the southwestern Iberian Peninsula[122; 166] and in Greece[160]. Between 126 and 120 ka, southwestern Iberia experienced warm and relatively humid climate as indicated by the expansion of the Mediterranean forest (Fig. 6b), while a deciduous oak forest is found in northwestern Iberia[122]. Here the beginning of the Eemian interglacial was actually marked by the expansion of pioneer species 1 ky prior to the establishment of Mediterranean forest conditions suggesting pre-cool and wet conditions[122]. Annual precipitation in this same region was around 800 mm and the warmest month mean temperature must have varied between 20 and 24 °C while the coldest month is likely to have experienced around 5 °C[122]. In northwestern Iberia, precipitation levels were similar but temperatures were lower, close to 18 °C in the warmest month and 3 °C in the coldest month. Recent studies on the isotopic composition of water in fluid inclusions ($\delta D_{(H2O)}$) of two stalagmites and oxygen isotopes of mammal's teeth phosphate ($\delta^{18}O_{(PO4)}$) in the Soyons Cave, Rhone Valley, France, are also indicating comparable contrasting seasonal temperatures during the same time interval with mean summer and winter values of 16 °C and 2 °C, respectively[167]. The Mediterranean climate of southern Iberia was gradually replaced by oceanic (cool and wet) conditions, that were well established between 120 and 116 ka, and turned into warm and dry conditions between 116 and 110 ka[122; 166]. At latitudes north of 36 °N but further to the east, the climatic phases described for the northwestern Iberian margin are also detected in the Ioannina record (Greece)[159]. In central Italy the coldest month temperatures were similar to the ones registered in the southwestern Iberian margin, that is, 4 – 5 °C[161].

In the Levant, the Israeli speleothem $\delta^{13}C$ records indicate higher abundances of C3 plants (e.g. trees), that is, humid and cool conditions, especially during the time of S5[146; 148].

During the last 450 ky MIS 5e stands out as the warmest interglacial within the Mediterranean Sea. The warm periods preceding MIS 5e were MIS 7 and MIS 9e (338 – 324 ka). MIS 7 includes the three warm substages MIS 7e (246 – 229 ka), 7c (216.8 – 206.8 ka) and 7a (200 – 190 ka) of which MIS 7e is the warmest in the Antarctic ice core records (e.g.[123]). Sapropels 9, 8 and 7 are associated with these substages, respectively. Relative sea level data for the Mediterranean Sea exists only for MIS 7a when sea level was between -9 and -18 m lower than at present[130]. SST in the Mediterranean region were fairly similar during all three substages, but on average 1°C colder than during MIS 5e[149; 158; 168; 169]. Similar to MIS 5e, SSTs were warmer in the eastern basin (by about 1 °C) than the western basin[149]. Also comparable to MIS 5e, SST at site 90 (borehole PRAD1-2[169]) in the central Adriatic Sea started to decline earlier than in the Alboran Sea (site 44/ODP site 977[158; 170]) and off southwestern Portgual (MD01-2443[168]) during MIS 7e and 9e. In the Alboran Sea surface water records and off southwestern Portugal all three MIS 7 substages were recorded as long warm

periods. In the subsurface waters (*N. pachyderma* (r) record of[170]), on the other hand, only MIS 7e and 7a were continuously warm. During MIS 7c subsurface waters in the Alboran Sea warmed only during the later phase, similar to the $U^{K'}_{37}$ –SST at site 90 indicating that the two records might be linked via the LIW formed in the Adriatic Sea. For MIS 9e only few SST data exists within the Mediterranean Sea. The $U^{K'}_{37}$ –SST record at site 90[169] indicates values (around 17.2°C) similar to MIS 7a and thus colder than during MIS 5e and at site 136 in the Levantine basin 21.5°C were reached during the formation of sapropel 10[149]. Along the western Portuguese margin, average SST decreased from 19.5 °C at 37.8 °N (core MD01-2443[168]) to 19.2 °C at site 1[171] and to values around 18.5 °C at site 10[172] and were therefore within the MIS 5e range (Fig. 7).

In the pollen records the MIS 7 substages and MIS 9e also show differences to MIS 5e. Although all three MIS 7 substages and MIS 9e were associated with a forest expansion (e.g.[173; 174; 175]), the forested periods were shorter than the MIS substages[121] and the forest during MIS 7c was more diverse than the one during MIS 7e[159; 174]. For MIS 9e, on other hand, the southern Iberian pollen record of core MD01-2443[121; 176] –opposite to northern Iberia[172]– reveals a short tree pollen maximum that is replaced by a higher abundance of Ericacaea pollen in the later phase of the interglacial. A much stronger climate contrast to MIS 5e is, however, observed in the records from the Levant. The higher lake level in the Lake Lisan/ Dead Sea system, the formation of travertines and the prevalence of C3 plants (trees) as shown by the lighter $\delta^{13}C$ data from the Soreq cave clearly indicate MIS 7 as a much wetter period than MIS 5e[144; 146].

3.2 High Frequency Variations: The case of MIS 3

The millennial-scale climate variability consisting of cycles of wamer (interstadial) and colder (stadial) periods were first described in detail in ice core records from Greenland (*e.g.*[177; 178]) but can be found in climate records all over the world[179]. The abrupt warming at the transition from a stadial to an interstadial is referred to as Dansgaard-Oeschger event and the cycles are called Dansgaard-Oeschger cycles[180] and consist of a Greenland interstadial (GI) and a Greenland stadial (GS)[165]. During some of the GS occurred the well-known Heinrich ice-rafting events in the North Atlantic ocean (*e.g.*[181]) that due to their supply of freshwater into the North Atlantic's convection areas led to a shutdown of the Atlantic Meridional Overturning Circulation (AMOC) (*e.g.*[5]). During a "regular" GS AMOC was slowed down, but also shallower than today. As a result of the reduced convection in the North Atlantic the interface between the North Atlantic Deep Water (NADW) and the Antarctic Bottom Water (AABW) shoaled and the AABW filled the water column up to 2000 m water depth (*e.g.*[182; 183]). The duration of a Heinrich ice-rafting event varied with a (apparent) longer duration in more northern latitudes and closer to the calving ice-sheets and a shorter towards the southern edge of the North Atlantic's ice-rafted debris belt (*e.g.*[184]). Since icebergs themselves did not enter the Mediterranean Sea –just their meltwater– it is impossible to clearly distinguish a Heinrich event in that region. Thus we are following Sanchez-Goñi and Harrison[184] and use the term Heinrich stadial (HS) for those GS associated with a Heinrich event. The temporal duration of a HS is equal to the associated GS as recorded in the Greenland ice core records and thus sometimes longer than the ice-rafting event itself. For the timeslices discussed here we selected HS 4 and the subsequent GI 8. Heinrich event 4 was one of the major ice-rafting events during MIS 3 and thus had a strong climatic impact. GI 8, on the other hand, was one of the longer lasting GI (*e.g.*[165]). HS 4 lasted between 39.92 and 38.46 calendar (cal) ka before present (BP = AD 1950) in the GISP2 chronology (*e.g.*[178]) and between 39.81 and 38.31 cal ka in the GICC05 chronology of the NGRIP ice core[165]; note that GICC05 ages are before AD 2000). The respective age ranges for GI 8 are 38.44 – 36.22 cal ka BP (GISP2) and 38.29 – 36.55 cal ka (NGRIP). The waxing and waning of the continental ice sheets left their imprints in the MIS 3 sea level record (see[185] for a recent review) and can also be detected in the Mediterranean Sea where flooding of the Gulf of Lions continental shelf occurred in general by the onset of the GI following a HS (site 58 – PRGL1[128]).

High-resolution SST records for the Mediterranean Sea are sparse and concentrated in the western basin. Both $U^{K'}_{37}$ -SST records from the Alboran Sea reveal the GI/ GS cycles with warmer SST during the GI (*e.g*. Fig. 8g; sites 41 and 44[158; 186]). Coldest SST during MIS 3 occurred during the HS, especially HS 4, both in the Alboran Sea (Fig. 8g) and north off Menorca (site 61[187]). For the central basin the data of site 88 in the Thyrrenhian Sea (core KET80-03[188]) exists and in the eastern basin the SST record of site 114 (core C69) in the southern Aegean Sea (Fig. 9[189]). Both sites experienced a cooling during HS 4. The temperature evolution in the Levantine basin is partly revealed by the planktonic foraminifera $\delta^{18}O$ records of sites 139 and 142 (cores 9501 and 9505[190]) but those two seem to follow more northern hemisphere insolation (Fig. 8e) rather than the millennial-scale pattern. The $\delta^{18}O$ records of both cores show, however, some oscillations during HS 4 indicating less stable surface water conditions.

On the western Iberian margin, SST records experienced the millennial-scale oscillations (Fig. 8b-d; *e.g*.[157]). SST were colder in the north where the impact of the southward advance of the Polar Front and thus the appearance of iceberg-bearing subpolar waters was felt more strongly (*e.g*.[191; 192; 157]). The southward shift of the Polar Front had a stronger impact north of 39°N because SST values in the Mediterranean Sea north of this latitude were not much colder than those offshore Portugal during HS 4 (Fig. 9 top). Likewise SST south of this latitude was similar on the Portuguese margin and in the Mediterranean Sea. Only the Gulf of Cadiz record of site 18 (core MD99-2339) stands out with the warmest mean SST but this location experienced only short-term cooling episodes during HS 4 (Fig. 8d[193]) as this site was located close to the boundary separating the colder northern surface waters from the Azores Current derived waters to the south. For the younger HS 2 and 1 Penaud *et al.*[194] could show that the waters off Morocco had clearly a different origin from those in the Alboran Sea and Rogerson *et al.*[195] revealed that the Azores Front penetrated into the Gulf of Cadiz. In comparison to the Gulf of Cadiz data, the Alboran Sea mean values –for sites 41 and 44– appear relatively cold but one needs to keep in mind that the Alboran Sea $U^{K'}_{37}$ data reflects annual mean temperatures and those in the Gulf of Cadiz summer SST. Mg/ Ca-based temperatures derived from the shells of *G. bulloides*, a surface dwelling foraminifera species, from site 41 (core MD95-2043) give a mean value of 14.5 ±0.8 °C for HS 4 (Cacho, unpubl. data) and thus in the range of the site 18 (core MD99-2339) value.

For the GI 8 timeslice, the major boundary was again located near 39°N, especially on the Portuguese margin (Fig. 9 bottom; Table 2sm). One pecularity associated with GI 8 –and only with this GI– is that the planktonic foraminifera faunas recorded colder SST at the beginning of the GI than in the end and not an immediate warming at the onset of the GI (Fig. 8b, d[157]). The $U^{K'}_{37}$ - SST values for the two Alboran Sea sites (41 and 44) and site 142 (core 9505) off Israel with 14.2 – 14.4 °C are again mean annual SST which might explain why they are so much colder than the SST recorded off the southern Portuguese margin or in the southern Aegean Sea. Also for this timeslice the *G. bulloides* Mg/ Ca temperatures for site 41 (core MD95-2043) are significantly warmer with 18.4 ±1.0 °C (Cacho, unpubl. data) and more in the range of those off southern Portugal.

For the Mediterranean Sea itself few evidence exists for the impact of millennial-scale climate change on ocean productivity. The various paleoproductivity proxy records generated for site 41 (core MD95-2043; *e.g*. Fig. 8h[196]) indicate that in the Alboran Sea productivity was reduced during stadials and high during interstadials. Productivity during HS 4 was comparable to other HS or GS and during GI 8 to other GI. However, maxima in interstadial productivity occurred not at the beginning of a GI but lateron. The site 84 (ODP Site 963) abundance record of *F. profunda*, a deep dwelling coccolith species that is anticorrelated with the chlorophyll a concentration, also shows millennial-scale variations that seem to support reduced/ increased productivity during stadials/ interstadials[156]. Site 114 (core C69) in the southern Aegean Sea recorded a TOC peak at the onset of GI 8 indicating the formation of an organic-rich layer[189]. If hydrographic conditions during the formation of this layer were similar to those during sapropel formation than the increase in organic

matter could result from enhanced productivity.

More evidence for productivity variations is available for the western Iberian margin. A latitudinal transect compiled by Salgueiro *et al.*[157] revealed that the same boundary affecting the SST variations also existed in regard to productivity. North of 39°N the southward migrating subpolar surface waters inhibited upwelling and thus led to reduced productivity during HS and GS. South of this boundary productivity during HS and GS varied –sometimes reduced, sometimes not. During HS 4 export productivity was increased at site MD95-2042 and even higher than during GI 8. North of 39°N productivity increased during the GI to levels similar to the interglacial ones[157]. GI 8 stands a bit out because off Cape Finisterre (site 7 – core SU92-03) productivity –like SST– increased only towards the end of the GI. Coccolith evidence from the Gulf of Cadiz supports high phytoplankton productivity during interstadials[197], consistent with the total alkenone concentration data from sites 5 and 9 (cores MD95-2042 and MD95-2040) on the western Iberian margin[198]. Voelker *et al.*[199], on the other hand, showed for site 18 (core MD99-2339) in the central Gulf of Cadiz that export productivity –estimated from the planktonic foraminifera fauna– was high during HS 1, 2 and 3, potentially linked to frontal upwelling. Export productivity at this site was also high during HS 4 but increased even further and remained high during GI 8[200].

Ventilation of the Western Mediterranean Deep Water (WMDW) strongly followed the millennial-scale variations (Fig. 10c, d; sites 41 and 61[187; 201]) with better ventilation during the GS and most parts of the HS and poor ventilation during the GI. This relationship is opposite to the one observed in the deep North Atlantic ocean, *e.g.* at site 5 (core MD95-2042; Fig. 10h), where the AMOC proxies indicate a slowdown during GS and a shutdown during most HS that led to a shoaling of the interface between NADW and AABW. Consequently, a seesaw pattern existed between the ventilation state of the deep Mediterranean Sea and Atlantic Ocean[187]. The high resolution record of site 61 (core MD99-2343), however, revealed that deep convection in the Gulf of Lions –driving WMDW ventilation– was interrupted during parts of the HS, such as HS 4 (Fig. 10c), due to the capping by less saline surface waters entering through the Strait of Gibraltar[187]. In general, the WMDW current off Menora had a higher flow speed during most of the HS and all GS (Fig. 10a,b; site 61[202]) supporting formation of WMDW by deep convection in the Gulf of Lions. Off Corsica, the grain size record of site 72 (core MD01-2434) from 800 m water depth[203] also recorded an increase in bottom current strength during all the GS and HS hinting to enhanced production of intermediate depth water masses, such as Levantine Intermediate Water (LIW), in the eastern Mediterranean. Currently, benthic stable isotope data for MIS 3 exists for only one intermediate depth core site in the Mediterranean Sea, M69/1-348 recovered in the Alboran Sea from 802 m water depth and covering the last 34 cal ky BP. The benthic $\delta^{13}C$ record of this core reveals a pattern similar to sites 61 and 41 (cores MD99-2343 and MD95-2043) with better ventilation during GS 5 and 4 (Schönfeld, unpubl. data). Thus it is appears that convection, most likely stronger than today, took place in both Mediterranean basins during the cold climate periods of MIS 3. Since surface waters were colder during GS and HS than today or during GI (Fig. 8, 8) the deeper and intermediate waters of the Mediterranean Sea should also have been colder and the deep water temperature (DWT) record of site 41 (core MD95-2043) from the Alboran Sea (Fig. 10f[204]) confirms this. The DWT and benthic $\delta^{18}O$ records do, however, not mimick each other (Fig. 10e,f) indicating that the $\delta^{18}O$ signal –a pattern similar to core MD95-2043 is also seen in the Sicily Strait at site 84 (ODP Site 963[156])– is partly driven by salinity changes.

Since production of both intermediate and deep water masses took place in the Mediterranean Sea both of them likely contributed to the MOW in the Gulf of Cadiz. Grain size records from core sites in the Gulf of Cadiz indicate the formation of contourite layers (grain size maxima, *e.g.* Fig. 10g) during GS and HS revealing that bottom current strength was not only enhanced in the Mediterranean Sea but also in the upper and lower MOW levels (sites 23 and 18[193; 205]). Because signal responses in mean grain size and benthic $\delta^{13}C$ at site 18 (core MD99-2339) were similar to

those of sites 41 and 61 (cores MD95-2043 and MD99-2343) in the deep western Mediterranean Sea, Voelker *et al.*[193] postulated that WMDW contributed more than at present to the deeper MOW during GS and HS.

The millennial-scale variations also affected the vegetation in the wider Mediterranean region. Several short-term events of forest expansion and reduction have been detected in Europe and in particular in some Mediterranean continental sites (*e.g.*[174; 206; 207]) and tentatively correlated with the GS - GI cycles and the North Atlantic Heinrich events (*e.g.*[206; 208; 209; 210; 211; 212; 213]). However, this correlation is not direct and based on independent chronologies that preclude the perfect match[214]. Marine sequences, in turn, usually present continuous, long records and can be used for direct sea-land correlations. In recent years large efforts have been made to understand the vegetation response to millennial-scale climate changes using sediment cores from the eastern North Atlantic mid-latitudes and the Mediterranean Sea[191; 214; 215; 216; 217; 218; 219; 220; 221; 222; 223]. Based on these studies, the strong/weak reduction of Mediterranean forests is likely the result of cold/cool conditions while the expansion of these floristic associations reflects warm conditions. Also, the growth/decline of semi-desert plants might be associated with dry/wet conditions (Fig. 8).

HS 4 was characterized by cold or extremely cold and dry conditions in the Mediterranean region that not only affected the vegetation –a shift to a steppic flora[209; 216]– but also lake levels, such as site 149 (Lake Lisan[144; 224]) or site 65 (Les Echets[225]), and precipitation as reflected in speleothem $\delta^{18}O$ records[145; 146; 226; 227]; Fig. 8f). The arid conditions were associated with increased intensity of Saharan winds (site 41; Fig. 8i; [228; 229]) and Saharan dust has also been found in Italy[230]. The shift to a dominance of steppic and thus C4 plants (e.g., grasses, herbs) is also seen in the Sofular speleothem $\delta^{13}C$ data and Fleitmann *et al.*[227] could show that a ≈100 year phase lag existed between the climate change and ecosystem response. Pollen data from extremely high resolution Iberian margin records, however, indicate a more complex pattern for HS4 composed of alternated cold and wet /cool and dry phases[191; 215; 216; 217; 222].

GI 8, on the other hand, was associated with wetter conditions (Fig. 9 bottom) resulting in higher lake levels and increased precipitation (Fig. 8f). A gradual temperature increase from 47 to 35 °N is depicted from pollen records. North of 45 °N, GI 8 was detected in only few sequences such as site 30 (core MD04-2845) in the Bay of Biscaye[217] and at site 79 (Azzano Decimo) in northern Italy[231]. Both records are marked by the slight expansion of temperate and Mediterranean forests (Fig. 8j, k), reflecting cool/relatively warm and wet conditions. A recent review of European vegetation records revealed that during the last glacial the temperate forest's northern limit was displaced further south to latitudes around 45 °N in comparison to 60 °N today[214]. South of 45 °N, GI 8 is more evident in high-resolution marine and terrestrial pollen records (Fig. 8j, k). Relatively warm and wet conditions were detected between 44 and 40 °N; moderate warm and wet conditions between 40 and 37 °N and warm and wet conditions, above 37 °N (Fig. 9 bottom; Table 2sm).

3.3 Deglaciation(s): The Case of the Last Glacial-Interglacial Transition (LGIT)

The deglaciation is the transition period between the end of a glacial and the beginning of the subsequent interglacial. Here we will concentrate on the last deglacial period, the transition from the Last Glacial Maximum (LGM) at 21 cal ka BP to the Holocene. The increase in high-latitude summer insolation that followed the LGM, favored the northern hemisphere ice sheets' retreat and triggered a 120-130 m increase in global sea level [232; 233; 234; 235] (starting around 19 cal ka BP) that led to a gradual deepening of the (shallower) straits and to flooding of the northern Adriatic Sea (e.g.[236]). The last deglaciation is marked by a succession of accelerated melting events superimposed on a smooth continuous sea level rise, the so-called melt-water peaks (mwp) 1A occurring at ~ 14 cal ka BP and mwp 1B around 11.3 cal ka BP[237; 238]. Millennial-scale climate variability, which includes two extreme cold episodes: Heinrich event/ stadial 1 (HS 1; Fig.10) and the Younger Dryas (YD; Fig. 11), further interrupted the deglaciation warming trend. HS1 is the result of abrupt and massive

icebergs discharges into the North Atlantic region (*e.g.*[181]) while the YD is related to catastrophic drainage episodes of the proglacial Lake Agassiz[239]. Between HS1 and the YD, a short warm phase occurred, the Bølling-Allerød episode (B-A; *e.g.* [239; 240; 241; 242; 243; 244; 245])

Figure 11 shows a W-E transect of $U^{K'}_{37}$ - SST records from the Iberian margin to the eastern Mediterranean basins for the above described period (21 to 9 cal ka BP). A SST increase from the LGM to the Holocene emerges as the general deglaciation pattern, with a more evident SST rise between the end of the YD and the beginning of the Holocene. The Holocene temperatures are close to 20 ºC almost all along the transect, but warmer values are observed in the Gulf of Cadiz (around 22 ºC) at sites 41 and 44 (Table 1) and in the easternmost Levantine basin with values around 24 ºC (site 145 - Table 1).

The LGM was associated with generally cool sea-surface conditions, with SST close to 12 ºC in the Alboran Sea and central basin, 14 ºC in the southwestern Iberian margin and around 16 ºC in the Levantine Basin (Fig. 11). This data shows a southwestern Iberian margin and Alboran Sea 4-6 °C colder in the LGM than today while the central and Levantine basins SST were around 8 ºC colder. The $U^{K'}_{37}$ -SST estimates for the LGM indicate lower values (by 1-2 °C) than those determined by Hayes *et al* [246] based on planktonic foraminifera faunas, especially in the eastern Mediterranean Sea, where new data (site 144) points to a 6 °C cooling[247] confirming the alkenone values from the nearby site 136 (Table 1, [149; 248]).

The HS 1 and YD events were well imprinted on the Iberian margin and Alboran Sea records. However, the cold HS1 signal is less evident in the central and Levantine basin compared to the other sites (Fig. 11). The YD cold event was well recorded in the Tagus mud patch (site 14) (Fig. 11, Table 1) with cold temperatures close to 8 ºC but less severe (~12 ºC) although well recorded, in other Iberian margin sites and in the western and central Mediterranean basins. In the Levantine basin (sites 140 and 144) and also for the northern Red Sea core (site 145, Figs. 4 and 10), a cooling episode also interrupted the LGIT but occurred about 2 ky earlier than the YD and as a consequence the rapid SST rise preceded the one at the other sites.

The B-A interstadial interval was recorded at most sites with SSTs around 2-4 º C colder than the Holocene.

Two areas stand out in the compilation, *i.e.* the Adriatic Sea (site 90[169]), and the Red Sea (site 145[249]). The Adriatic Sea (despite the low resolution record) recorded extremely cold conditions during HS 1 with SST close to 3 ºC. Afterward the SST rose to around 10 ºC during the B-A and decreased to 8 ºC during the YD. The transition to the Interglacial is recorded as a gradual SST increase until the early Holocene. A similar pattern occurred in the Marmara Sea (site 127[250]) with SST increasing from 6 ºC during the YD to 20 ºC at 9 cal ka BP. In contrast to these cold conditions, the site located in the Red Sea experienced warmer SST during the whole period with the warmest values during the Holocene (26 ºC) and only 2 ºC lower SST during the LGM. The interval between 18 and 14.5 cal ka BP shows the lowest values around 20 ºC and the rapid increase to interglacial conditions occurred at the end of this interval (site 145 in Figs. 4 and 10).

In summary, the "Mediterrannean" $U^{K'}_{37}$ -SST record for the last deglaciation shows lower values in the Adriatic Sea during HS 1 and in the Tagus mud patch area off Lisbon during the YD. Warmer conditions were recorded during the present interglacial with values close to 20 ºC and with around 4- 6 ºC lower values during the B-A interstadials. The LGIT is marked by a rapid SST increase, in its last warming phase, in the southwestern Iberian Margin, the Alboran Sea and the central Mediterranean basin.

Reconstruction of a δw W-E transect, combining $\delta^{18}O$ of planktonic foraminifera (*Globigerina bulloides* and *Globigerinoides ruber*) and $U^{K'}_{37}$ -SSTs, reveals a progressive isotopic enrichment of the surface water from the North Atlantic to the Levantine basin, except for a slight depletion in the central Mediterranean Sea[247]. This result indicates that the salinity gradient was steeper during the LGM than today. Although δw values in the central Mediterranean basin are slightly lighter than

today, δw increased sharply from the Sicily Strait to the East, suggesting a higher salinity gradient in the eastern basin. Therefore, even though colder temperatures may account for less evaporation at the LGM, the eastern Mediterranean Sea underwent higher excess evaporation over precipitation than today. Lake level curves support this with a lowering in the Lake Lisan/Dead Sea system (site 149[224; 251]) and in Lake Tiberias (Jordan Valley[252; 253]) during HS 1 and HS 2. Halite deposit in the paleo-Dead Sea during the YD has been interpreted as reflecting extreme arid conditions (*e.g.*[251]), although according to the Levantine basin δw curve, HS 1 was more arid than the YD. Speleothem $\delta^{18}O$ records from Israeal[146] agree with the lake level fluctuations with the most positive values during the YD, i.e. lowest rainfall.

LGIT related variations in productivity for the area, have been investigated by many authors (*e.g.* [254; 255; 256; 257; 258; 259; 260]). Although controversial results arise when different proxies are compared, strong changes in primary productivity and an organic rich layer (ORL) has been described from the Alboran deglaciation sediments, at a time of no sapropel deposition in the eastern Mediterranean (*e.g.*[54; 261]). In the central Mediterranean Sea, surface water productivity increased during the colder climate phases of the LGIT, i.e. the LGM, the YD and the century-scale cold oscillations within the B-A interstadial complex[236; 262; 263] with the colder conditions often aiding deep winter mixing and thus nutrient replenishment. Increased productivity in the Adriatic Sea during the B-A cold oscillations might, on the other hand, be linked to nutrients supplied by the Po river[236; 262]. In the upwelling centres along the western Iberian margin, summer export productivity was high during the LGM, crashed during HS 1, especially in the northern region, and then increased again during the YD[157]. YD levels were, however, lower than during the LGM and more comparable to the early Holocene.

Conditions in the deeper water masses were also affected by the deglacial climate oscillations. During the LGM, the WMDW was well ventilated (Fig. 10d, e; sites 41 and 61[187; 201]) indicating that deep-water convection took place in the Gulf of Lions. The glacial WMDW was also relatively cold (Fig. 10f[204]). Furthermore, the UP10 record of site 61 (core MD99-2343; Figs. 4 and 9a[202]) reveals that the current strength of the WMDW branch near Menorca was highly variable. Benthic isotopes records from intermediate-depth core sites in the Aegean and Leventine Seas reveal that the LIW was also well ventilated from the LGM to the YD[264] and indicate continuous LIW formation in those regions. Records from the Adriatic Sea, on the other hand, indicate that deep convection was interrupted in the Adriatic Sea, especially during the YD[236]. Studies in the Gulf of Cadiz and along the southern Portuguese margin showed that the lower MOW settled deeper in the water column (lower boundary near 2000 m) during the LGM[265; 195], but current strength was partly also enhanced in the upper MOW core (site 23 - core MD99-2341[205]).

During HS 1 and the YD, the WMDW was less well ventilated (in contrast to the LIW), but relatively cold. The WMDW's current strength off Menorca declined from the LGM until the transition from the YD to the Holocene. Nevertheless, the current strength related records of site 61 (Fig. 10a, b) indicate that periods with a stronger current existed during parts of HS 1 and the YD. Similar to the MIS 3 GS and HS, the enhanced WMDW flow during the later phase of HS 1 might have contributed to the increased current strength of the lower MOW core in the Gulf of Cadiz (Fig. 10g[193]). However, the grain size record at site 72 (core MD01-2434), collected from 800 m water depth east off Corsica, also reveals maxima during HS 1 and the YD[203] indicating that current strength was also enhanced close to the LIW level –concordant with the evidence of LIW formation in the eastern basins[264]– so that strengthening of the MOW might more be related to the LIW which contributes much more to the export through the Strait of Gibraltar. The YD contourite layer formed in the Gulf of Cadiz is well known and recorded in water depths bathed by the lower as well as the upper MOW core[193; 205; 266]. Because epibenthic foraminifera species become sparse to absent in the Holocene no stable isotope data exists for the deeper Mediterranean Sea (WMDW level) younger than 11.2 cal ka BP (Fig. 10). Thus, WMDW conditions at the beginning of the Holocene can only

be deducted from site 61 (core MD99-2343) through grain size and Si/ Al records, both of which show an extended minimum at the transition into the Holocene indicating a sluggish WMDW current. LIW production in the eastern basin remained relative strong until about 11 cal ka BP and then declined towards the period of sapropel S 1 formation[264; 267].

On land, and in particular in western Iberian Peninsula and western Mediterranean region the climate was cool and relatively wet[218; 219; 220; 222; 268; 269; 270]. These cool and wet conditions were probably the response to a more vigorous AMOC than during the previous HS 2 as testified by $^{231}Pa/^{230}Th$ measurements which estimate a AMOC slowdown of 30-40% or less during this period[245; 271] as also predicted by numerical climate models[5]. In contrast, further east the climate seems to have been relatively drier during the LGM, as shown by pollen sequences from Italy (*e.g.*[207; 209; 210]), Greece [273]and the Black[212], Tyrrhenian[272] and southern Aegean Seas[189].

As during HS 4, the continental climate became extremely cold and dry during the HS 1 episode as revealed by several pollen sequences (*e.g.*[120; 159; 189; 207; 209; 212; 218; 219; 268; 269; 270; 272; 273; 274; 275; 276]). However, a complex pattern composed by two or even three phases (cold-wet and cool-dry; cold-wet, cool-dry and cold-wet) is detected in a few high resolution pollen records from the western Iberian margin and the Alboran Sea[191; 220; 222]. A similar complex pattern has also been observed in a high resolution lacustrine record in central Italy (Lake Albano)[277; 278].

During the B-A warm period, numerous marine and terrestrial pollen sequences (*e.g.*[207; 212; 220; 221; 222; 268; 270; 273; 276; 279; 280; 281; 282; 283; 284; 285; 286; 287; 288; 289]) reveal warm and wet conditions along the entire Mediterranean region, supported by lake levels increases such as in Lake Albano[278]. Furthermore, high-resolution pollen sequences show that this period was punctuated by centennial-scale climatic variations such as the Older Dryas and the intra-Allerød events (*e.g.*[274; 269; 290; 291]). This complexity of vegetation changes during the B-A event parallel the rapid episodes detected in the Greenland ice cores during the Greenland interstadial 1 known as GI-1e, d, c, b, and a following the INTIMATE event stratigraphy (e.g.[292]).

The YD is marked by a strong/moderate reduction of the temperate-mediterranean forests and the high/moderate expansion of semi-desert plants in the Mediterranean region which indicate cold/cool and dry/relatively dry conditions, respectively (see B-A references above). The vegetation changes linked to this short event appear to be more drastic at latitudes above 42 °N and in high altitudinal sites rather than in lower latitude records (*e.g.*[293]). Also the conditions became less cold and dry further east (*e.g.*[294]).

3.4 Holocene climate

General North Hemispheric Climate

The last period discussed in this Mediterranean compilation corresponds to the interglacial period in which we presently live, the Holocene. This relatively warm period started at about 11.7 cal ka BP[295] and has generally been considered to be an epoch of climate stability, compared to the rapid and intense variability that characterized the last glacial[240] (see section 3.2). However, more high-resolution studies, completed within the last decade, have revealed the existence of significant short-term decadal to centennial climate variability[296].

In general terms, most of the extra-tropical Holocene records suggest maximum temperatures right at the beginning of the Holocene, during the so-called Holocene Climatic Optimum – HO (centred at 9 cal ka BP), followed by a continuous and pronounced trend towards cooler conditions [297; 298; 299; 300]. In the tropics, the same period shows roughly the reverse trend[301]. These changes are associated with changes in the terrestrial orbit[302], which led to markedly stronger seasonality in the Northern Hemisphere during the HO, with increased annual-mean insolation at high-latitudes and reduced at low latitudes. Nevertheless, an increasing number of high-resolution regional studies

reveal the existence of differences in magnitude and intensity of this trend which, is also indicative of the parallel action of regional processes of different intensity[303].

Climatic oscillations of short duration are, to some extent, superimposed on this general Holocene evolution, and, in the literature, these have been associated with a combination of internal climate system variability and external forcings (see, e.g.[304]). Variability at this timescale was first identified in the North Atlantic and linked to an external forcing in the form of changes in the intensity of the solar activity[305] although the physical mechanisms to establish the link within the climate system remain somewhat unclear. These authors found that periods of less intense solar activity were associated with relatively cold conditions and larger number of icebergs, the last of which is believed to have been the Little Ice Age (LIA) that followed a time of warmer climatic conditions known as the Medieval Warm Period (MWP). These two periods are well differentiated in the northern hemisphere and a large range of historical documentation is available – they are therefore discussed separately and in detail in Chapter 2.

Within the Holocene centennial oscillations identified in the North Atlantic[305], the one that left the strongest imprint was the so called "8.2" event, a cold period whose occurrence was centred at 8.2 cal ka BP[306; 307.] It is well marked in the Greenland ice cores and with a climatic expression in most of the Northern Hemisphere records. The 8.2 ka event shows many of the typical characteristics as the most prominent glacial cold events (i.e., Heinrich events). The 8.2 ka event is believed to have been forced by the rapid discharge of freshwater from pro-glacial Lakes Agassiz and Ojibway through Hudson Bay and the Hudson Strait into the Labrador Sea[308] or into the Arctic Ocean[309] marking the final demise of the Laurentide ice sheet.

The Holocene in the Mediterranean Region

In the Mediterranean region, the most abundant Holocene temperature data are $U^{K'}_{37}$-SST records and their evaluation reveals a HO development following the previously described northern hemisphere extratropical cooling trend[300; 299], best marked off western Iberia and in the western Mediterranean (*e.g.*[310; 311]). After maximum SST values, a 1 ºC cooling trend towards present day is observed in the western Iberian margin and the Alboran Sea[158; 310]. A pattern also visible in other more central regions of the Mediterranean, although more intense at the Tyrrhenian Sea, north of Sicily, with a 1.5 ºC cooling[310]. Another SST record north of Menorca confirms the maximum at the beginning of the Holocene and a cooling trend of 1ºC during the Holocene (Herrera and Cacho, unpubl. data), but SST records from the south of Sicily and Eastern Levantine basin do not show a clear cooling pattern and support comparable temperatures during the early and late Holocene[247; 312].

This Holocene SST evolution seems to be better established in the marine records than in the terrestrial ones, given the complexity to separate the thermal from the hydrologic imprint on these. One of the few continuous atmospheric records is from lake Redó in the central Pyrenees[313]. This record shows marked millennial-scale oscillations, but the warmer temperatures are still observed at the beginning of the Holocene[313].

Pollen records are direct indicators of the vegetation type and state, and as such, they correspond to an integral of the atmospheric temperature and humidity conditions. Several efforts have been made to reconstruct the atmospheric temperature from pollen sequences both from northern and southern Europe, and the results found in southern France and the northern Iberian Peninsula point to minimum temperatures at the beginning of the Holocene followed by a continuous warming trend of 2 ºC towards the Present[314]. However, these reconstructions do not agree with other reconstructions (also pollen based) that also show 1–2 ºC higher temperatures at the beginning of the Holocene relatively to present-day values[315]. Although this might still be a problem connected to the small number of available records, it also reveals the difficulty of reconstructing atmospheric temperatures from pollen. Indeed, important variations in the hydrologic conditions are clearly detected for the Mediterranean from pollen information, suggesting that precipitation might be more important than

temperature in defining the terrestrial vegetation. Such variations have allowed the separation of three intervals in the Holocene for the circum-Mediterranean region: (1) a primarily humid period (11.5-7 cal ka BP); (2) a transition phase (7-5.5 cal ka BP), and (3) a more recent arid period (5.5-0 cal ka BP)[316]. Southern European lake levels also indicate a primarily humid beginning for the Holocene and drier conditions after 5 cal ka BP[317]. This evolution is quite well recorded in the Iberian Peninsula, but the variations do not appear to be synchronous[318]. In the Pyrenees the period of maximum humidity is concentrated at 9-8 cal ka BP, where the arid phase starts around 8-7.5 cal ka BP[319; 320]. The Lake Banyoles pollen record confirms an initial humid phase in Catalunya for the Holocene [321], while the salines in the Ebro valley point to more arid conditions after 5 ka BP[322].

In terms of oceanic primary productivity, diatom data for both western Iberia and the Alboran basin point to the early-mid Holocene as the time of the lowest productivity level of the last 23 cal ky BP[254; 255; 260] and indicate a re-establishment of more productive conditions towards the Recent (± 3 cal ka BP). Very low productivity conditions are also indicated for the Algero–Balearic basin by Ba_{excess} data[261], the Gulf of Lion by benthic foraminifera data[323] and the Tyrrenian Sea, by planktonic foraminifera assemblages[324]. In contrast, in the eastern Mediterranean, higher abundances of crenarchaeol and alkenones support increased productivity in a high-nutrient stratified environment[312] as also shown by major and minor trace element distributions and solid phase phosphorous contents in a core from the Cretan Ridge[325]. However, the early Holocene sediments of the Alboran Sea show the formation of an ORL (e.g.[326; 327; 328]). A layer that although not found in other parts of the western Mediterranean, corresponds in time to manganese-rich layers in the Balearic basin[329] and layers containing organic traces in the Tyrrhenian Sea[330].

ORL / Sapropel formation is associated with either high flux of organic matter to the sea floor from high productivity conditions at the surface or increased preservation of organic matter in the ocean bottom due to deep waters devoid of oxygen. Given the indication of low primary production shown by the traditional productivity proxies, such as diatoms, for the Alboran Sea, this ORL was associated to a deep oxygen-depleted environment[328]. Besides, this layer is coeval with the deposition of the well-known sapropel S1 in the eastern Mediterranean, which occurred during the early Holocene in two phases S1a (10.8 – 8.8 cal ka BP) and S1b (7.8 – 6.1 cal ka BP) interrupted at about 8.2 ka BP[331; 332; 333; 334].

S1 is just the last of a large number of sapropel layers, occurring over a long time interval, in the eastern Mediterranean. Its formation is related to global changes in climate and circulation that derived from strong freshwater run-off of nutrients and resulted in enhanced stratification of the water column, increased productivity and reduction of dense water formation (see section 2.1). In the western Mediterranean one needs to also consider the Mediterranean in its relation to the Atlantic Ocean. As can be read in Chapters 0 and 3, the fact that the Gibraltar Strait is the Mediterranean Sea's sole connection to the Atlantic Ocean results in a west to east sea surface salinity and SST increase and a corresponding productivity decrease[335; 336; 337]. The inflowing Atlantic surface waters have their main influence in the western basin, while the strong evaporation towards the central and eastern basins leads to a 1.7 psu increase in salinity (S). The resulting rise in water density, associated with the cold dry Arctic air that penetrates into the eastern Mediterranean region during the winter, leads to the formation of deep waters in the Levantine (LIW) and Ionian Basins (see chapters 0 and 3). This dense Mediterranean water is pumped over the sill of Gibraltar, and exported as MOW into the Atlantic where its presence is easily depicted by both higher T and S at depths between 600 and 1200 m. The salinity of the Atlantic Ocean surface waters depend on the freshwater budget, but the salinity of the intermediate layer depends on processes occurring in the North Atlantic (Labrador and Norwegian Seas), where those waters are formed.

The primary sources of precipitation in the Mediterranean region over the Holocene period have typically been associated with two main processes: (1) fronts that originate in the NE Atlantic Ocean, passing over Europe and the Mediterranean Sea, generally associated with cyclonic "storm"

systems[338], and (2) the monsoonal system that originates in the tropical Atlantic or the southern Indian Ocean, passes over NE Africa, and is associated with the low-latitude rainfall system (cf. [132]).

The monsoonal system fluctuates in time reaching maximum strength during periods of maximum insolation in the Northern Hemisphere summer[105; 132]. As mentioned above, the major forcing for the Holocene climatic optimum, was the strong northern hemisphere extratropical insolation along with a marked increase in seasonality [302], which is known to have had also a strong impact in the tropical, subtropical and Mediterranean precipitation regime at the beginning of the Holocene (e.g.[11; 339; 299]). Such so, that presently deserted regions in the African continent were then marked by humid conditions determined by a strong African monsoon[105; 340]. The northward extension of the summer African monsoon is widely simulated by climate modelling experiments using General Circulation Models (GCMs), and is enhanced by both vegetative feedbacks over North Africa (e.g.[341]) and oceanic processes (e.g.[342]). Despite this, most GCMs appear to underestimate the extent of the northward shift in precipitation relative to palaeo-observations under mid-Holocene-like conditions[11; 339].

These changes mean that sapropel S1 was deposited simultaneously in the western and eastern Mediterranean basins, under warmer and wetter climatic conditions that are likely to have reduced or even nullified the present day Atlantic-Mediterranean salinity gradient, and consequently reduced deep water formation and bottom ventilation[264]. The reconstructed surface salinity record for the Gulf of Lion shows strong negative excursions confirming the low salinity of the Atlantic surface water entering the Mediterranean at the time[323], coinciding with elevated discharge of the Nile River (*e.g.*[105; 141; 343; 344]). Furthermore, although it is perhaps unlikely that direct monsoonal precipitation (of tropical origin) reached the southern coastline of the Eastern Mediterranean (consistent with the so-called "monsoon-desert" proposed by[345], discussed in the Holocene context by Brayshaw *et al*.[346] and in agreement with palaeo-data from the Red Sea[249]) rivers from the Tibesti Mountains, formed as a result of a northward shift of the monsoonal belt over Africa, are additional sources of freshwater into the Eastern Mediterranean during this period[143; 190; 347; 348]. In addition to the monsoonal precipitation, there is evidence for stronger rainfall on the entire Mediterranean Sea from Atlantic sources[349; 350; 351], perhaps consistent with enhanced winter storm activity in the Mediterranean during the earlier part of the Holocene[352] and stronger westerly mean flow over southern Europe and the Mediterranean (consistent with the pollen-based study of Bonfils *et al*[353], although it should be noted that GCM simulations of the associated atmospheric circulation anomalies over the Atlantic and Europe remain highly uncertain[354]). At around the same period, the influx of fresher Black Sea water[355; 356] was also contributing to a fresher Mediterranean Sea.

HO in the Mediterranean Region

The hydrologic information gathered from pollen data as well as oxygen isotopic composition measured in lakes and speleothems for HO, a period contained in the first phase of the S1 deposition time (Fig. 12), is consistent with widespread wet and warm conditions in the landmass surrounding the Mediterranean as a whole. As to the SST, the $U^{K'}_{37}$ data contained in the figure (Fig. 12), to the exception of the 25 ºC found at site 145 in the Red Sea, and considering the standard deviation (Table 3sm), reveals values that are very similar across the entire basin with a mean Mediterranean SST of 18.8 ± 1.8 ºC and 18.6± 2.05 ºC in the western basin, 18.3±1.93 ºC in the central basin and 19.8±1.21 ºC in the eastern basin. Planktonic foraminiferal assemblages dominated by the species *Globigerinoides ruber* together with other warm-water species confirm the presence of warm surficial waters in most of the basin (e.g.[139; 263; 347; 357; 358; 359]). Foraminiferal estimated SSTs (Table 3sm) as well as TEX86-based SST although showing higher values relatively to the $U^{K'}_{37}$ -SST, which probably indicates increased seasonality in the early Holocene[312], confirm widespread warm conditions throughout the Mediterranean. This observation supports a major reduction of the modern thermal gradient, as suggested by Rohling and De Rijk[360]. Furthermore, the presence of infaunal and

low oxygen tolerant benthic foraminifera species throughout the central and eastern basins, points to a decrease of the oxygen content into the sediment levels[136; 323; 357]. Anoxic conditions confirmed by de Lange[334] for the whole eastern Mediterranean basin below 1.8 km during the entire period of sapropel S1 formation (10.8 to 6.1 ka cal. BP) sustain the hypothesis that during the first phase of S1 deposition (S1a), the entire Mediterranean Sea suffered a major change in circulation towards poor ventilation conditions[361; 362].

Climate simulations of the HO with sufficient resolution to discern the detailed topography of the Mediterranean are scarce. However, recent work by Brayshaw *et al*[346; 352], using a nested regional climate model within a global GCM, provides a picture that broadly concurs with the description above in that the Mediterranean was generally wetter during the HO (particularly in the north and east), with a considerably stronger seasonal cycle of surface temperatures (summer temperatures are much warmer, particularly over land in the south and east of the basin, consistent with the large-scale response of most climate models[11]). However, somewhat in contrast to the surface temperature changes inferred from proxy evidence, the annual-mean surface temperature in Brayshaw *et al*[346] shows little change or even a slight reduction over much of the basin (in their model, this is consistent with a response to reduced atmospheric greenhouse gas concentrations in their HO period experiments).

The 8.2 event in the Mediterranean Region

Several paleoclimatic records from Greenland, Europe and America show evidence of a rapid reorganisation of the atmospheric system occurring exactly at this time (the 8.2 event[296; 307; 363]). The agreement observed between the periodicity of the Holocene abrupt events marked in the westernmost Mediterranean region and the cooling events of the North Atlantic region support a strong Atlantic-Mediterranean climatic link at high-frequency time intervals. Furthermore, proxies for deep-water conditions reveal the occurrence of episodes of deepwater overturning reinforcement in the western Mediterranean basin, which not only supports the good ventilation conditions needed to stop the formation of the ORL in the Alboran Sea[328] but also interrupted sapropel S1 in the Eastern Mediterranean Basin[331; 333]. Furthermore, it also indicates a rapid response of the Mediterranean thermohaline circulation to climate change in the North Atlantic, and, stresses the importance of atmospheric processes in linking climate variability between high- and mid-latitudes. A mechanism similar to one defended by Cacho *et al*.[328] and Sierro *et al*.[187] for the glacial Dansgaard-Oeschger variability has also been proposed to explain the Holocene cooling events by Frigola *et al*.[364]. That is, a strengthened westerly system enhancing the marine overturning cell in the Gulf of Lion would lead to a more efficient formation of Mediterranean Deep Waters in both the eastern and western Mediterranean[328; 364; 365] and to the enhancement of deep circulation.

Spatial distribution of climate conditions at 8.2 cal ka BP within the Mediterrannean region is shown in Figure 13 and compiled in Table 4ms. The temperatures documented in the $U^{K'}_{37}$ -SST records relatively to the HO values are 0.7 ºC lower (for the entire basin). The western basin shows a lower difference between 8.2 ka and HO (0.4 ^{o}C) while a larger difference (1.3 ^{o}C) is found in the eastern basin (Table 3sm). Lower temperature and/or humidity are also indicated by planktonic foraminifera $\delta^{18}O$ values from the central Aegean Sea[366], and low Ca-contents in the Black Sea[355]. This sea-surface cooling is coupled with sharply smaller contents of the marine and terrestrial biomarkers in the water column and point to reductions of organic fluxes or more active oxidation on the seafloor and stronger water column ventilation[367]. An inference also supported by the benthic foraminiferal records (*e.g.*[331; 356; 368]).

Most high-resolution pollen sequences from the Mediterranean region show a slight decrease of temperature during the 8.2 ka (e.g.[189; 221; 276; 316]). Pollen records from the Adriatic Sea indicate an increase in high-altitude trees (Abies and Picea[369]) possibly related to a slight temperature decrease in the continental climate, perhaps induced by an increase in intensity of the northeastern and eastern

winds. Nevertheless, the presence of the Mediterranean taxa that require mild winters indicates that winter temperatures did not drastically decrease[370].

South of 42 °N, in the central and eastern Mediterranean regions (e.g.[207; 221; 316; 371; 372; 373; 374; 375; 376]) and northern Aegean Sea[189; 276; 332; 377; 378; 379; 380; 381] dry conditions persisted during the 8.2 ka event. The prevalence of arid conditions in northeastern Africa and the Middle East has also been documented by multiproxy data ([382] and references within). In contrast, pollen sequences located north of 42 °N, such as those from the northwestern Iberian margin as well as the ones from the Swiss and French Jura mountains detect an increase in precipitation[220; 383; 384].

The terrestrial records however, do not show any major change, except in the Pyrenees where the signal is towards relatively cold and arid conditions[319]. On the other hand, archeologic evidence from the Ebro depression point to a quite strong impact on the neolitic settlings in the region. This period appears to coincide with the period known in the region as the "archeologic silence", moment in which most of the higher altitude sites were abandoned[385].

Model reconstructions focusing on the short-lived '8.2 ka cal BP event' anomaly convincingly link this event to a reduction of the AMOC due to a meltwater pulse (*e.g.*[307; 386; 387]). Sortable silt size (a proxy of deep current flow speed) records for the Gadar and the Erik Drift (cores MD99-2251 and MD03-2665, respectively[388; 389]), sites under the influence of the Iceland Scotland and the total integrated Nordic Seas overflows[390; 391; 392] show cooling and deep-water circulation disturbance at virtually the same time. Specifically, a reduction in NADW production slightly precedes and spans the sea surface cooling event, in striking agreement with the sequence of events found by the above mentioned climate models.

However, this data compilation shows a stronger impact of this event on the eastern basin, confirming severe far-field impacts of this North Atlantic events in Mediterranean basins such as the Aegean Sea[365], which are isolated from the North Atlantic oceanic circulation, pointing to a signal transmitted through atmospheric processes as proposed by Ariztegui *et al.*[332] and Rohling *et al.*[347; 393], has shown that the event at 8.2 ka coincided in time with intensifications of the Siberian High, as reflected in the GISP2 nss [K^+] record. This ice peak in K+ also coincides with periods of dry Indian monsoon (Qunf Cave $\delta^{18}O$ speleothem record[394]), hinting at large (hemispheric) scale teleconnections during the early Holocene on centennial timescales[363; 365].

Some insight into these large-scale teleconnections can, perhaps, be gained through the so-called "AMOC shutdown" experiments using GCMs[307]. Many of these experiments can, in some senses, be considered to be a "forced" version of the 8.2 ka event (whereby the sinking water in the high latitude North Atlantic is completely shutdown by applying a large freshwater pulse or hosing). Such simulations typically indicate markedly cooler temperatures over the whole Northern Hemisphere extratropics[395] and weaker precipitation (lower temperatures are associated with reduced atmospheric humidity despite increased storm activity; e.g.[396]). Although precipitation is reduced over Europe and almost all of the Mediterranean, this change is not uniform (e.g., results presented by Brayshaw *et al.*[397] suggest that the precipitation signal is particularly weak in the south-east corner of the Mediterranean basin). However, it is important to note that many of these experiments are performed against a "recent" background climate rather than conditions specifically pertaining to the 8.2 ka event.

In modern times, outbreaks of cold northerly air masses strongly affect the Aegean winter SST regime, impacting on the rates of Aegean deep water formation and consequently on the ventilation of the entire eastern Mediterranean Sea (see Chapter 0 and [398; 399; 400]). It may well be that the frequency and/or intensity of such events varies in association with the North Atlantic Oscillation[401], generating a stronger signal on the eastern than on the western Mediterranean, where the signal appears to be transmitted mainly via thermohaline circulation.

This relation between relative aridity and cold temperatures is however not likely to have been maintained during the whole Holocene, given that during the cold LIA conditions the glaciers of the

Pyrenees have greatly expanded[402] and evidence for strong precipitation and even increased flooding have been found in the littoral Catalan[403] and off the west coast of the Iberian Peninsula[404; 405].

Acknowledgments
This work is a result of the MedCLIVAR program, an ESF à la carte program which has provided the funds for meeting(s) that helped shape this contribution. I would like to thank those who provided preprints or unpublished material that was used in this chapter. Thanks are also due to Alessandra Asioli and Alan Haywood whose comments on a previous version have been greatly appreciated.

REFERENCES TEXT AND TABLES

1. J. Zachos, M. Pagani, L. Sloan, E. Thomas, K. Billups, *Science* 292, 686 (2001).
2. W. Ruddiman, *Earth's Climate Past and Future*. W. F. Ruddiman., W. H. F. a. Co., Eds., (NY, 2nd Ed, 2007).
3. A. Berger, M. F. Loutre, *Planetary Science Letters* 111, 369 (1992).
4. J. Imbrie, K. P. Imbrie, *Progress in Physical Geography* 6, 606 (1979).
5. A. Ganopolski, S. Rahmstorf, *Nature* 409, 153 (2001).
6. C. Lyell, *Principles of geology, being an attempt to explain the former changes of the Earth's surface, by reference to causes now in operation*. J. Murray, Ed. 1 (London, 1830).
7. G. Fischer, G. W. (eds.), *Use of Proxies in Paleoceanography: Examples from the South Atlantic*. (Springer, Berlin, 1999).
8. S. Solomon *et al.*, Eds *Climate Change 2007: The Physical Science Basis Contribution of Working Group I to the Fourth Assessment Report of the Intergovernmental Panel on Climate Change* (Cambridge University Press, 2007).
9. J. Kennett, *Marine Geology*. pp. 813 (Prentice-Hall, London, 1982).
10. R. S. Webb, *Nature* 385, 695 (1997).
11. P. Braconnot *et al.*, *Climate of the Past* 3, 261 (2007).
12. G. Siani *et al.*, *Science* 294, 1917 (2001).
13. P. Sabatier *et al.*, *Radiocarbon* 52, 91 (2010).
14. F. Rögl, *Geologica Carpathica* 50, (1999).
15. F. Rögl, H.-J. Hansen, *Ann. Naturhist. Mus. Wien* 111A, 15 (2009).
16. S. K. Hüsing *et al.*, in *Geodynamics of Collision and Collapse at the Africa-Arabia-Eurasia subduction zone,* D. J. J. Van Hinsbergen, M. A. Edwards, R. Govers, Eds. 311, 107-132 (Geological Society of London Special Publication, London, 2009).
17. H. M. Schulz, A. Bechtel, R. F. Sachsenhofer, *Global and Planetary Change* 49, 163 (2005).
18. M. B. Allen, H. A. Armstrong, *Palaeogeography, Palaeoclimatology, Palaeoecology* 265, 52 (2008).
19. S. V. Popov, A. S. Stolyarov, *Israel Journal of Earth Sciences* 45, 161 (1996).
20. R. F. Sachsenhofer, B. Stummer, G. Georgiev, *Marine and Petroleum Geology* 26, 57 (2009).
21. F. Rögl, *Ann. Naturhist. Mus. Wien* 99A, 279 (1998).
22. G. Clauzon *et al.*, *Basin Research* 17, 437 (2005).
23. M. Harzhauser, W. E. Piller, *Palaeogeography, Palaeoclimatology, Palaeoecology* 253, 8 (2007).
24. S. V. Popov *et al.*, *Palaeogeography, Palaeoclimatology, Palaeoecology* 236, 91 (2006).
25. G. Ramstein, F. Fluteau, J. Besse, S. Joussaume, *Nature* 386, 788 (1997).
26. F. Fluteau, G. Ramstein, J. Besse, *Journal of Geophysical Research-Atmospheres* 104 11995 (1999).
27. L. Gentil, *C. R. Acad. Sci. Paris*, 167 (1918).
28. K. J. Hsü, W. B. F. Ryan, M. B. Cita, *Nature* 242, 240 (1973).
29. K. J. Hsü *et al.*, *Nature* 267, 399 (1977).
30. M. B. Cita, R. C. Wright, W. B. F. Ryan, A. Longinelli, *Messinian palaeoenvironments*. K. J. Hsü, L. Montadert, Eds., (US. Government Printing Office, Washington, 1978).

31. L. Montadert, J. Sancho, J. P. Fail, J. Debyser, E. Winnock, *C. R. Acad. Sci. Paris* 271, 812 (1970).
32. J. Lofi *et al.*, *Marine Geology* 217, 1 (2005).
33. J. G. Lofi *et al.*, in CISEM 2008 *The Messinian Salinity Crisis from mega-deposits to microbiology- A consensus Report,* F. Briand, Ed., 83 (2008).
34. A. Decima, F. C. Wezel, in *Initial Reports of the Deep Sea Drilling Project,* W. B. F. Ryan, K. J. Hsu, Eds. 13, 1234 (US Government Printing Office, Washington, DC, 1973).
35. M. Roveri, M. A. Bassetti, F. Ricci Lucchi, *Sedimentary Geology* 140, 201 (2001).
36. M. Roveri, S. Lugli, V. Manzi, B. C. Schreiber, *Terra Nova* 20, 438 (2008).
37. M. Roveri, M. V., *Palaeogeography, Palaeoclimatology, Palaeoecology* 238, 386 (2006).
38. V. Manzi, S. Lugli, F. Ricci-Lucchi, M. Roveri, *Sedimentology* 52, 875 (2005).
39. V. Manzi *et al.*, *Palaeogeography, Palaeoclimatology, Palaeoecology* 251, 470 (2007).
40. V. Manzi, S. Lugli, M. Roveri, B. C. Schreiber, *Sedimentology* 56, 1937 (2009).
41. F. J. Hilgen, W. Krijgsman, *Terra Nova* 11, 16 (1999).
42. W. Krijgsman, F. J. Hilgen, I. Raffi, F. J. Sierro, D. S. Wilson, *Nature* 400, 652 (1999).
43. F. J. Hilgen, *Earth Planet, Sci. Lett* 107, 349 (1991).
44. J. M. Rouchy, A. Caruso, *Sedimentary Geology* 188-189, 35 (2006).
45. R. Butler, W. H. Lickorish, M. Grasso, H. M. Pedley, L. L. Ramberti, *Geological Society of America Bulletin* 107 425 (1995).
46. G. Clauzon, J. P. Suc, F. Gautier, A. Berger, M. F. Loutre, *Geology* 24 363 (1996).
47. R. Riding, J. C. Braga, J. M. Martin, I. M. Sanchez-Almazo, *Marine Geology* 146, 1 (1998).
48. J. C. Braga *et al.*, *Sedimentary Geology* 188, 131 (2006).
49. CIESM, in CISEM 2008 *The Messinian Salinity Crisis from mega-deposits to microbiology- A consensus Report,* F. Briand, Ed., 3 (2008).
50. T. J. Kouwenhoven, M. S. Seidenkrantz, G. J. van der Zwaan, *Palaeogeogr. Palaeoclimatol. Palaeoecol* 152, 259 (1999).
51. T. J. Kouwenhoven, F. J. Hilgen, G. J. van der Zwaan, *Palaeogeogr. Palaeoclimatol. Palaeoecol* 18, 303 (2003).
52. M. S. Seidenkrantz, T. J. Kouwenhoven, F. J. Jorissen, N. J. Shackleton, G. J. Van der Zwaan, *Marine Geology* 163, 387 (2000).
53. F. J. Sierro *et al.*, *Palaeogeogr. Palaeoclimatol. Palaeoecol.* 190, 289 (2003).
54. F. J. Sierro *et al.*, *Marine Geology* 153, 137 (1999).
55. F. J. Sierro, W. Krijgsman, F. J. Hilgen, J. A. Flores, *Palaeogeogr. Palaeoclimatol. Palaeoecol* 168, 143 (2001).
56. E. Van Assen, K. F. Kuiper, N. Barhoun, W. Krijgsman, F. J. Sierro, *Palaeogeogr. Palaeoclimatol. Palaeoecol* 238, 15 (2006).
57. M. Fenton, S. Geiselhart, E. J. Rohling, C. Hemleben, *Marine Micropaleontology* 40, 277 (2000).
58. W. Krijgsman, F. J. Hilgen, A. Fortuin, F. J. Sierro, *Sedimentary Geology* 140, 43 (2001).
59. E. J. Rohling *et al.*, *Nature Geoscience* 1, 38 (2008).
60. F. Gautier, G. Clauzon, J. P. Suc, J. Cravatte, D. Violanti, *Comptes Rendus de l´Academie des Sciences Serie II* 318 1103 (1994).
61. G. J. De Lange, W. Krijgsman, *Marine Geology* 275, 273 (2010).
62. S. Lugli, V. Manzi, M. Roveri, C. Schreiber, *Palaeogeography, Palaeoclimatology, Palaeoecology* 297, 83 (2010).
63. W. Krijgsman, P. T. Meijer, *Marine Geology* 253, 73 (2008).
64. G. Clauzon, in *Initial Reports of the Deep Sea Drilling Project,* W. B. F. Ryan, K. J. Hsü, Eds. 13, 1251. (Washington, DC, 1973).
65. E. van der Laan, S. Gaboardi, F. J. Hilgen, L. J. Lourens, *Paleoceanography* 20, (2005).
66. F. J. Hilgen, K. F. Kuiper, W. Krijgsman, E. Snel, E. Van der Laan, *Stratigraphy* 4, 231 (2007).
67. P. T. Meijer, *Earth Planet. Sci. Lett.* 248, 471 (2006).
68. P. T. Meijer, W. Krijgsman, *Earth Planet. Sci. Lett.* 240, 510 (2005).
69. M. Roveri, V. Manzi, M. A. Bassetti, M. Merini, F. Ricci Lucchi, *Giornale di Geologia* 60, 119 (1998).

70. R. Flecker, R. M. Ellam, *Sedimentary Geology* 188-189, 189 (2006).
71. M. N. Çagatay *et al.*, *Sedimentary Geology* 188-189, 171 (2006).
72. S. Lugli, M. Manzi, M. Roveri, in CISEM 2008 *The Messinian Salinity Crisis from mega-deposits to microbiology- A consensus Report,* F. Briand, Ed., .67 (2008).
73. J.-P. Suc, *Nature* 307, 429 (1984).
74. S. Iaccarino, A. Bossio, in *Proc. O.D.P., Sci. Res,* R. Zahn, M. C. Comas, A. Klaus, Eds. 161, 529 (Ocean Drilling Program, College Station, TX, 1999).
75. A. R. Fortuin, W. Krijgsman, *Sediment. Geology* 160, 213 (2003).
76. J. M. Rouchy *et al.*, *Sedimentary Geology* 145, 93 (2001).
77. J. M. Rouchy *et al.*, *Sedimentary Geology*. 163 (2003).
78. J. M. Rouchy, A. Caruso, C. Pierre, M. M. Blanc-Valleron, M. A. Bassetti, *Palaeogeography, Palaeoclimatology, Palaeoecology* 254, 386 (2007).
79. J. Aguirre, I. M. Sánchez-Almazo, *Sedimentary Geology* 168, 71 (2004).
80. M. A. Bassetti, P. Miculan, F. J. Sierro, *Sedimentary Geology* 188-189, 279 (2006).
81. A. Guerra-Merchán *et al.*, *Palaeogeography, Palaeoclimatology, Palaeoecology* 285, 264 (2010).
82. D. A. Hodell, J. H. Curtis, F. J. Sierro, M. E. Raymo, *Paleoceanography* 16, 164 (2001).
83. E. van der Laan, E. Snel, E. De Kaenel, F. J. Hilgen, W. Krijgsman, *Paleoceanography* 21, (2006).
84. S. Duggen, K. Hoernle, P. van den Bogaard, L. Rupke, J. P. Morgan, *Nature* 422, 602 (2003).
85. F. J. Sierro, S. Ledesma, J. A. Flores, in CISEM 2008 *The Messinian Salinity Crisis from mega-deposits to microbiology- A consensus Report,* F. Briand, Ed., 45 (2008).
86. P. L. Blanc, *Geodinamica Acta* 15, 303 (2002).
87. N. Loget, J. Van den Driessche, *Sedimentary Geology* 188-189, 341 (2006).
88. D. Garcia-Castellanos *et al.*, *Nature* 462, 778 (2009).
89. S. Fauquette, J. Guiot, S. J. P., *Palaeogeography, Palaeoclimatology, Palaeoecology* 144, 183 (1998).
90. J. O. Fauquette, J. P. Suc, J. Guiot, *Paleogeography, Palaeoclimatology, Palaeoecology,* 152 15 (1999).
91. G. Jimenez-Moreno, S. Fauquette, J. P. Suc, *Review of Paleobotany and Palinology*. (in press).
92. L. J. Lourens *et al.*, *Paleoceanography* 11, 391 (1996).
93. R. Sprovieri *et al.*, *Paleoceanography* 21, (2006).
94. S. M. Popescu *et al.*, in *Quaternary International*. (2010).
95. H. J. Dowsett, M. A. Chandler, M. M. Robinson, *Philosophical Transactions of the Royal Society* 367, 69 (2009).
96. J. Van Der Burgh, H. Visscher, D. L. Dilcher, W. M. Kurschner, *Science* 260, 1788 (1993).
97. A. K. Tripati, C. D. Roberts, R. A. Eagle, *Science* 326, 1394 (2009).
98. A. M. Haywood, B. W. Sellwood, P. J. Valdes, *Geology* 28, 1063 (2000).
99. A. Jost *et al.*, *Climate of the Past* 5, 585 (2009).
100. G. H. Haug, R. Tiedemann, *Nature* 393, 673 (1998).
101. L. E. Lisiecki, M. Raymo, *Paleoceanography*, 20, pp. PA1003 (2005).
102. N. Combourieu-Nebout, S. Fauquette, P. Quezel, *Bulletin de la Societe Geologique de France* 171 271 (2000).
103. F. J. Hernandez-Molina *et al.*, *Deep Sea Research, Part II* 53, 1420 (2006).
104. N. Khelifi *et al.*, *Geology* 37, 811 (2009).
105. M. Rossignol-Strick, V. Nesteroff, P. Olive, C. Vergnaud-Grazzini, *Nature* 295, 105 (1982).
106. R. C. Thunell, D. F. Williams, P. R. Belyea, *Marine Geology* 59, 105 (1984).
107. E. J. Rohling, *Marine Geology* 122, 1 (1994).
108. A. Cramp, G. O`Sullivan, *Marine Geology* 1-4, 11 (1999).
109. R. Wehausen, H.-J. Brumsack, in *Proc. Ocean Drilling Program, Scientific Results,* A. H. F. Robertson, K.-C. Emeis, C. Richter, A. Camerlenghi, Eds, 160,. 207-217 (Ocean Drilling Program, College Station, Tx, 1998),
110. F. J. Hilgen, *Earth and Planetary Science Letters* 104, 226 (1991).
111. D. Kroon *et al.*, in *Proc. Ocean Drilling Program, Scientific Results,* A. H. F. Robertson, K.-C. Emeis, C. Richter, A. Camerlenghi, Eds., 160, 181-189 (Ocean Drilling Program, College Station, 1998).
112. K.-C. Emeis *et al.*, in *Proc. Ocean Drilling Program, Scientific Results,* A. H. F. Robertson, K.-C. Emeis, C.

Richter, A. Camerlenghi, Eds.), 160, 309-331 (Ocean Drilling Program, College Station, Tx, 1998).
113. L. Diester-Haass, C. Robert, H. Chamley, in *Proc. Ocean Drilling Program, Scientific Results,* A. H. F. Robertson, K.-C. Emeis, C. Richter, A. Camerlenghi, Eds. 160, 227- 248 (Ocean Drilling Program, College Station, Tx, 1998).
114. M. Milankovitch, *Theorie Mathematique des Phenomenes Thermiques produits par la Radiation Solaire.*, (Gauthier-Villars Paris, 1920).
115. J. D. Hays, J. Imbrie, N. J. Shackleton, *Science* 194, 1121 (1976).
116. J. R. Petit *et al.*, *Nature* 399, 429 (1999).
117. J. Jouzel *et al.*, *Science* 317, 793 (2007).
118. L. Loulergue *et al.*, *Nature* 453, 383 (2008).
119. N. J. Shackleton, N. D. Opdyke, *Quaternary Research* 3, 39 (1973).
120. P. C. Tzedakis *et al.*, *Earth and Planetary Science Letters* 150, 171 (1997).
121. P. C. Tzedakis, K. H. Roucoux, L. de Abreu, N. J. Shackleton, *Science* 306, 2231 (2004).
122. M. F. Sánchez-Goñi *et al.*, *Earth and Planetary Science Letters* 231, 111 (2005).
123. EPICA Members, *Nature* 429, 623 (2004/06/10, 2004).
124. P. C. Tzedakis *et al.*, *Nature Geoscience* 2, 751 (2009).
125. N. J. Shackleton, M. F. Sanchez-Goni, D. Pailler, Y. Lancelot, *Global and Planetary Change* 36, 151 (2003).
126. G. J. Kukla *et al.*, *Quaternary Research* 58, 2 (2002).
127. W. G. Thompson, S. L. Goldstein, *Science* 308, 401 (2005).
128. F. J. Sierro *et al.*, *Quaternary Science Reviews* 28, 2867 (2009).
129. F. Marra, F. Florindo, E. Boschi, *Paleoceanography*. 23 (2008).
130. E. Bard, F. Antonioli, S. Silenzi, *Earth and Planetary Science Letters* 196, 135 (2002).
131. J. A. Dorale *et al.*, *Science* 327, 860 (2010).
132. M. Rossignol-Strick, *Palaeogeogr. Palaeoclimatol. Palaeoecol.* 49, 237 (1985).
133. S. Weldeab *et al.*, *Palaeogeography, Palaeoclimatology, Palaeoecology* 190, 121 (2003).
134. G. Schmiedl *et al.*, *Palaeogeography, Palaeoclimatology, Palaeoecology* 190, 139 (2003).
135. G. Marino *et al.*, *Geology* 35, 675 (2007).
136. F. J. Jorissen, *Marine Geology* 153, 91 (1999).
137. J. S. L. Casford *et al.*, *Paleoceanography* 17, 14 (2002).
138. E. J. Rohling, F. J. Jorissen, C. V. Grazzini, W. J. Zachariasse, *Marine Micropaleontology* 21, 191 (1993).
139. F. J. Jorissen *et al.*, *Marine Micropaleontology,* 21, 169 (1993).
140. R. Cheddadi, M. Rossignol-Strick, *Paleoceanography* 10, 291 (1995).
141. A. E. Scrivner, D. Vance, E. J. Rohling, *Geology* 32, 565 (2004).
142. A. H. Osborne, G. Marino, D. Vance, E. J. Rohling, *Quaternary Science Reviews* 29, 2473 (2010).
143. E. J. Rohling *et al.*, *Earth and Planetary Science Letters* 202, 61 (2002).
144. N. Waldmann, A. Torfstein, M. Stein, *Geology*, 567 (2010).
145. M. Bar-Matthews, A. Ayalon, A. Kaufman, G. J. Wasserburg, *Earth and Planetary Science Letters* 166, 85 (1999).
146. M. Bar-Matthews, A. Ayalon, M. Gilmour, A. Matthews, C. J. Hawkesworth, *Geochimica et Cosmochimica Acta* 67, 3181 (2003).
147. A. Frumkin, D. C. Ford, H. P. Schwarcz, *Quaternary Research* 51, 317 (1999).
148. A. Frumkin, D. C. Ford, H. P. Schwarcz, *Global Biogeochem. Cycles* 14, 863 (2000).
149. K.-C. Emeis *et al.*, in *Paleoceanography*. 18 (2003).
150. M. T. J. van der Meer *et al.*, *Earth and Planetary Science Letters* 262, 594 (2007).
151. E. J. Rohling, E. C. Hopmans, J. S. Sinninghe Damstè, in *Paleoceanography*. 21, PA2018 (2006).
152. F. Martinez-Ruiz, M. Kastner, A. Paytan, M. Ortega-Huertas, S. M. Bernasconi, *Paleoceanography* 15, 200 (2000).
153. E. J. Rohling, W. W. C. Gieskes, *Paleoceanography* 4, 531 (1989).
154. E. J. Rohling *et al.*, *Marine Micropaleontology* 50, 89 (2004).

155. U. Struck, K.-C. Emeis, M. Voß, M. D. Krom, G. H. Rau, *Geochimica et Cosmochimica Acta* 65, 3249 (2001).
156. A. Incarbona *et al.*, *Marine Micropaleontology* 69, 26 (2008).
157. E. Salgueiro *et al.*, *Quaternary Science Reviews* 29, 680 (2010).
158. B. Martrat *et al.*, *Science* 306, 1762 (2004).
159. P. C. Tzedakis, J. F. McManus, H. Hooghiemstra, D. W. Oppo, T. A. Wijmstra, *Earth and Planetary Science Letters* 212, 197 (2003).
160. P. C. Tzedakis, M. R. Frogley, T. H. E. Heaton, *Global and Planetary Change* 36, 157 (2003).
161. J. R. M. Allen, B. Huntley, *Quaternary Science Reviews* 28, 1521 (2009).
162. N. Thouveny *et al.*, *Nature* 371, 503 (1994).
163. R. Sprovieri, E. Di Stefano, A. Incarbona, D. W. Oppo, *Quaternary Science Reviews* 25, 2332 (2006).
164. D. W. Oppo, J. F. McManus, J. L. Cullen, *Quaternary Science Reviews* 25, 3268 (2006).
165. NGRIP members, *Nature* 431, 147 (2004).
166. M. F. Sanchez-Goni, F. Eynaud, J. L. Turon, N. J. Shackleton, *Earth and Planetary Science Letters* 171, 123 (1999).
167. V. Gardien *et al.*, paper presented at the AGU Meeting, St. Francisco, 2010.
168. B. Martrat *et al.*, *Science* 317, 502 (2007).
169. A. Piva *et al.*, in *Geochemistry Geophysics Geosystems*. 9 (2008).
170. B. Gonzalez-Mora, F. J. Sierro, J. Schönfeld, in *Geochem. Geophys. Geosyst.* 9 (2008).
171. T. Rodrigues, A. H. L. Voelker, J. O. Grimalt, F. Abrantes, F. Naughton, in *Paleoceanography*. (in press).
172. S. Desprat, M. F. Sanchez Goñi, J. F. McManus, J. Duprat, E. Cortijo, *Clim. Past* 5, 53 (2009).
173. M. Reille, V. Andrieu, J.-L. de Beaulieu, P. Guenet, C. Goeury, *Quaternary Science Reviews* 17, 1107 (1998).
174. M. Follieri, M. Giardini, D. Magri, L. Sadori, *Quaternary International* 47-48, 3 (1998).
175. T. A. Wijmstra, A. Smit, *Acta bot. neerl* 25, 297 (1976).
176. K. H. Roucoux, P. C. Tzedakis, L. de Abreu, N. J. Shackleton, *Earth and Planetary Science Letters* 249, 307 (2006).
177. S. J. Johnsen *et al.*, *Nature* 359, 311 (1992).
178. P. M. Grootes, M. Stuiver, *Journal of Geophysical Research* 102, 26 (1997).
179. A. H. L. Voelker, *Quaternary Science Reviews* 21, 1185 (2002).
180. W. S. Broecker, G. H. Denton, *Geochimica et Cosmochimica Acta* 53, 2465 (1989).
181. G. Bond *et al.*, *Nature* 365, 143 (1993).
182. D. W. Oppo, S. Lehman, *Paleoceanography* 10, 901 (1995).
183. L. Vidal *et al.*, *Earth and Planetary Science Letters* 146, 13 (1997).
184. M. F. Sanchez-Goñi, S. P. Harrison, *Quaternary Science Reviews* 29, 2823 (2010).
185. M. Siddall, E. J. Rohling, W. G. Thompson, C. Waelbroeck, *Reviews of Geophysics*. (2008).
186. I. Cacho *et al.*, *Paleoceanography* 14, 698 (1999).
187. F. J. Sierro *et al.*, *Paleoceanography*. 20, PA2019 (2005).
188. M. Paterne *et al.*, *Paleoceanography* 14, 626 (1999).
189. M. Geraga, S. Tsaila-Monopolis, C. Ioakim, G. Papatheodorou, G. Ferentinos, *Palaeogeography, Palaeoclimatology, Palaeoecology* 220, 311 (2005).
190. A. Almogi-Labin *et al.*, *Quaternary Science Reviews* 28, 2882 (2009).
191. F. Naughton *et al.*, *Earth and Planetary Science Letters* 284, 329 (2009).
192. F. Eynaud *et al.*, in *Geochemistry Geophysics Geosystems*. 10 (2009).
193. A. H. L. Voelker *et al.*, *Earth and Planetary Science Letters* 245, 39 (2006).
194. A. Penaud *et al.*, *Quaternary Science Reviews* 29, 1923 (2010).
195. M. Rogerson, E. J. Rohling, P. P. E. Weaver, J. W. Murray, *Paleoceanography*. 20, PA3007 (2005).
196. A. Moreno, I. Cacho, M. Canals, J. O. Grimalt, A. Sanchez-Vidal, *Palaeogeography, Palaeoclimatology, Palaeoecology* 211, 205 (2004).
197. E. Colmenero-Hidalgo *et al.*, *Palaeogeography, Palaeoclimatology, Palaeoecology* 205, 317 (2004).
198. D. Pailler, E. Bard, *Palaeogeography, Palaeoclimatology, Palaeoecology* 181, 431 (2002).

199. A. H. L. Voelker, L. de Abreu, J. Schönfeld, H. Erlenkeuser, F. Abrantes, *Geochem. Geophys. Geosyst.* 10 (2009).
200. A. H. L. Voelker, J. Schönfeld, S. M. Lebreiro, F. Abrantes, *to be submitted to Marine Micropaleontology*, (in prep.).
201. I. Cacho, J. O. Grimalt, F. J. Sierro, N. Shackleton, M. Canals, *Earth and Planetary Science Letters* 183, 417 (2000).
202. J. Frigola *et al.*, *Quaternary International* 181, 88 (2008).
203. N. Touyet *et al.*, Geo-Temas,11 171 2010.
204. I. Cacho, N. Shackleton, H. Elderfield, F. J. Sierro, J. O. Grimalt, *Quaternary Science Reviews* 25, 3294 (2006).
205. S. Toucanne *et al.*, *Palaeogeography, Palaeoclimatology, Palaeoecology* 246, 354 (2007).
206. F. Burjachs, R. Julià, *Quaternary Research* 42, 308 (1994).
207. D. Magri, *Review of Palaeobotany and Palynology* 106, 171 (1999).
208. S. A. G. Leroy, S. Giralt, P. Francus, G. Seret, *Quaternary Science Reviews* 15, 189 (1996).
209. J. R. M. Allen *et al.*, *Nature* 400, 740 (1999).
210. J. R. M. Allen, W. A. Watts, B. Huntley, *Quaternary International* 73/ 74, 91 (2000).
211. F. Guiter *et al.*, *Quaternary International* 111, 59 (2003).
212. K. A. Arslanov, P. M. Dolukhanov, N. A. Gei, *Quaternary International* 121 (2007).
213. V. Margari, P. L. Gibbard, C. L. Bryant, P. C. Tzedakis, *Quaternary Science Reviews* 28, 1317 (2009).
214. W. J. Fletcher *et al.*, *Quaternary Science Reviews*. (in press).
215. M. F. Sánchez-Goñi, J. L. Turon, F. Eynaud, S. Glendreau, *Quaternary Research* 54, 394 (2000).
216. M. F. Sánchez-Goñi *et al.*, *Climate Dynamics* 19, 95 (2002).
217. M. F. Sánchez-Goñi *et al.*, *Quaternary Science Reviews* 27, 1136 (2008).
218. K. H. Roucoux, N. J. Shackleton, L. de Abreu, J. Schönfeld, P. C. Tzedakis, *Quaternary Research* 5, 128 (2001).
219. K. H. Roucoux, L. de Abreu, N. J. Shackleton, P. C. Tzedakis, *Quaternary Science Reviews* 24, 1637 (2005).
220. F. Naughton *et al.*, *Marine Micropaleontology* 62, 91 (2007).
221. W. J. Fletcher, T. Boski, D. Moura, *The Holocene* 17, 481 (2007).
222. W. J. Fletcher, M. F. Sanchez Goñi, *Quaternary Research* 70, 451 (2008).
223. V. Margari *et al.*, *Nature Geosci* 3, 127 (2010).
224. Y. Bartov, S. L. Goldstein, M. Stein, Y. Enzel, *Geology* 31, 439 (2003).
225. L. Ampel, B. Wohlfarth, J. Risberg, D. Veres, *Quaternary Science Reviews* 27, 1493 (2008).
226. D. Genty *et al.*, *Nature* 421, 833 (2003).
227. D. Fleitmann *et al.*, *Geophys. Res. Lett.* 36 (2009).
228. A. Moreno *et al.*, *Quaternary Research* 58, 318 (2002/11, 2002).
229. A. Moreno *et al.*, *Quaternary Science Reviews* 24, 1623 (2005).
230. B. Narcisi, *Journal of Quaternary Science* 16, 245 (2001).
231. R. Pini, C. Ravazzi, M. Donegana, *Quaternary Science Reviews* (2009).
232. R. G. Fairbanks, *Paleoceanography* 5, 937 (1990).
233. R. G. Fairbanks *et al.*, *Quaternary Science Reviews*. 24, 1781 (2005).
234. W. R. Peltier, R. G. Fairbanks, *Quaternarty Science Reviews* 25, 3322 (2006).
235. J. D. Stanford *et al.*, *Palaeogeography* 21, (2006).
236. A. Asioli *et al.*, *Quaternary Science Reviews* 20, 1201 (2001).
237. E. Bard, B. Hamelin, D. Delanghe-Sabatier, *Science* 327, 1235(2010).
238. E. Bard *et al.*, *Geophysical Research Letters* 23, 1473 (1996).
239. J. T. Teller, D. W. Leverington, J. D. Mann, *Quaternary Science Reviews* 21, 879 (2002).
240. W. Dansgaard *et al.*, *Nature* 264, 218 (1993).
241. K. A. Hughen, J. T. Overpeck, L. C. Peterson, S. Trumbore, *Nature* 380, 51 (1996).
242. J. Iversen, *Danmarks Geol. Unders* 80, 87 (1954).
243. S. J. Johnsen *et al.*, *Journal of Quaternary Science* 16, 299 (2001).
244. L. D. Keigwin, S. J. Lehman, *Paleoceanography* 9, (1994).
245. J. F. McManus, R. Francois, J.-M. Gherardi, L. D. Keigwin, S. Brown-Leger, *Nature* 428, 834 (2004).

246. A. Hayes, M. Kucera, N. Kallel, L. Sbaffi, E. J. Rohling, *Quaternary Science Reviews* 24, 999 (2005).
247. L. Essallami, M. A. Sicre, N. Kallel, L. Labeyrie, G. Siani, *Geochemistry Geophysics Geosystems*. 8 (2007).
248. K. C. Emeis *et al.*, *Palaeogeography Palaeoclimatology Palaeoecology* 158, 259 (2000).
249. H. W. Arz, F. Lamy, J. Paetzold, P. J. Mueller, M. Prins, *Science* 300, 118 (2003).
250. M. Sperling *et al.*, *Palaeogeography, Palaeoclimatology, Palaeoecology* 190, (2003).
251. M. Stein, A. Torfstein, I. Gavrieli, Y. Yechieli, *Quaternary Science Reviews* 29, 567 (2010).
252. N. Hazan, M. Stein, S. Marco, *Isr. J. Earth-Sci* 53, 199 (2004).
253. S. A. Robinson, S. Black, B. W. Sellwood, P. J. Valdes, *Quaternary Science Reviews* 25, 1517 (2006).
254. F. Abrantes, *Mar. Micropaleontol.* 13, 76 (1988).
255. F. Abrantes, *Mar. Micropaleontol.* 17, 285 (1990).
256. M. H. Caralp, *Marine Micropaleontology* 13 265 (1988).
257. P. P. E. Weaver, C. Pujol, *Palaeogeogr. Palaeoclimatol. Palaeoecol.* 64, 35 (1988).
258. C. Vergnaud-Grazzini, C. Pierre, *Paleoceanography* 6, 519 (1991).
259. J. Targarona, Utrecht University (1997).
260. M. A. Bárcena *et al.*, *Palaeogeography, Palaeoclimatology, Palaeoecology* 167, 337 (2001).
261. F. J. Jimenez-Espejo *et al.*, *Palaeogeography, Palaeoclimatology, Palaeoecology* 246, 292 (2007).
262. F. Sangiorgi, L. Capotondi, H. Brinkhuis, *Palaeogeography, Palaeoclimatology, Palaeoecology* 186, 199 (2002).
263. R. Sprovieri, E. Di Stefano, A. Incarbona, M. E. Gargano, *Palaeogeography, Palaeoclimatology, Palaeoecology* 202, 119 (2003).
264. G. Schmiedl *et al.*, in *Quaternary Science Reviews* (in press).
265. J. Schönfeld, R. Zahn, *Palaeogeography, Palaeoclimatology, Palaeoecology* 159, 85 (2000).
266. C. Vergnaud-Grazzini *et al.*, *Oceanologica Acta* 12, 305 (1989).
267. T. Kuhnt, G. Schmiedl, W. Ehrmann, Y. Hamann, N. Andersen, *Palaeogeography, Palaeoclimatology, Palaeoecology* 268, 106 (2008).
268. K. P. Boessenkool, H. Brinkhuis, J. Schönfeld, J. Targarona, *Global and Planetary Change* 30, 33 (2001).
269. N. Combourieu-Nebout *et al.*, *Geology* 30, 863 (2002).
270. J. L. Turon, A.-M. Lézine, M. Denèfle, *Quaternary Research* 59, 88 (2003).
271. J. M. Gherardi *et al.*, *Earth and Planetary Science Letters* 240, 710 (2005).
272. M. Rossignol-Strick, *Quaternary Science Reviews* 14, 893 (1996).
273. I. T. Lawson, M. Frogley, C. Bryant, R. Preece, P. C. Tzedakis, *Quaternary Science Reviews* 23, 1599 (2004).
274. J. L. de Beaulieu, M. Reille, *Boreas* 13, 111 (1984).
275. N. Combourieu Nebout *et al.*, in *Proceedings ODP, Scientific Results,* R. Zahn, M. C. Comas, A. Klaus, Eds. 161, 457-468 (Ocean Drilling Program, College Station, TX, 1999).
276. N. Combourieu Nebout *et al.*, *Clim. Past* 5, 503 (2009).
277. P. Guilizzoni *et al.*, *Journal of Paleolimnology* 23, 117 (2000).
278. C. Chondrogianni *et al.*, *Quaternary International* 122, 31 (2004).
279. M. Reille, J. L. Beaulieu, in *Quaternary type sections: imagination or reality?,* S. C. e. Rose J, Ed. 79-89 (Balkema, Rotterdam, 1989).
280. M. Follieri, D. Magri, L. Sadori, *Quaternary International* 3/4, 81 (1989).
281. H. F. Lamb, U. Eicher, V. R. Switsur, *Journal of Biogeography* 16, 65 (1989).
282. M. Rossignol-Strick, N. Planchais, *Nature* 342, 413 (1989).
283. R. Cheddadi, M. Rossignol-Strick, M. Fontugne, *Marine Geology* 100, 53 (1991).
284. M. Reille, J. J. Lowe, *Quaternary Science Reviews* 12, 47 (1993).
285. J. R. M. Allen, B. Huntley, W. A. Watts, *Journal of Quaternary Science* 11, 125 (1996).
286. M. C. Peñalba, M. Arnold, J. Guiot, J.-C. Duplessy, J.-L. de Beaulieu, *Quaternary Research* 48, 205 (1997).
287. C. Muñoz-Sobrino, P. Ramil-Rego, L. Gómez-Orellana, *Vegetation History and Archaeobotany* 13, 1 (2004).
288. J. Atanassova, I. Stefanova, *Vegetation History and Archaeobotany* 12, 1 (2003).
289. A. Bordon, O. Peyron, A.-M. Lézine, S. Brewer, E. Fouache, *Quaternary International* 200, 19 (2009).
290. P. González-Sampériz *et al.*, *Quaternary International* 140, 4 (2005).

291. M. Magny *et al.*, *Quaternary Science Reviews* 25, 414 (2006).
292. J. J. Lowe *et al.*, *Quaternary Science Reviews* 27, 6 (2008).
293. F. Naughton, J.-F. Bourillet, M. F. Sanchez Goni, J.-L. Turon, J.-M. Jouanneau, *The Holocene* 17, 939 (2007).
294. S. Bottema, *Quaternary Science Reviews* 14 883 (1995).
295. M. Walker *et al.*, *Journal of Quaternary Science* 24, 3 (2009).
296. P. A. Mayewski *et al.*, *Quaternary Research* 62, 243 (2004).
297. P. DeMenocal *et al.*, *Quaternary Science Reviews* 19, 347 (2000).
298. P. DeMenocal, J. Ortiz, T. Guilderson, M. Sarnthein, *Science* 288, 2198 (2000).
299. O. Marchal *et al.*, *Quaternary Science Reviews* 21, 455 (2002).
300. J. H. Kim *et al.*, *Quaternary Science Reviews* 23, 2141 (2004).
301. E. Jansen *et al.*, in *Climate Change 2007: The Physical Science Basis Contribution of Working Group I to the Fourth Assessment Report of the Intergovernmental Panel on Climate Change.,* S. Solomon *et al.*, Eds. 433-497 (Cambridge University Press, 2007).
302. A. L. Berger, *Journal of Atmospheric Sciences* 35, 2362 (1978).
303. H. Renssen *et al.*, *Nature Geoscience* 2, 411 (2009).
304. M. Debret *et al.*, *Quaternary Science Reviews*, 2675 (2009).
305. G. Bond *et al.*, *Science* 294, 2130 (2001).
306. R. B. Alley *et al.*, *Geology* 25, 483 (1997).
307. R. B. Alley, A. M. Agustsdottir, *Quaternarty Science Reviews* 24, 1123 (2005).
308. D. C. Barber *et al.*, *Nature* 400, 344 (1999).
309. A. Born, A. Levermann, *Geochem. Geophys. Geosyst*. 11 (2010).
310. I. Cacho *et al.*, *Paleoceanography* 16, 40 (2001).
311. T. Rodrigues, J. O. Grimalt, F. Abrantes, J. A. Flores, S. M. Lebreiro, *Geochem. Geophys. Geosyst.* 10, Q07U06 (2009).
312. I. S. Castañeda *et al.*, *Paleoceanography*. 25, PA1208 (2010).
313. S. Pla, J. Catalan, *Climate Dynamics* 24, 263 (2005).
314. B. A. S. Davis, S. Brewer, A. C. Stevenson, J. Guiot, *Quaternary Science Reviews* 22, 1701 (2003).
315. B. Huntley, I. C. Prentice, *Science* 241, 687 (1988).
316. G. Jalut, A. Esteban Amat, L. Bonnet, T. Gauquelin, M. Fontugne, *Palaeogeography, Palaeoclimatology, Palaeoecology* 160, 255 (2000).
317. S. P. Harrison, G. Digerfeldt, *Quaternary Science Reviews* 12, 233 (1993).
318. J. S. Carrión *et al.*, *Quaternary Science Reviews* 26, 1455 (2007).
319. P. Gonzalez-Samperiz *et al.*, *Quaternary Research* 66, 38 (2006).
320. M. Morellón *et al.*, *Quaternary International* 181, 15 (2008).
321. R. Perez-Obiol, R. Julia, *Quaternary Research* 41, 91 (1994).
322. P. González-Sampériz *et al.*, *Palaeogeography, Palaeoclimatology, Palaeoecology* 259, 157 (2008).
323. T. Melki *et al.*, *Palaeogeography, Palaeoclimatology, Palaeoecology* 279, 96 (2009).
324. G. Ciampo, *Glob. Planet. Change* 40, 151 (2004).
325. G. Gennari, F. Tamburini, D. Ariztegui, I. Hajdas, S. Spezzaferri, *Palaeogeography, Palaeoclimatology, Palaeoecology* 273, 239 (2009).
326. Shipboard Scientific Party, *Sites 963, 964, 966, 967, 969*. Proc. ODP, Init. Rep. 160, 972 (1996).
327. Shipboard Scientific Party, *Sites 974, 975, 976, 979.*, Proc. ODP, Init. Rep. 161, 972 (1996).
328. I. Cacho, J. O. Grimalt, M. Canals, *Journal of Marine Systems* 33-34, 253 (2002).
329. M. Canals-Artiguas, Univ. Barcelona (1980).
330. N. Kallel, M. Paterne, L. D. Labeyrie, J. C. Duplessy, M. Arnold, *Palaeogeogr., Palaeoclimat. Palaeoecol* 135, 97 (1997).
331. E. J. Rohling, F. J. Jorissen, H. C. De Stigter, *Journal of Micropalaeontology* 16, 97 (1997).
332. D. Ariztegui *et al.*, *Palaeogeography, Palaeoclimatology, Palaeoecology* 158, 215 (2000).
333. D. Mercone, J. Thomson, R. H. Abu-Zied, I. W. Croudace, E. J. Rohling, *Marine Geology* 177, 25 (2001).

334. G. J. De Lange *et al.*, *Nature Geoscience*. 1 (2008).
335. D. Antoine, A. Morel, J.-M. Andre, *Journal of Geophysical Research* 100, 16 (1995).
336. P. Malanotte-Rizzoli *et al.*, *Dynamics of Atmospheric and Oceans* 29, 365 (1999).
337. N. Pinardi, E. Masetti, *Palaeogeography, Palaeoclimatology, Palaeoecology* 158, 153 (2000).
338. M. Rindsberger, M. Magaritz, I. Carmi, D. Gilad, *Geophysical Research Letters* 10, 43 (1983).
339. P. Braconnot *et al.*, *Climate of the Past* 3, (2007).
340. S. E. Calvert, B. Nielsen, M. R. Fontugne, *Nature* 359, 223 (1992).
341. M. Claussen, J. Fohlmeister, A. Ganopolski, V. Brovkin, *Geophysical Research Letters*. 33. (2006)
342. Y. Zhao *et al.*, *Climate Dynamics* 25, 777 (2005).
343. M. Fontugne *et al.*, in *Late Quaternary Chronology and Paleoclimate of the eastern Mediterranean,* O. Bar-Yosef, R. S. Kra, Eds. . 75–88 (1994).
344. S. E. Calvert, M. R. Fontugne, *Paleoceanography* 16, 78 (2001).
345. M. J. Rodwell, B. J. Hoskins, *Quarterly Journal of the Royal Meteorological Society* 122, 1385 (1996).
346. D. J. Brayshaw, C. M. R. Rambeau, S. Smith, The *Holocene*, (in press b).
347. E. J. Rohling, P. A. Mayewski, A. Hayes, R. H. Abu-Zied, J. S. L. Casford, *Climate Dynamics* 18, 587 (2002).
348. A. H. Osborne *et al.*, *Proceedings of the National Academy of Sciences* 105, 16444 (2008).
349. N. Kallel *et al.*, *Oceanologica Acta* 20, 697 (1997).
350. M. Bar-Matthews, A. A., K. A., *Geology* 169, 145 (2000).
351. N. Roberts *et al.*, *Quaternary Science Reviews* 1(2008).
352. D. J. Brayshaw, B. Hoskins, E. Black, *Phil Trans Roy Soc* (in press).
353. C. Bonfils, N. de Noblet-Ducoudre, J. Guiot, P. Bartlein, *Climate Dynamics* 23, (2004).
354. R. M. Gladstone *et al.*, *Geophysical Research Letters*. 32 (2005).
355. A. Bahra, F. Lamy, H. Arz, H. Kuhlmann, G. Wefer, *Marine Geology,* 214, 309 (2005).
356. A. E. Aksu, D. Yasar, P. J. Mudie, *Palaeogeography, Palaeoclimatology, Palaeoecology* 116, 71 (1995).
357. A. Asioli, *Mem. Ist. ital. Idrobiol.* , 55, 197 (1996).
358. G. Siani, M. Paterne, C. Colin, *Journal of Quaternary Science* 25, 808 (2010).
359. L. Sbaffi, F. C. Wezel, G. Curzi, U. Zoppi, *Global and Planetary Change* 40, 201 (2004).
360. E. J. Rohling, S. D. Rijk, *Marine Geology* 153, 57 (1999).
361. S. de Rijk, A. Hayes, E. J. Rohling, *Marine Geology* 153, 337 (1999).
362. P. G. Myers, E. J. Rohling, *Quat. Res* 55, 98 (2000).
363. E. J. Rohling, H. Palike, *Nature* 434, 975 (2005).
364. J. Frigola *et al.*, *Paleoceanography* 22, 1 (2007).
365. G. Marino *et al.*, *Quat. Sc. Rev.* 28, 3246 (2009).
366. M. Geraga, C. Ioakim, V. Lykousis, S. Tsaila-Monopolis, G. Mylona, *Palaeogeography, Palaeoclimatology, Palaeoecology* 287, 101 (2010).
367. A. Gogou *et al.*, *Palaeogeography, Palaeoclimatology, Palaeoecology* 256, 1 (2007).
368. T. Kuhnt, G. Schmiedl, W. Ehrmann, Y. Hamann, C. Hemleben, *Marine Micropaleontology* 64, 141 (2007).
369. S. Giunta *et al.*, *Palaeogeography, Palaeoclimatology, Palaeoecology* 190, 39 (2003).
370. F. Sangiorgi *et al.*, *Journal of Quaternary Science* 18, 723 (2003).
371. C. Peñalba, *Journal of Ecology* 82, 815 (1994).
372. C. Muñoz-Sobrino, P. Ramil-Rego, L. Gómez-Orellana, R. A. Díaz Varela, *Boreas* 34, 381 (2005).
373. J. S. Carrión, A. Andrade, K. D. Bennett, C. Navarro, M. Munuera, *The Holocene* 11, 635 (2001).
374. G. Jalut *et al.*, in *The Mediterranean Basin: The Last Two Climatic Extremes. Explanatory notes of the maps. Two maps, scale 1:5 000 000 N,* Petit-Maire, B. Vrielinck, Eds. 37-57 (2005).
375. D. Magri, I. Parra, *Earth and Planetary Science Letters* 200, 401 (2002).
376. W. Tinner *et al.*, *Quaternary Science Reviews* 28, 1498 (2009).
377. U. Kotthoff *et al.*, *The Holocene* 18, 1019 (2008).
378. U. Kotthoff *et al.*, *Quaternary Science Reviews* 27, 832 (2008).
379. H. F. Lamb *et al.*, *Nature* 373, 134 (1995).

380. H. F. Lamb, S. van der Kaars, *The Holocene* 5, 400 (1995).
381. R. Cheddadi, H. F. Lamb, J. Guiot, S. van der Kaars, *Climate Dynamics* 14, 883 (1998).
382. L. M. Kiage, K.-B. Liu, *Progress in Physical Geography* 30, 633 (2006).
383. M. Magny, J. Guiot, P. Schoellammer, *Quaternary Research* 56, 170 (2001).
384. W. Tinner, A. F. Lotter, *Geology* 29, 551 (2001).
385. P. Gonzalez-Samperiz *et al.*, *Quaternary Research* 71, 121 (2009).
386. A. N. LeGrande *et al.*, *Proceedings of the National Academy of Sciences* 103, 837 (2006).
387. A. P. Wiersma, H. Renssen, *Quaternary Science Reviews* 25, 63 (2006).
388. C. R. W. Ellison, M. R. Chapman, I. R. Hall, *Science* 312, 1929 (2006).
389. H. F. Kleiven *et al.*, *Science* 319, 60 (2008).
390. B. Hansen, S. Østerhus, *Progress in Oceanography* 45, 109 (2000).
391. B. Hansen, W. R. Turrell, S. Østerhus, *Nature* 411, 927 (2001).
392. S. Hunter *et al.*, *Deep-Sea Research I* 54, 2036 (2007).
393. P. A. Mayewski *et al.*, *Journal of Geophysical Research* 102, 26 (1997).
394. D. Fleitmann *et al.*, *Science* 300, 1737 (2003).
395. M. Vellinga, R. A. Wood, *Climatic Change* 54, 251 (2002).
396. D. Jacob *et al.*, in *Geophysical Research Letters*. 32 (2005).
397. D. J. Brayshaw, T. Woollings, M. Vellinga, *Journal of Climate* 22, 3146 (2009).
398. A. Theocharis, D. Georgopoulos, *Continental Shelf Research* 13, 919 (1993).
399. W. H. Roether *et al.*, *Science* 271, 333 (1996).
400. V. Zervakis, E. Krasakopoulou, D. Georgopoulos, E. Souvermezoglou, *Deep-Sea Res., I* 50, 53 (2003).
401. M. N. Tsimplis, S. A. Josey, *Geophys. Res. Lett.* 28, 803 (2001).
402. R. Copons, J. Bordonau, in *El Glaciarismo surpirenaico: nuevas aportaciones,* C. M. Bono, J. G. Ruíz, Eds. 111–124 (Geoforma Ediciones, Logroño, Spain, 1994).
403. M. B. Vallve, J. Martin-Vide, *Climatic Change* 38, 473 (1998).
404. F. Abrantes *et al.*, *Quaternary Science Reviews* 24, 2477 (2005).
405. F. Abrantes *et al.*, *Climate Research*, (in press).
406. N. J. Shackleton, M. A. Hall, E. Vincent, *Paleoceanography* 15, 565 (2000).
407. R. N. Drysdale, G. Zanchetta, J. C. Hellstrom, A. E. Fallick, J. X. Zhao, in *Geophysical Research Letters*. 32, L24708 (2005).
408. R. N. Drysdale *et al.*, *Science* 325, 1527 (2009).
409. J. Laskar *et al.*, *Astronomy and Astrophysics* 428, 261 (2004).
410. W. J. Fletcher, M. F. Sanchez Goñi, O. Peyron, I. Dormoy, *Clim. Past* 5, 203 (2010).
411. T. Rodrigues, J. O. Grimalt, F. Abrantes, F. Naughton, J.-A. Flores, *Quaternary Science Reviews* 29, 1853 (2010).
412. H. Hooghiemstra, H. Stalling, C. O. C. Agwu, L. M. Dupont, *Review of Palaeobotany and Palynology* 74, 1 (1992).
413. A.-M. Lézine, M. Denèfle, *Geology* 25, 119 (1997).
414. L. C. Skinner, H. Elderfield, *Paleoceanography* 22, (2007).
415. M. Vautravers, N. J. Shackleton, *Paleoceanography* 21, 1 (2006).
416. M. F. Sánchez-Goñi, A. Landais, I. Cacho, J. Duprat, L. Rossignol, *Geochemistry, Geophysics, Geosystems* 10 (2009).
417. A. H. L. Voelker, L. de Abreu, in *Abrupt Climate Change: Mechanisms, Patterns, and Impacts,* H. Rashid, V. Polyak, L. G. Thompson, Eds. (AGU, Washington, D.C., submitted).
418. L. Santos, M. F. Sanchez-Goni, *The Holocene* 13, 461 (2003).
419. L. Gómez-Orellana, P. Ramil-Rego, C. Muñoz Sobrino, *Quaternary Research* 67, 438 (2007).
420. C. Muñoz-Sobrino, P. Ramil-Rego, M. A. Rodríguez Guitián, *Vegetation History and Archaeobotany* 10, 7 (2001).
421. C. Muñoz-Sobrino, P. Ramil Rego, M. Rodríguez Guitián, *Vegetation History and Archaeobotany* 6, 215 (1997).
422. F. Marret, J.-L. Turon, *Marine Geology* 118, 107 (1994).

423. A. Moreno *et al.*, *Global and Planetary Change* 71, 218 (2010).
424. F. Florschütz, J. Menéndez Amor, T. A. Wijmstra, *Palaeogeography, Palaeoclimatology, Palaeoecology* 10, 233 (1971).
425. A. Pons, M. Reille, *Palaeogeography, Palaeoclimatology, Palaeoecology* 66, 243 (1988).
426. M. J. Gil-García, M. Dorado-Valiño, A. Valdeolmillos Rodríguez, M. B. Ruiz-Zapata, *Quaternary International* 93, 13 (2002).
427. J. S. Carrión, *Quaternary Science Reviews* 21, 2047 (2002).
428. J. S. Carrión, *Ecosistemas* 3, 13 (2003).
429. F. J. Jimenez-Espejo *et al.*, *Geochem. Geophys. Geosyst.* 9 (2008).
430. J. S. Carrión, M. Dupré, *New Phytologist* 134, 177 (1996).
431. J. S. Carrión, B. Van Geel, *Review of Palaeobotany and Palynology* 106, 209 (1999).
432. M. Reille, V. Andrieu, *Vegetation History and Archaeobotany* 4, 1 (1995).
433. D. Genty *et al.*, *Quaternary Science Reviews* 29, 2799 (2010).
434. M. Morellón *et al.*, *Quaternary Science Reviews* 28, 2582 (2009).
435. B. L. Valero-Garcés, E. Zeroual, K. Kelts, in *Paleohydrology and Environmental Change,* G. Benito, Ed. 67-80 (1998).
436. C. Beaudouin, G. Jouet, J.-P. Suc, S. Berné, G. Escarguel, *Quaternary Science Reviews* 26, 1037 (2007).
437. M. Reille, J. L. de Beaulieu, *Palaeogeography, Palaeoclimatology, Palaeoecology* 80, 35 (1990).
438. J. L. de Beaulieu, M. Reille, *Vegetation History and Archaeobotany* 1, 233 (1992).
439. C. Beaudouin *et al.*, *Marine and Petroleum Geology* 22 845 (2005).
440. H. Doose *et al.*, in *Proceedings ODP, Scientific Results,* R. Zahn, M. C. Comas, A. Klaus, Eds.161, 489-503 (Ocean Drilling Program, College Station, TX, 1999).
441. J. L. de Beaulieu, M. Reille, *Palaeogeography, Palaeoclimatology, Palaeoecology* 72, 147 (1989).
442. F. David, *Comptes rendus de l' Académie des Sciences Paris, Sciences de la vie / Life Sciences* 324, 373 (2001).
443. M. Reille, J. Gamisans, J.-L. de Beaulieu, V. Andrieu, *New Phytologist* 135, 547 (1997).
444. R. N. Drysdale *et al.*, *Earth and Planetary Science Letters* 227, 215 (2004/11/15, 2004).
445. I. Rouis-Zargouni *et al.*, *Palaeogeography Palaeoclimatology Palaeoecology* 285, 17 (2010).
446. D. Magri, L. Sadori, *Vegetation History and Archaeobotany* 8, 247 (1999).
447. G. Canali *et al.*, *Palaeogeography, Palaeoclimatology, Palaeoecology* 253, 300 (2007).
448. D. Ariztegui, C. Chondrogianni, A. Lami, P. Guilizzoni, E. Lafargue, *Journal of Paleolimnology* 26, 283 (2001).
449. M. Follieri, D. Magri, B. Narcisi, in *Lecture Notes in Earth Sciences Paleolimnology of European Maar Lakes,* F. W. Negendank, B. Zolitschka, Eds. 49. 95-107 (Springer-Verlag, Berlin 1993).
450. D. Magri, *Review of Palaeobotany and Palynology* 81, 313 (1994).
451. S. Frisia *et al.*, *Quaternary Research* 66, 388 (2006).
452. L. Sadori *et al.*, *Quaternary International* 225, (2010).
453. M. Rossignol-Strick, *Quaternary Science Reviews* 14, 893 (1995).
454. J. R. M. Allen, W. A. Watts, E. McGee, B. Huntley, *Quaternary International* 88, 69 (2002).
455. W. A. Watts, J. R. M. Allen, B. Huntley, *Quaternary Science Reviews* 15, 133 (1996).
456. W. A. Watts, J. R. M. Allen, B. Huntley, *Palaeogeography, Palaeoclimatology, and Palaeoecology* 155, 83 (2000).
457. S. Favaretto, A. Asioli, A. Miola, A. Piva, *Quaternary International* 190 89 (2008).
458. N. Combourieu-Nebout, M. Paterne, J.-L. Turon, G. Siani, *Quaternary Science Reviews* 17, 303 (1998).
459. M. Rossignol-Strick, N. Planchais, M. Paterne, D. Duzer, *Quaternary Science Reviews* 11, 415 (1992).
460. S. Giunta, K.-C. Emeis. DOI: 10.1594/PANGAEA.438366 (2006).
461. F. Sangiorgi *et al.*, *Paleoceanography*. 23 (2008).
462. L. Löwemark *et al.*, *Palaeogeography, Palaeoclimatology, Palaeoecology* 239, 406 (2006).
463. M. R. Frogley, P.C. Tzedakis, T.H.E. Heaton, *Science* 285, 1886 (1999).
464. P. C. Tzedakis, I. T. Lawson, M. R. Frogley, G. M. Hewitt, R. C. Preece, *Science* 297, 2044 (2002).
465. P. C. Tzedakis, *Philosophical Transactions of the Royal Society London* B 345, 403 (1994).

466. S. Bottema, *Palaeohistoria* 21, 20 (1979).
467. E. D. Bozilova, S. B. Tonkov, *New Phytologist* 148, 315 (2000).
468. P. C. Tzedakis, *Journal of the Geological Society* 156, 425 (1999).
469. S. Tonkov, G. Possnert, E. D. Bozilova, *Vegetation History and Archaeobotany* 16, 15 (2006).
470. B. Wohlfarth *et al.*, *Quaternary Science Reviews* 20, 1897 (2001).
471. L. Björkman, A. Feurdean, K. Cinthio, B. Wohlfarth, G. Possnert, *Quaternary Science Reviews* 21, 1039 (2002).
472. A. Feurdean, V. Mosbrugger, B. P. Onac, V. Polyak, D. Veres, *Quaternary Research* 68, 364 (2007).
473. A. Feurdean, , Stockholm University (2004).
474. J. Pross *et al.*, *Geology* 37, 887 (2010).
475. T. A. Wijmstra, *Acta Botanica Neerlandica* 18, 511 (1969).
476. I. Tantau, M. Reille, J.-L. de Beaulieu, S. Farcas, *Journal of Quaternary Sciences* 21, 49 (2006).
477. L. Vidal *et al.*, *Paleoceanography*. 25 (2010).
478. P. J. Mudie, A. Rochon, A. E. Aksu, *Marine Geology* 190, 233 (2002).
479. A. Vaks *et al.*, *Earth and Planetary Science Letters* 249, 384 (2006).
480. H. P. Affek, M. Bar-Matthews, A. Ayalon, A. Matthews, J. M. Eiler, *Geochimica et Cosmochimica Acta* 72, 5351 (2008).
481. A. Schramm, M. Stein, S. L. Goldstein, *Earth and Planetary Science Letters* 175, 27 (2000).
482. N. Waldmann, M. Stein, D. Ariztegui, A. Starinsky, *Quaternary Research* 72, 1 (2009).
483. A. Vaks *et al.*, *Quaternary Research* 59, 182 (2003/3, 2003).
484. J. Niklewski, W. van Zeist, *Acta Botanica Neerlandica* 19, 737 (1970).

LIST OF TABLES and FIGURES

records presented were linked for their respective age models. b) Foraminifera fauna based SST record of core MD95-2040 off northern Portugal[157]. c) Alkenone based SST record of core MD01-2444 of southwestern Portugal[168]. d) Foraminifera fauna based SST record of core MD99-2339 in the Gulf of Cadiz[200]. e) $\delta^{18}O$ record of planktonic foraminifera *G. ruber* white from core 9501 south off Cyprus[190] and June 21st insolation at 65°N (grey curve[409]). f) Speleothem $\delta^{18}O$ record from Sofular cave in northern Turkey[227]. Note that the speleothem's U/ Th chronology diverges from the GISP 2 chronology (a) for some of the Greenland interstadials (GI) and is more conform with the GICC05 chronology of the NGRIP ice core[165]. g) to j) Records from core MD95-2043 in the Alboran Sea: g) Alkenone based SST[186]; h) Ba_{excess} data indicating biogenic Ba and thus productivity[196]; i) Modelled Endmember (EM) 1 reflects the intensity of Saharan winds[229]; j) Sum of pollen representing the Temperate Mediterranean Forest[410], higher percentages of which indicate warmer and more humid conditions in southern Spain. k) Percentage of wooden taxa as recorded in Lago Grande di Monticchio in central Italy[210]. j) Mean Temperature of the Coldest month (MTCO) estimated from the pollen data of Lago Grande di Monticchio[210]. Grey bar marks the interval of Heinrich stadial (HS) 4, grey rectangle that of GI 8. Additional GI are listed in a) and f).

Figure 9 - Map showing sites covering MIS 3 and mean SST values (Table 1) for Heinrich Stadial 4 (top) and for Greenland Interstadial 8 (bottom).

Figure 10 - Evidence for Mediterranean deep water variability during the last 52 cal ky BP in comparison to a MOW record and depth changes in the boundary between NADW and AABW on the Portuguese margin. a) to c): Records of core MD99-2343 from 2391 m water depth with the UP10 grain size data in a), Si/ Al in b) –both of which reflect bottom current strength[202; 364]– and the benthic foraminifera $\delta^{13}C$ record in c) with higher $\delta^{13}C$ values reflecting a better ventilation and thus formation of WMDW in the Gulf of Lions[187]. d) to f) Conditions in the deep Alboran Sea, core MD95-2043 from 1841 m water depth with the benthic foraminifera $\delta^{13}C$ (d) and $\delta^{18}O$ (e) data and deep water temperatures (DWT) estimated from benthic foraminifera Mg/ Ca data in f)[201; 204]. On the Atlantic side, the mean grain size in the fraction <63µm measured in core MD99-2339 (g) shows changes in the bottom current strength, *i.e.* the lower MOW core[193]. In the deeper western Iberian margin the benthic foraminifera $\delta^{13}C$ record of core MD95-2042 (h[406]) reflects changes in the strength of the Atlantic Meridional Overturning Circulation (AMOC) with AABW ($\delta^{13}C < 0.5‰$) bathing the site's depth of 3146 m during colder climate intervals when AMOC was reduced, and NADW being present during warmer intervals when AMOC was strong.

Figure 11 – W-E transect of $U^{K'}_{37}$ -SST records from the Iberian margin to the eastern Mediterranean basins for the LGIT period (21 to 8 cal ka BP). On the left, in grey are plotted $d^{18}O$ record of the Greenland ice core GRIP (GICC05 age scale) and the insolation curve at 65ºN[302]. The SST records are organized from left (W) to right (E) and are numbered according to the site numbers in Table 1 and Fig. 4, original work is referenced in the main Table 1.

Figure 12 - Climate conditions in the Holocene Optimum period (9 ± 0.250 cal ka BP) for the Mediterranean region. SST estimated through Uk37 on marine cores. Qualitative information derived from pollen data in marine cores as well as other proxies from lakes, peat bogs, lagoons and speleothem records. Map legend as in figure 4. Original work referenced in Table 1.

Figure 13 - Climate conditions at 8.2 cal ka BP (± 0.250 cal ka BP) for the Mediterranean region. SST estimated through Uk37 on marine cores. Qualitative information derived from pollen data in marine cores as well as other proxies from lakes, peat bogs, lagoons and speleothem records. Map legend as in figure 4. Original work referenced in Table 1.

Site_ID	Site name	Latitude	Longitude	Elevation / Water depth	Archive Map	Archive type	Time-slice	References
1	MD03-2699	39.04	-10.67	-1895	Marine	Marine core	LGIT; HO; 8.2ka	*411*
2	M16004-1	29.83	-10.65	-1512	Marine	Marine core	MIS 5e; MIS 3	*412*
3	MD95-2039	40.57	-10.33	-3381	Marine	Marine core	MIS 3; LGIT	*218 ; 219*
4	SU 81-18	37.77	-10.21	-3135	Marine	Marine core	LGIT; HO; 8.2 ka	*130; 270*; *413*
5	MD95-2042	37.81	-10.15	-3146	Marine	Marine core	MIS 5e; MIS 3; LGIT; HO; 8.2 ka	*122; 125; 157; 166; 198; 215; 216; 406*
6	MD01-2444	37.57	-10.13	-2656	Marine	Marine core	MIS 5e; MIS 3; LGIT; HO; 8.2ka	*168*; *414; 415*; *223*
7	SU92-03	43.20	-10.11	-3005	Marine	Marine core	MIS 5e; MIS 3	*157*
8	8057B	37.68	-10.08	-2811	Marine	Marine core	LGIT; 8.2ka	*412*
9	MD95-2040	40.58	-9.86	-2465	Marine	Marine core	MIS 5e; MIS 3	*157*
10	MD03-2697	42.17	-9.70	-2164	Marine	Marine core	LGIT; HO; 8.2ka	*220; 293*
11	MD99-2331	42.15	-9.69	-2110	Marine	Marine core	MIS 5e; MIS 3; LGIT	*122; 191 ; 217 ;220; 416*
12	MD95-2041	37.83	-9.52	-1123	Marine	Marine core	MIS 3	*417*
13	SO75-6KL	37.94	-9.51	-1281	Marine	Marine core	LGIT	*268*
14	D13882	38.63	-9.45	-88	Marine	Marine core	LGIT; HO; 8.2ka	*311*
15	Santo Andre lagoon	38.08	-8.78	2.7	Continental	Lagoon core	HO	*418*
16	M39029-7	36.04	-8.23	-1917	Marine	Marine core	MIS 3	*197*
17	M15669-1	34.88	-7.82	-2030	Marine	Marine core	MIS 3	*412*
18	MD99-2339	35.88	-7.53	-1170	Marine	Marine core	MIS 3	*193; 199; 200*
19	Guadiana basin	37.27	-7.45	0	Continental	Estuary core	LGIT; HO; 8.2ka	*221*
20	Area longa	43.60	-7.30	0	Continental	Terrestrial core	MIS 3	*419*
21	Lagoa de Lucenza	42.58	-7.12	1375	Continental	Terrestrial core	LGIT	*420*
22	Pozo do Carballal	42.71	-7.11	1330	Continental	Lake core	LGIT	*421*
23	MD99-2341+ GeoB5901	36.38	-7.07	-574	Marine	Marine core	HO; 8.2ka	*205*; *300*
24	M39008	36.37	-7.07	-576	Marine	Marine core	LGIT; HO; 8.2ka	*310*
25	KS 78007	34.32	-7.02	-700	Marine	Marine core	LGIT; HO	*422*
26	Suárbol	42.86	-6.85	1080	Continental	Peatbog core	LGIT	*421*
27	Laguna de la Roya	42.22	-6.77	1608	Continental	Lake core	LGIT; HO	*285*
28	Lleguna	42.12	-6.77	1050	Continental	peatbog core	LGIT	*287*
29	Tigalmamine	32.90	-5.35	1626	Continental	Lake core	HO; 8.2ka	*281*; *379; 380; 381*

30	MD04-2845	45.35	-5.22	-4100	Marine	Marine core	MIS 5e; MIS 3	*217*
31	El Pindar	43.38	-4.50		Speleothem	Speleothem	HO; 8.2ka	*423*
32	ODP Site 976	36.20	-4.30	-1108	Marine	Marine core	MIS 3; LGIT; HO; 8.2ka	*269; 275; 276*
33	TG-5	36.38	-4.25	-626	Marine	Marine core	HO; 8.2ka	*260*
34	Enol	43.18	-4.15		Continental	Lake / Peatbog core	HO; 8.2ka	*423*
35	Fuentillejo maar	38.93	-4.05		Continental	Lake core	HO; 8.2ka	(Vegas et al., in prep.)
36	Padul	37.00	-3.67	785	Continental	Lake core	LGIT; HO	*424*; *425*
37	Puerto de los tornos	43.15	-3.43	920	Continental	Peatbog core	8.2ka	*371*; *372*
38	KS8231	36.15	-3.27	-865	Marine	Marine core	HO; 8.2ka	*260*
39	Quintanar de la sierra	42.03	-3.02	1470	Continental	Marshland core	LGIT	*286*
40	Hoyos de Iregua	42.02	-2.75	1780	Continental	Lake core	LGIT; HO	*426*
41	MD95-2043	36.14	-2.62	-1841	Marine	Marine core	MIS 3; LGIT; HO; 8.2ka	*186*; *196; 201; 204; 216; 222; 228; 229*; *310*; *410; 416*
42	Siles lake	38.40	-2.50	1320	Continental	Lake core	LGIT	*427*
43	Villaverde	38.80	-2.37	900	Continental	Lake core	HO; 8.2ka	*373 ;374 ; 427*; *428; 306*
44	ODP Site 977A	36.03	-1.96	-1984	Marine	Marine core	MIS 5e; MIS 3; LGIT; HO; 8.2ka	*158*
45	TTR14-300G	36.36	-1.79	-1860	Marine	Marine core	HO; 8.2ka	*429*
46	Navarres peatbog	39.10	-0.68	225	Continental	Peatbog core	LGIT	*430*; *431*
47	El Portalet	42.80	-0.38	1802	Continental	Peatbog core	LGIT; HO; 8.2ka	*290; 319; 322; 385*
48	Biscaye	43.03	-0.07	410	Continental	Lake core	LGIT	*432*
49	Villars Cave, France	45.30	0.50		Speleothem	Speleothem	MIS 3	*226; 433*
50	Estanya	42.03	0.53		Continental	Lake core	HO; 8.2ka	*434*
51	Balcére	42.59	2.06	1764	Continental	Lake core	LGIT	*284*
52	La Borde	42.53	2.08	1660	Continental	Peatbog core	LGIT	*284*
53	Gourg Negre	42.63	2.22	2080	Continental	Peatbog core	LGIT	*284*
54	Lago de Banyoles	42.12	2.75	173	Continental	Lake core	MIS 3; LGIT; HO; 8.2ka	*321*; *435*
55	MD99-2349	42.82	3.73	-126	Marine	Marine core	LGIT	*436*
56	Lac du Bouchet	44.92	3.78	1200	Continental	Lake core	MIS 5e; MIS 3; LGIT	*173 ; 274*; *279*; *437*
57	Ribains/Landos/Velay 1	44.84	3.82	1080	Continental	Lake core	MIS 5e; LGIT	*274*; *279*; *438*
58	borehole PRGL1	42.69	3.84	-300	Marine	Marine core	MIS 5e; MIS 3	*128*
59	MD99-2348	42.70	3.85	-296	Marine	Marine core	LGIT	*128; 439*

60	M40/4-87SL	38.99	4.02	-1900	Marine	Marine core	MIS 5e	*149*; *133*
61	MD99-2343	40.50	4.03	-2391	Marine	Marine core	MIS 3; HO; 8.2ka	*187*; *202; 364*
62	MD99-2346	42.04	4.15	-2100	Marine	Marine core	HO; 8.2ka	*323*
63	MD99-2352	43.32	4.17	-70	Marine	Marine core	LGIT	*436*
64	ODP Site 975B	38.90	4.51	-2416	Marine	Marine core	MIS 5e; HO; 8.2ka	*261*; *429*; *440*
65	les Echets	45.81	4.92	267	Continental	Lake core	MIS 5e; MIS 3	*225 ; 274*; *441*
66	Lake Lautrey	46.59	5.86	788	Continental	Lake core	LGIT	*291*
67	Lac d'Annecy	45.80	6.13	445	Continental	Lake core	LGIT	*442*
68	Ételles	45.47	6.15	700	Continental	Lake core	LGIT	*442*
69	Le Locle	47.05	6.72	915	Continental	Lake core	LGIT; 8.2ka	*383*
70	Soppensee	47.09	8.08	596	Continental	Lake core	8.2ka	*384*
71	Lac de Creno	42.20	8.95	1310	Continental	Lake core	LGIT	443
72	MD01-2434	42.37	9.79	-800	Marine	Marine core	MIS 3	*203*
73	LC07	38.15	10.08	-488	Marine	Marine core	MIS 5e	*156*
74	Antro del Corchia	43.98	10.13	840	Speleothem	Speleothem	MIS 5e	*407 ; 408 ; 444*
75	MD04-2797	36.95	11.67	-771	Marine	Marine core	LGIT; HO; 8.2ka	*247*; *445*
76	Lagaccione	42.57	11.85	355	Continental	Lake core	MIS 3; LGIT	*207*
77	Lago di Vico	42.33	12.27	507	Continental	Lake core	MIS 3; LGIT; 8.2ka	*207*; *208*; *375; 446*
78	Lagoon of Venice	45.52	12.53	-2	Continental	Lagoon	MIS 3; LGIT	*447*
79	Azzano Decimo core	45.88	12.65	9.9	Continental	Terrestrial	MIS 3	*231*
80	Lake Gorgo Basso	37.62	12.65	6	Continental	Lake core	HO; 8.2ka	*376*
81	Albano	41.72	12.67		Continental	Lake core	HO; 8.2ka	*448*
82	Valle di Castiglione	41.89	12.76	44	Continental	Lake core	MIS 5e; MIS 3; LGIT	*449; 174*; *280*; *450*
83	Grotta di Carburangeli	38.17	13.16	22	Speleothem	Speleothem	HO; 8.2ka	*451*
84	ODP Site 963A + 963D	37.03	13.18	-470	Marine	Marine core	MIS 5e; HO; 8.2ka	*156*; *163*
85	BS79-38	38.41	13.58	-1489	Marine	Marine core	LGIT; HO; 8.2ka	*310*
86	BS79-33	38.26	14.03	-1282	Marine	Marine core	LGIT; HO; 8.2ka	*310*
87	Lago di Pergusa	37.52	14.30	674	Continental	Lake core	LGIT; HO	*452*
88	KET80-03	38.82	14.48	-1900	Marine	Marine core	MIS 3; LGIT	*188*; *282; 453*
89	CM92-43	42.88	14.72	-252	Marine	Marine core	8.2ka	*332*; *236*
90	PRAD1-2	42.68	14.77	-185.5	Marine	Marine core	MIS 5e; LGIT; HO; 8.2ka	*169*
91	Lago Grande di Monticchio	40.94	15.61	656	Continental	Lake core	MIS 5e; MIS 3	*161; 209*; *210*; *454*; *455*; *456*
92	SA03-1	41.50	17.18	-567	Marine	Marine core	LGIT	*457*

93	MD90-917	41.28	17.62	-1010	Marine	Marine core	LGIT	*358*; *458*
94	M25_4-KL11	36.75	17.72	-3376	Marine	Marine core	LGIT; HO; 8.2ka	*248*
95	KC01	36.25	17.74	-3640	Marine	Marine core	MIS 5e; HO; 8.2ka	*440*
96	IN68-9	41.80	17.92	-1234	Marine	Marine core	HO; 8.2ka	*361*
97	KET 8216	41.52	17.98	-1166	Marine	Marine core	LGIT; HO	*453; 459*
98	KS205	38.20	18.14	-2384	Marine	Marine core	MIS 5e	*143*
99	AD91-17	40.87	18.64	-844	Marine	Marine core	LGIT; HO; 8.2ka	*460*; *370*; *461*
100	M40/1-10	34.76	19.76	-2972	Marine	Marine core	HO; 8.2ka	*462*
101	BAN 84 09 GC	34.32	20.02	-3405	Marine	Marine core	LGIT; HO	*283*; *453*
102	Ioannina I	39.75	20.72	470	Continental	Lake core	LGIT	*294*
103	K6 lake maliq	40.77	20.78	-818	Continental	Lake core	LGIT; 8.2ka	*289*
104	Ioannina 284	39.75	20.85	319	Continental	Lake core	MIS 5e; MIS 3; LGIT	*463*; *464*; *273*
105	Ioannina 249	39.65	20.92	470	Continental	Lake core	MIS 5e	*465*
106	Lake Xinias	39.05	22.27	500	Continental	Lake core	MIS 3	466
107	Lake Sedmo Rilsko	41.88	23.02	2925	Continental	Lake core	LGIT; HO	*467*
108	Kopais	38.43	23.05	95	Continental	Lake core	MIS 3; MIS 5e	*468*
109	M40/ 4-71SL	34.81	23.19	-2827	Continental	Lake core	MIS 5e	*133*; *149*
110	Trilistnika lake	42.20	23.32	2216	Continental	Lake core	LGIT	*469*
111	Lake Kremensko-5	41.72	23.53	2124	Continental	Lake core	LGIT	*288*
112	Preluca Tiganului	47.81	23.53	730	Continental	Lake core	LGIT	*470*; *471*; *472*
113	Steregoiu	47.81	23.54	790	Continental	Lake core	LGIT	*472*; *473*
114	C69	36.55	24.21	-632	Marine	Marine core	MIS 3; LGIT; HO; 8.2ka	*189*
115	Tenaghi Philippon 2	40.97	24.22	40	Continental	Lake core	8.2ka	*474*
116	Tenaghi Philippon 1	41.17	24.33	40	Continental	Lake core	MIS 5e; MIS 3; LGIT	*120; 160; 175; 475*
117	AVRIG	45.72	24.38	400	Continental	Lake core	LGIT	*472*; *476*
118	GeoTü SL152	40.09	24.61	-978	Marine	Marine core	LGIT; 8.2ka	*377; 378*
119	ODP Site 971A	33.72	24.68	-2026	Marine	Marine core	MIS 5e	*135*; *143; 151*; *142*
120	M40/1-22	33.66	24.69	-2004	Marine	Marine core	HO; 8.2ka	*462*
121	ODP Site 969E	33.84	24.88	-2212	Marine	Marine core	MIS 5e	*133*; *149*
122	MNB3	39.15	25.00	-800	Marine	Marine core	LGIT; 8.2ka	*366*; *367*
123	Megali Limni basin	39.10	26.33	323	Continental	Lake core	MIS 3	*213*
124	LC21	35.67	26.58	-1522	Marine	Marine core	HO; 8.2ka, MIS 5e	*135*; *142*; *150; 361*
125	M40/4-67SL	34.81	27.30	-2158	Marine	Marine core	MIS 5e	*133*; *134*; *149*

126	MD01-2430	40.80	27.73	-580	Marine	Marine core	LGIT; HO	*477*
127	M44-1-KL71	40.84	27.76	-566	Marine	Marine core	HO; 8.2ka	*250*
128	MAR97-11	40.70	28.40	-111	Marine	Marine core	LGIT	*478*
129	Söğüt	37.05	29.88	1383	Continental	Lake core	LGIT	*294*
130	Abant	40.60	31.30	1375	Continental	Lake core	LGIT	*294*
131	Beyşehir	37.53	31.50	1120	Continental	Lake core	LGIT	*294*
132	Sofular Cave	41.42	31.93	700	Speleothem	Speleothem	MIS 3; HO	*227*
133	Yeniçağa	40.43	32.00	980	Continental	Lake core	LGIT	*294*
134	MD84642	32.67	32.57	-1260	Marine	Marine core	MIS 5e	*140*
135	KC20B	33.68	32.71	-882	Marine	Marine core	MIS 5e	*440*
136	ODP Site 967C	34.07	32.73	-2550	Marine	Marine core	MIS 5e; LGIT; HO; 8.2ka	*112*; *141; 143; 149; 151*; *248*
137	Akğöl Konya	37.50	33.73	1000	Continental	Lake core	LGIT	*294*
138	MD84627	32.22	33.75	-1185	Marine	Marine core	8.2ka	*140*
139	9501	34.53	33.98	-980	Marine	Marine core	MIS 3	*190*
140	GeoB7702-3	31.65	34.07	-562	Marine	Marine core	LGIT; HO; 8.2ka	*312*
141	GeoTü KL83	32.62	34.15	-1433	Marine	Marine core	MIS 5e	*133*; *134*
142	9509	32.02	34.27	-884	Marine	Marine core	MIS 3	*190*
143	MD84629	32.07	34.35	-745	Marine	Marine core	8.2ka	*140*
144	MD84632	32.78	34.37	-1425	Marine	Marine core	LGIT; HO; 8.2ka	*247*
145	GeoB5844-2	27.71	34.68	-963	Marine	Marine core	LGIT; HO; 8.2ka	*249*
146	Soreq Cave	31.45	35.03	400	Speleothem	Speleothem	MIS 5e; MIS 3; HO; 8.2ka	*145; 146; 479*; *480*
147	Jerusalem West Cave	31.78	35.15	700	Speleothem	Speleothem	MIS 5e	*147; 148*
148	Peqiin Cave	32.58	35.19	650	Speleothem	Speleothem	MIS 5e; MIS 3	*146*
149	Lake Lisan	31.21	35.31	410	Continental	Lake core	MIS 3; HO	*144; 224*; *251*; *481; 482*
150	Ma' ale Efrayim cave, Israel	32.00	35.50	250	Speleothem	Speleothem	MIS 3	*483*
151	Hula	33.17	35.58	300	Continental	Lake core	LGIT	*294*
152	Lâdik	40.92	36.02	800	Continental	Lake core	LGIT	*294*
153	Ghab	35.68	36.30	300	Continental	Lake core	LGIT; MIS 3	*294*; *484*
154	Dziguta River	43.02	41.02	120	Continental	River core	MIS 3; LGIT	*212*

Table 2 – Mean and standard deviation of the existing U37k' SST values for the Mediterranean Sea as a whole and its three main basins (western, central and eastern), at the time of the Holocene Optimum (HO) and the "8.2 event" as reported in figures 11 and 12. References for the original data on Table 1.

	SST HO	SST 8.2	ΔSST (HO-8.2)
WESTERN (9 sites W)			
Mean	19.2	18.8	0.4
StD	1.1	0.8	
CENTRAL (7 sites C)			
Mean	18.3	17.8	0.6
StD	1.9	1.5	
EAST (5 sites E)			
Mean	19.8	18.6	1.3
StD	1.2	1.4	
TOTAL (21 sites W-E)			
Mean	19.1	18.4	0.7
StD	1.4	1.2	

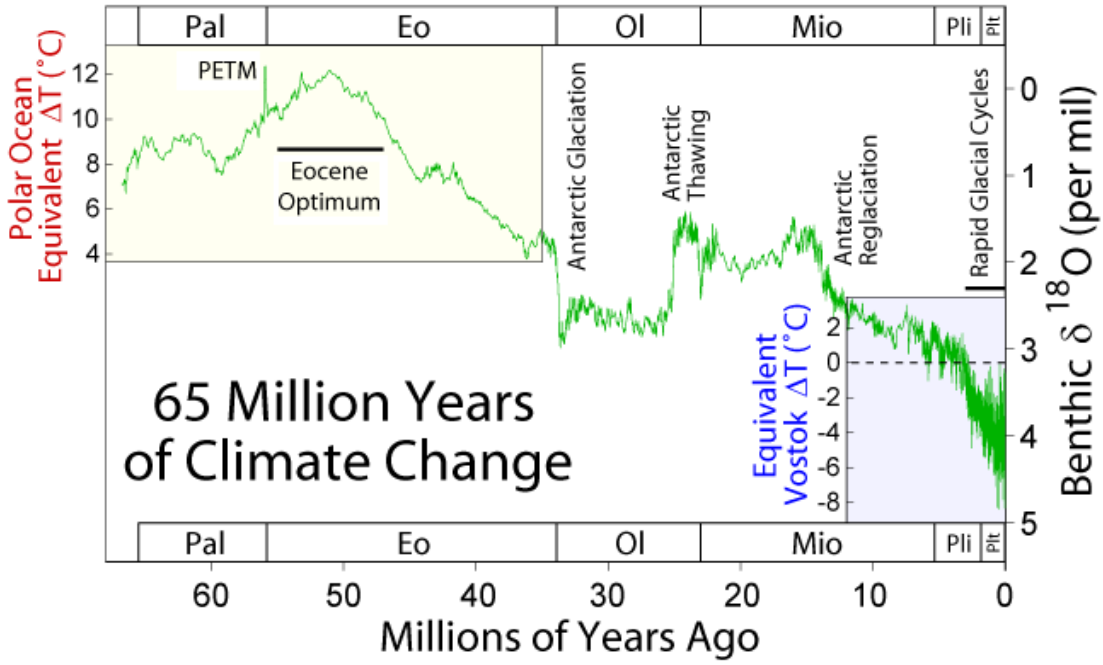

Figure 1 – Climate change between 65 million years ago and the Present (0) (after Zachos et al., 2001). The climate curve is the mean running line of all the existing deep-sea benthic foraminifer oxygen-isotope ($\delta^{18}O$) records from Deep Sea Drilling Project and Ocean Drilling Program sites. Benthic foraminifer $\delta^{18}O$ represents a combination of the temperature changes in this organisms' local living environment and changes in the isotopic composition of sea-water derived by the growth and retreat of continental ice sheets. The $\delta^{18}O$ temperature anomaly on the left axis (in red) was computed on the assumption of an ice-free ocean, reason why it applies only to the time preceding the onset of large-scale glaciation on Antarctica (about 35 million years ago). The $\delta^{18}O$ temperature anomaly for the most recent data (in blue) was computed considering the tight correlation between the oxygen isotope measurements of Lisiecki and Raymo (2005) and the temperature changes at the Vostok ice core established by Petit et al. (1999).

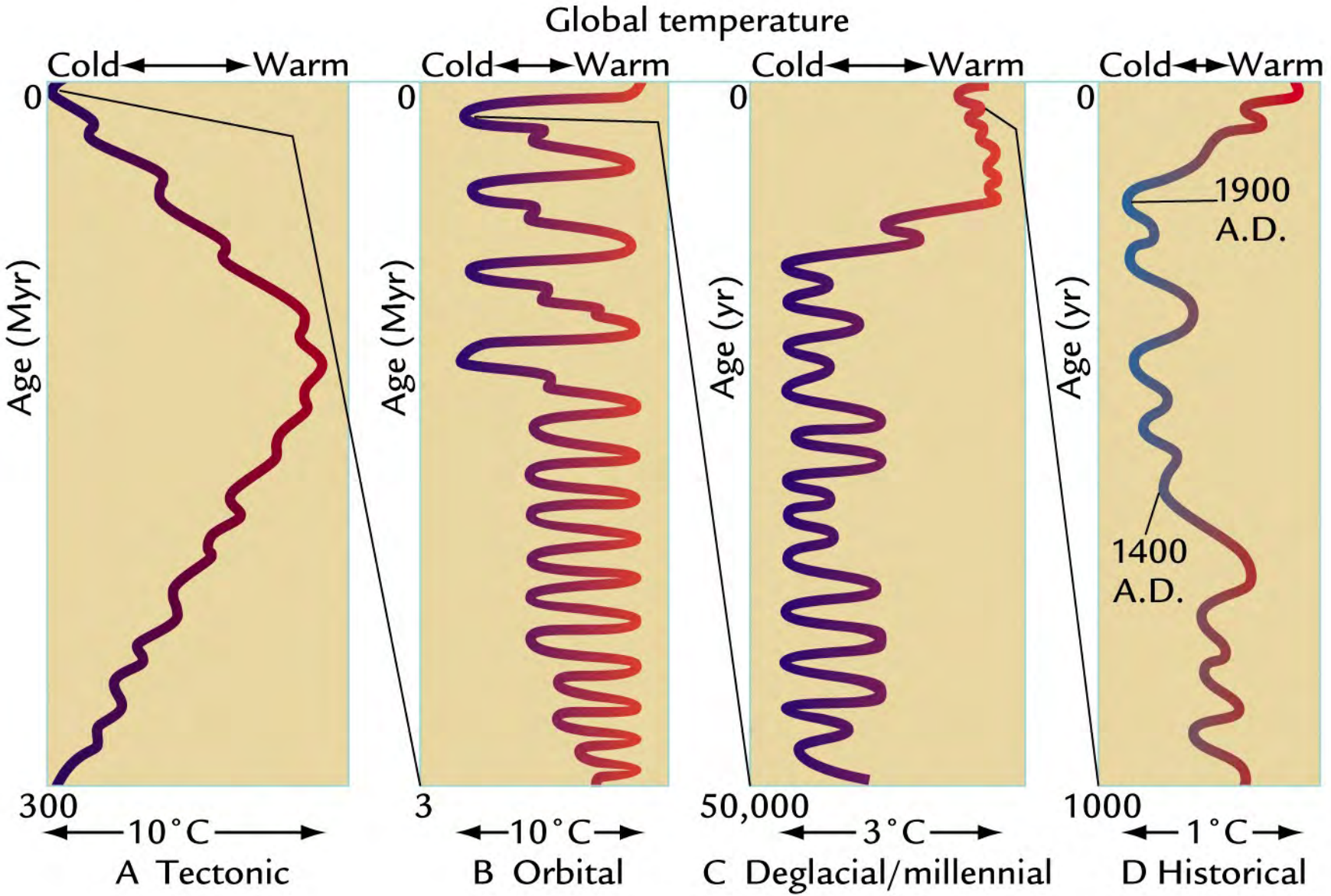
Global temperature
Cold
Warm
0
Age (Myr)
300
10°C
A Tectonic
Cold
Warm
0
Age (Myr)
3
10°C
B Orbital
Cold
Warm
0
Age (yr)
50,000
3°C
C Deglacial/millennial
Cold
Warm
0
Age (yr)
1900
A.D.
1400
A.D.
1000
1°C
D Historical

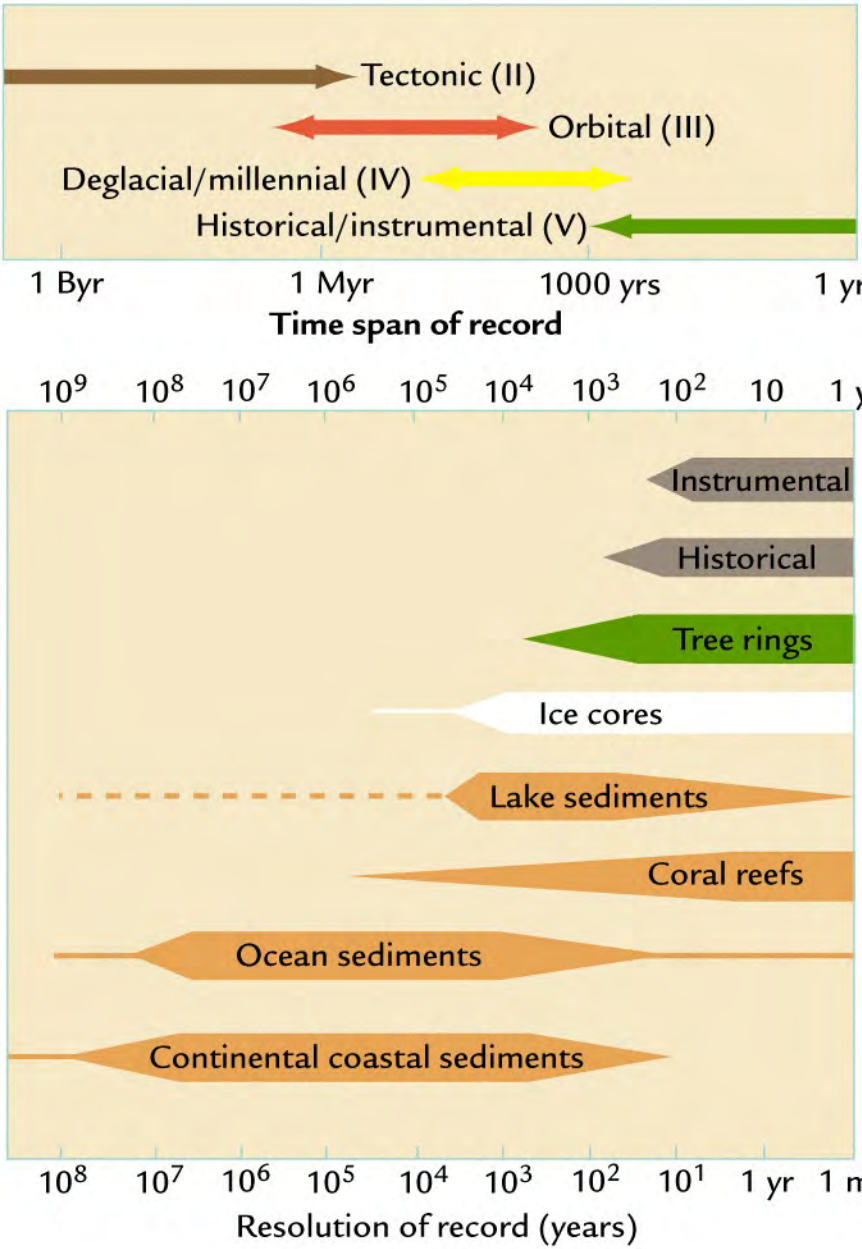
Tectonic (II)
Orbital (III)
Deglacial/millennial (IV)
Historical/instrumental (V)
1 Byr
1 Myr
1000 yrs
1 yr
Time span of record
10^9 10^8 10^7 10^6 10^5 10^4 10^3 10^2 10 1 yr
Instrumental
Historical
Tree rings
Ice cores
Lake sediments
Coral reefs
Ocean sediments
Continental coastal sediments
10^8 10^7 10^6 10^5 10^4 10^3 10^2 10^1 1 yr 1 mo
Resolution of record (years)

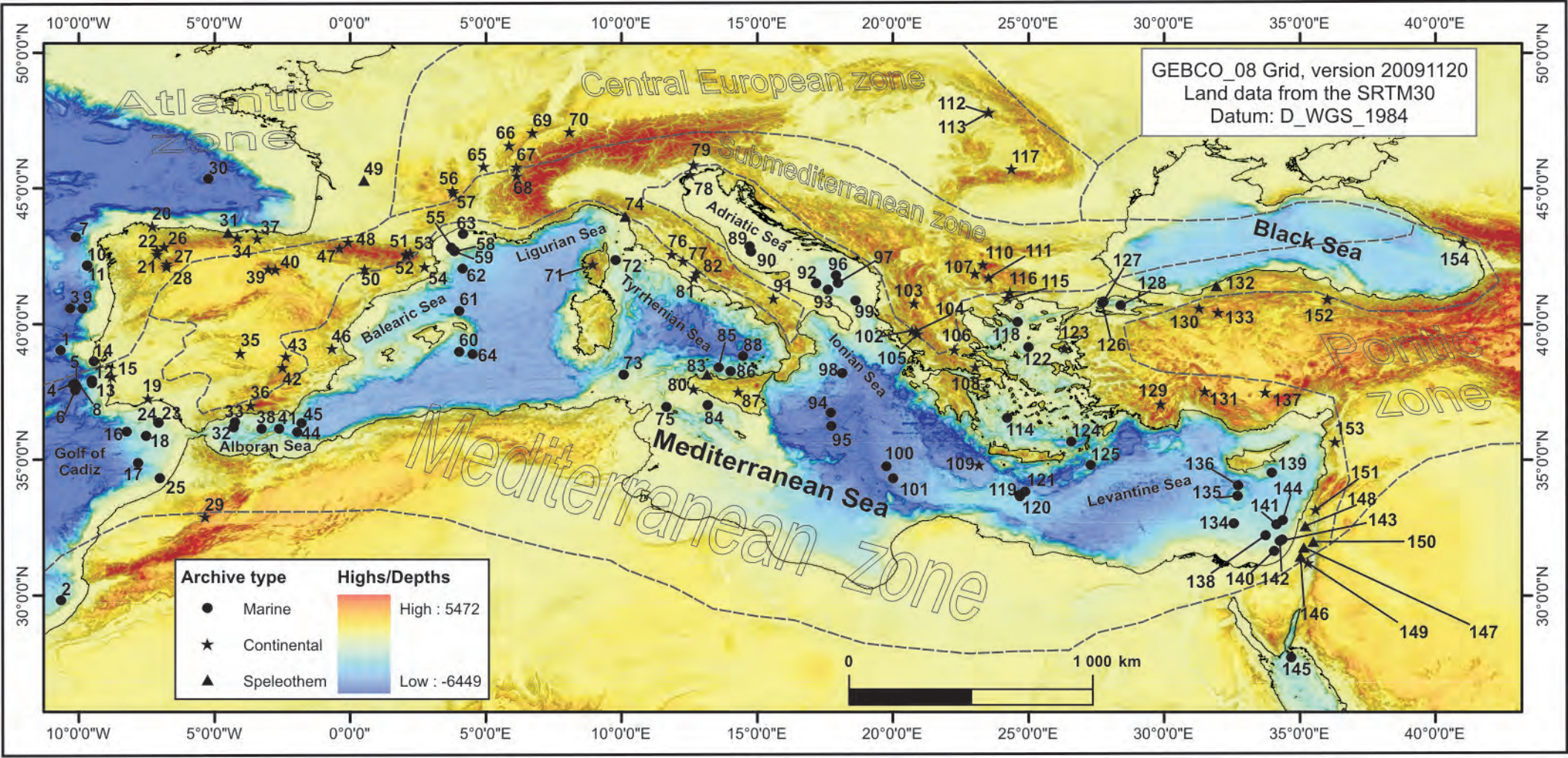
GEBCO_08 Grid, version 20091120
Land data from the SRTM30
Datum: D_WGS_1984
Atlantic zone
Central European zone
Submediterranean zone
Pontic zone
Mediterranean zone
Mediterranean Sea
Black Sea
Golf of Cadiz
Alboran Sea
Balearic Sea
Ligurian Sea
Tyrrhenian Sea
Adriatic Sea
Ionian Sea
Levantine Sea
Archive type
Marine
Continental
Speleothem
Highs/Depths
High : 5472
Low : -6449
0
1 000 km
10°0'0"W
5°0'0"W
0°0'0"
5°0'0"E
10°0'0"E
15°0'0"E
20°0'0"E
25°0'0"E
30°0'0"E
35°0'0"E
40°0'0"E
50°0'0"N
45°0'0"N
40°0'0"N
35°0'0"N
30°0'0"N

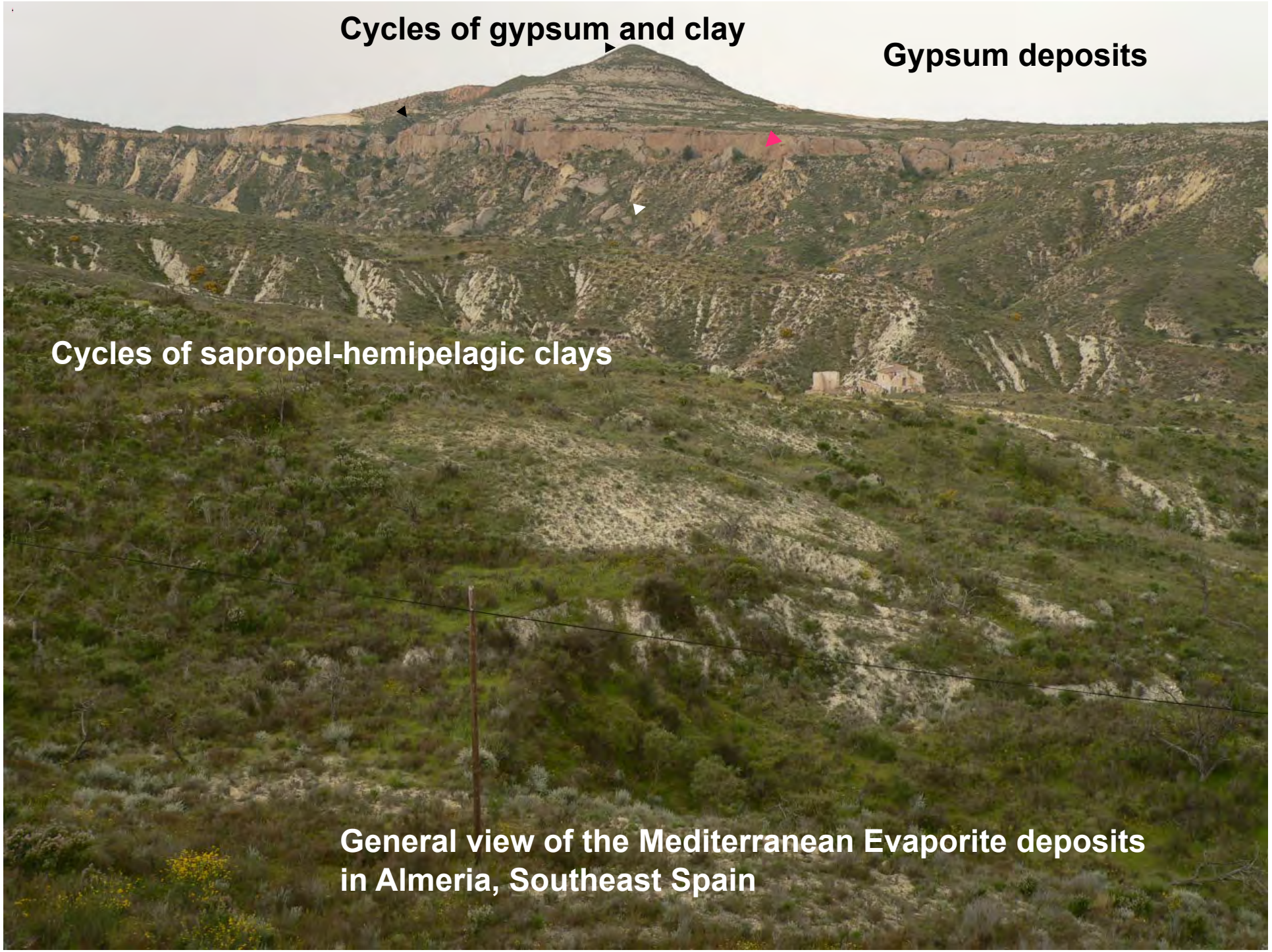
Cycles of gypsum and clay
Gypsum deposits
Cycles of sapropel-hemipelagic clays
General view of the Mediterranean Evaporite deposits
in Almeria, Southeast Spain

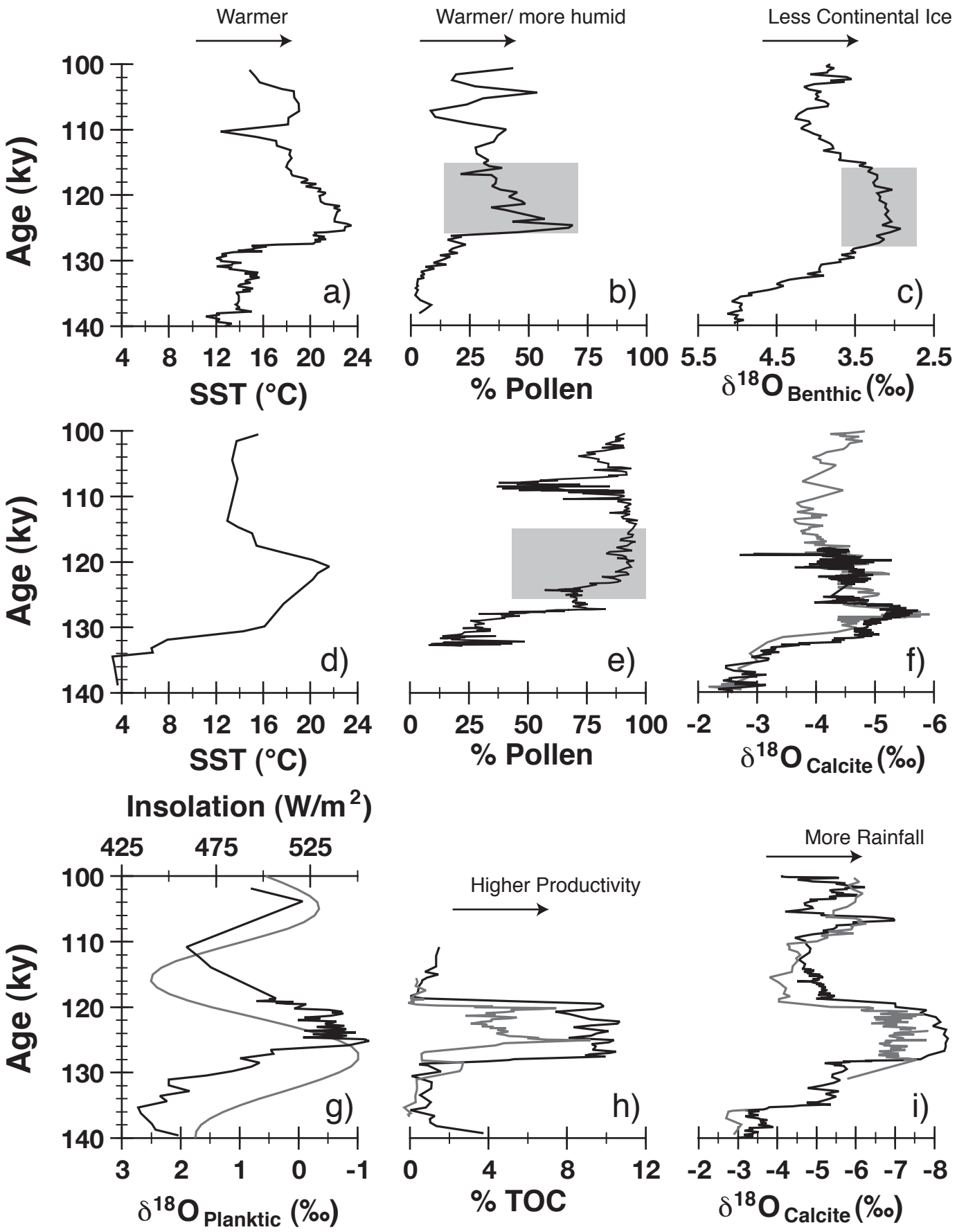
Warmer
Warmer/ more humid
Less Continental Ice
Age (ky)
100
110
120
130
140
a)
b)
c)
4 8 12 16 20 24
SST (°C)
0 25 50 75 100
% Pollen
5.5 4.5 3.5 2.5
δ18O Benthic (‰)
d)
e)
f)
-2 -3 -4 -5 -6
δ18O Calcite (‰)
Insolation (W/m2)
425 475 525
Higher Productivity
More Rainfall
g)
h)
i)
3 2 1 0 -1
δ18O Planktic (‰)
0 4 8 12
% TOC
-2 -3 -4 -5 -6 -7 -8
δ18O Calcite (‰)

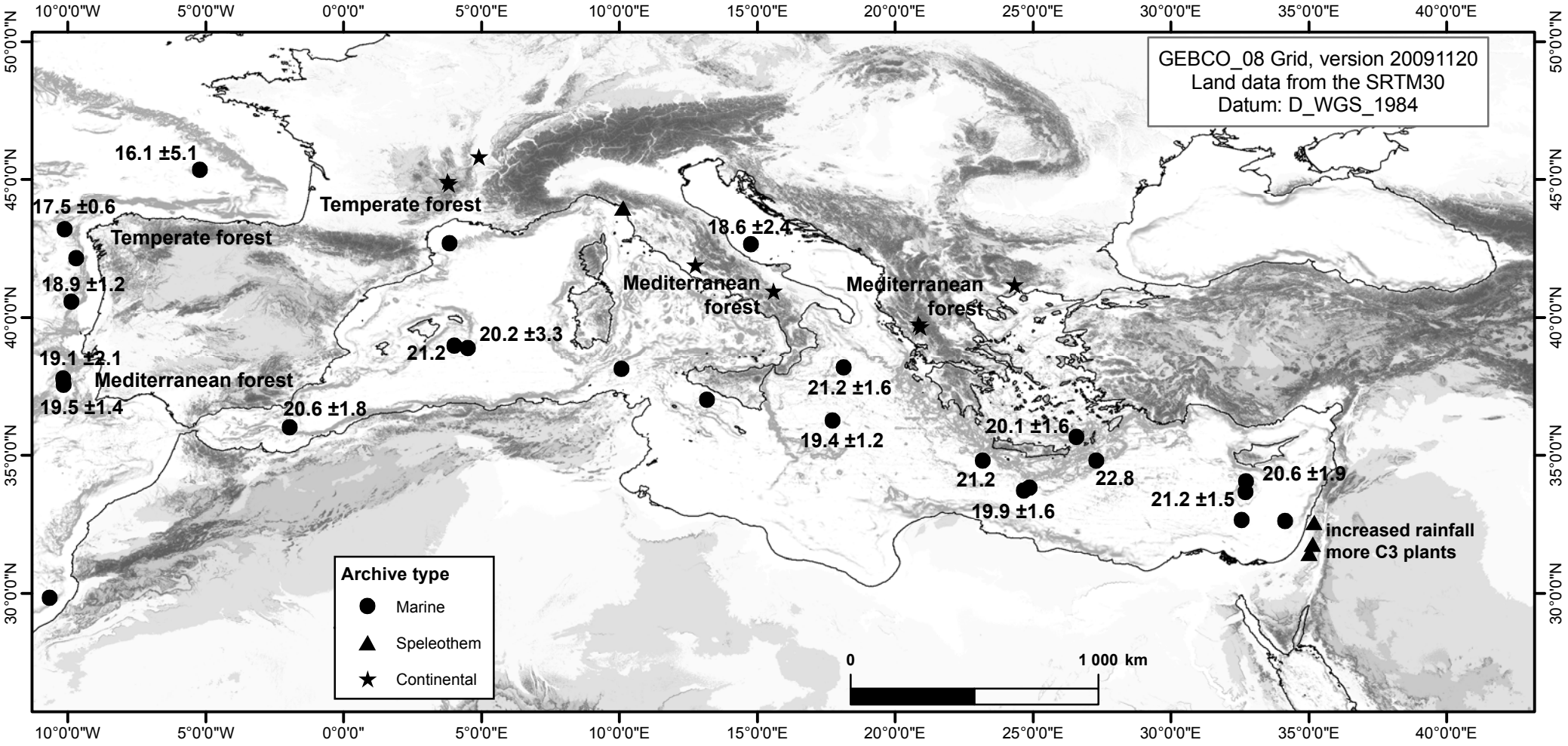
GEBCO_08 Grid, version 20091120
Land data from the SRTM30
Datum: D_WGS_1984
16.1 ±5.1
17.5 ±0.6
Temperate forest
Temperate forest
18.9 ±1.2
19.1 ±2.1
Mediterranean forest
19.5 ±1.4
20.6 ±1.8
21.2
20.2 ±3.3
18.6 ±2.4
Mediterranean forest
Mediterranean forest
21.2 ±1.6
19.4 ±1.2
20.1 ±1.6
21.2
22.8
19.9 ±1.6
21.2 ±1.5
20.6 ±1.9
increased rainfall
more C3 plants
Archive type
Marine
Speleothem
Continental
0
1 000 km
10°0'0"W
5°0'0"W
0°0'0"
5°0'0"E
10°0'0"E
15°0'0"E
20°0'0"E
25°0'0"E
30°0'0"E
35°0'0"E
40°0'0"E
50°0'0"N
45°0'0"N
40°0'0"N
35°0'0"N
30°0'0"N

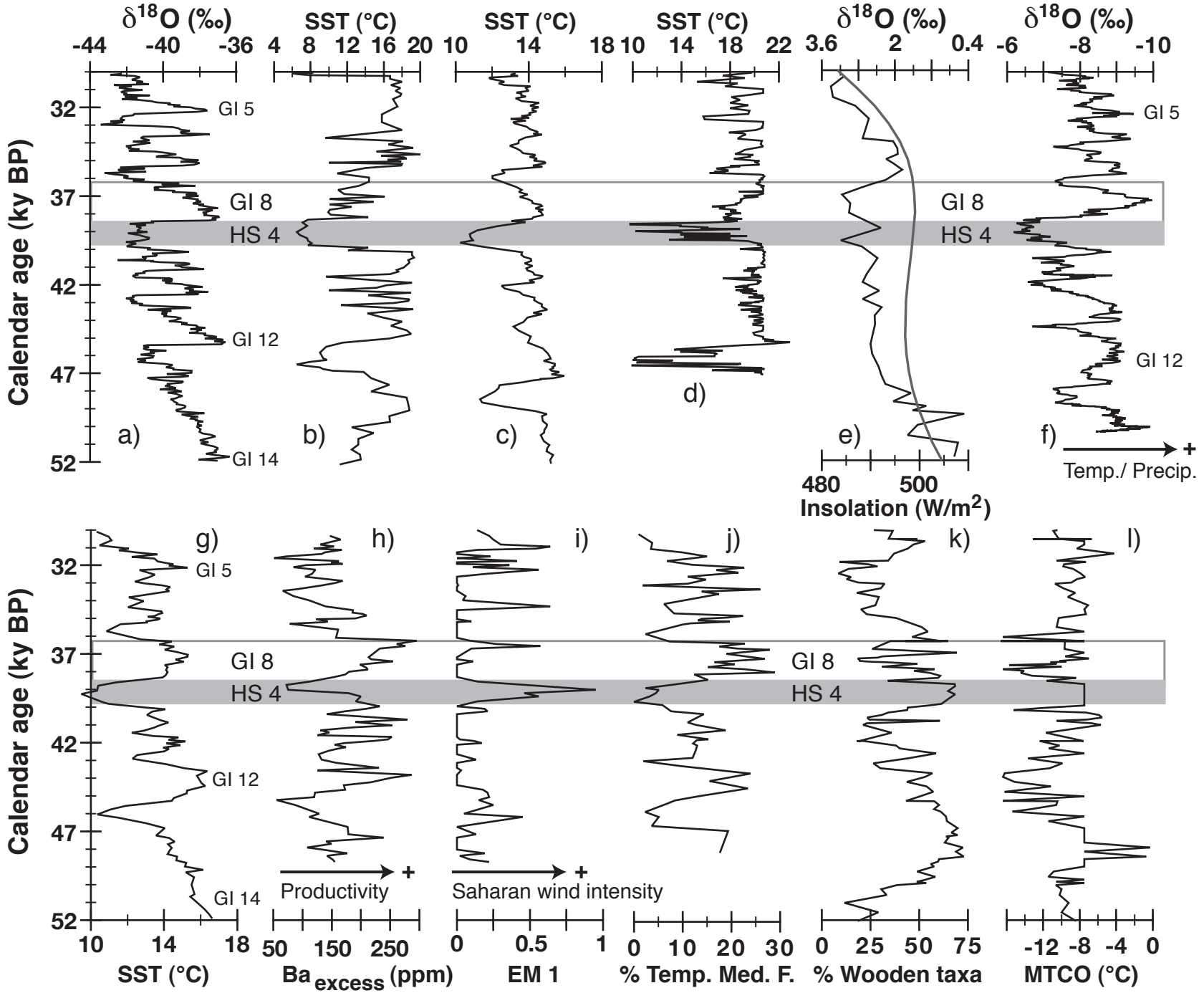
δ18O (‰)
-44 -40 -36
SST (°C)
4 8 12 16 20
SST (°C)
10 14 18
SST (°C)
10 14 18 22
δ18O (‰)
3.6 2 0.4
δ18O (‰)
-6 -8 -10
Calendar age (ky BP)
32
37
42
47
52
GI 5
GI 8
HS 4
GI 12
GI 14
a)
b)
c)
d)
e)
f)
480 500
Insolation (W/m2)
+
Temp./ Precip.
g)
h)
i)
j)
k)
l)
Productivity
Saharan wind intensity
10 14 18
SST (°C)
50 150 250
Ba excess (ppm)
0 0.5 1
EM 1
0 10 20 30
% Temp. Med. F.
0 25 50 75
% Wooden taxa
-12 -8 -4 0
MTCO (°C)

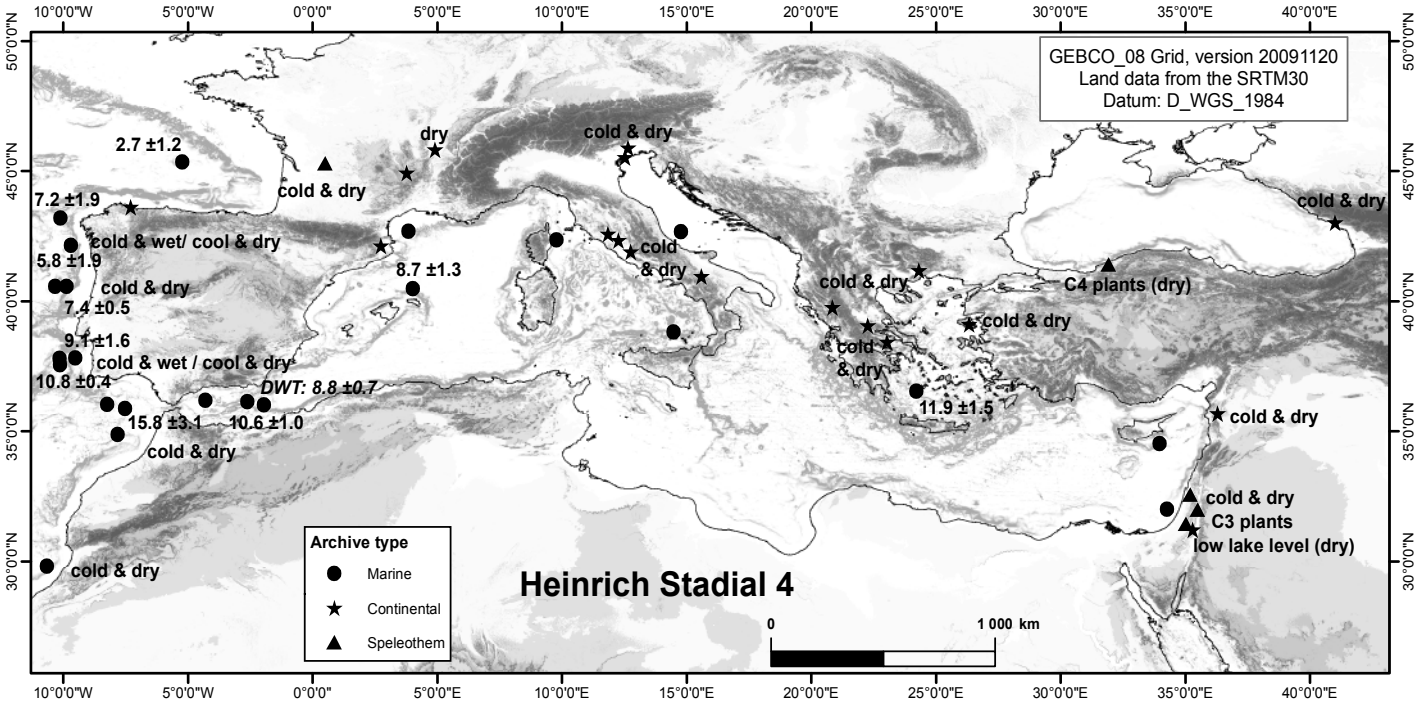
GEBCO_08 Grid, version 20091120
Land data from the SRTM30
Datum: D_WGS_1984
2.7 ±1.2
dry
cold & dry
cold & dry
7.2 ±1.9
cold & wet/ cool & dry
5.8 ±1.9
cold & dry
7.4 ±0.5
8.7 ±1.3
cold & dry
cold & dry
C4 plants (dry)
cold & dry
cold & dry
9.1 ±1.6
cold & wet / cool & dry
10.8 ±0.4
DWT: 8.8 ±0.7
15.8 ±3.1
10.6 ±1.0
cold & dry
11.9 ±1.5
cold & dry
cold & dry
C3 plants
low lake level (dry)
cold & dry
Archive type
Marine
Continental
Speleothem
Heinrich Stadial 4
0
1 000 km

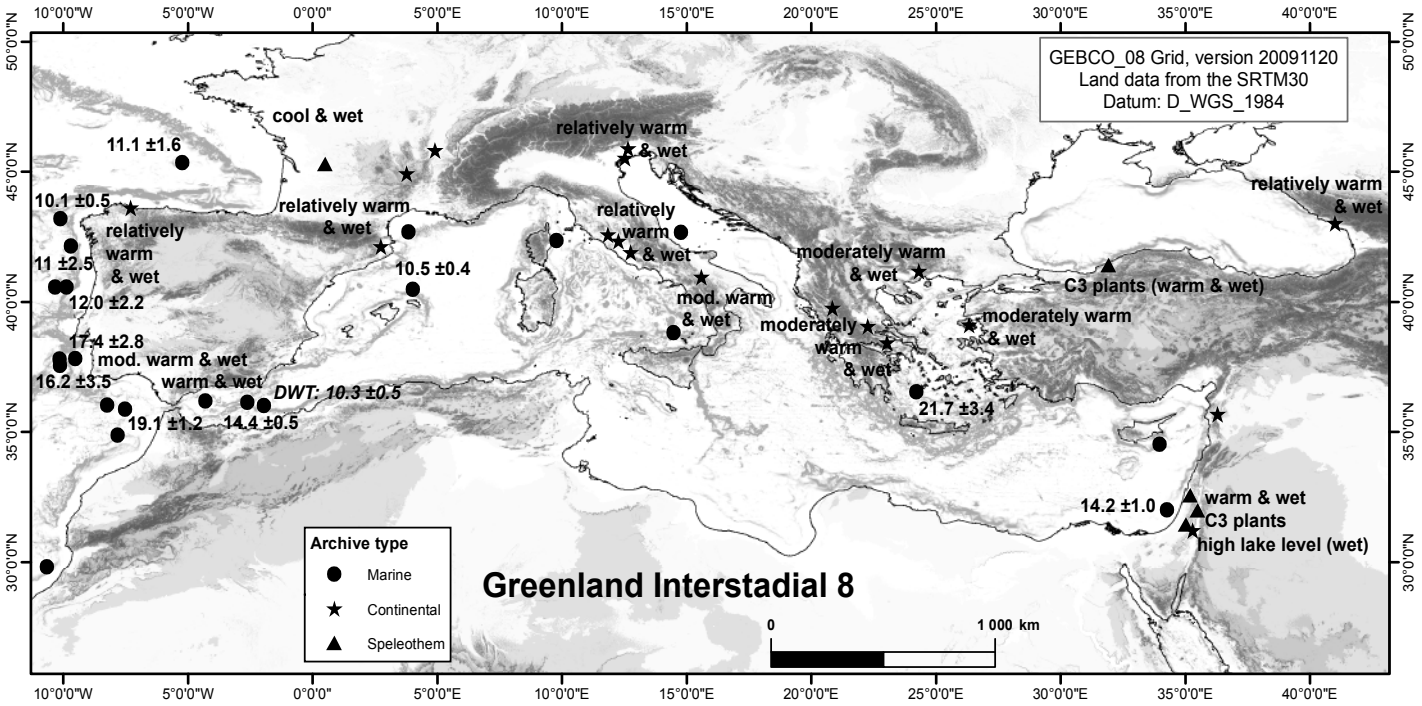
GEBCO_08 Grid, version 20091120
Land data from the SRTM30
Datum: D_WGS_1984
cool & wet
11.1 ±1.6
relatively warm & wet
relatively warm & wet
relatively warm & wet
10.1 ±0.5
relatively warm & wet
11 ±2.5
10.5 ±0.4
12.0 ±2.2
mod. warm & wet
moderately warm & wet
C3 plants (warm & wet)
moderately warm & wet
moderately warm & wet
17.4 ±2.8
mod. warm & wet
16.2 ±3.5
warm & wet
DWT: 10.3 ±0.5
19.1 ±1.2
14.4 ±0.5
21.7 ±3.4
14.2 ±1.0
warm & wet
C3 plants
high lake level (wet)
Archive type
Marine
Continental
Speleothem
Greenland Interstadial 8
0
1 000 km

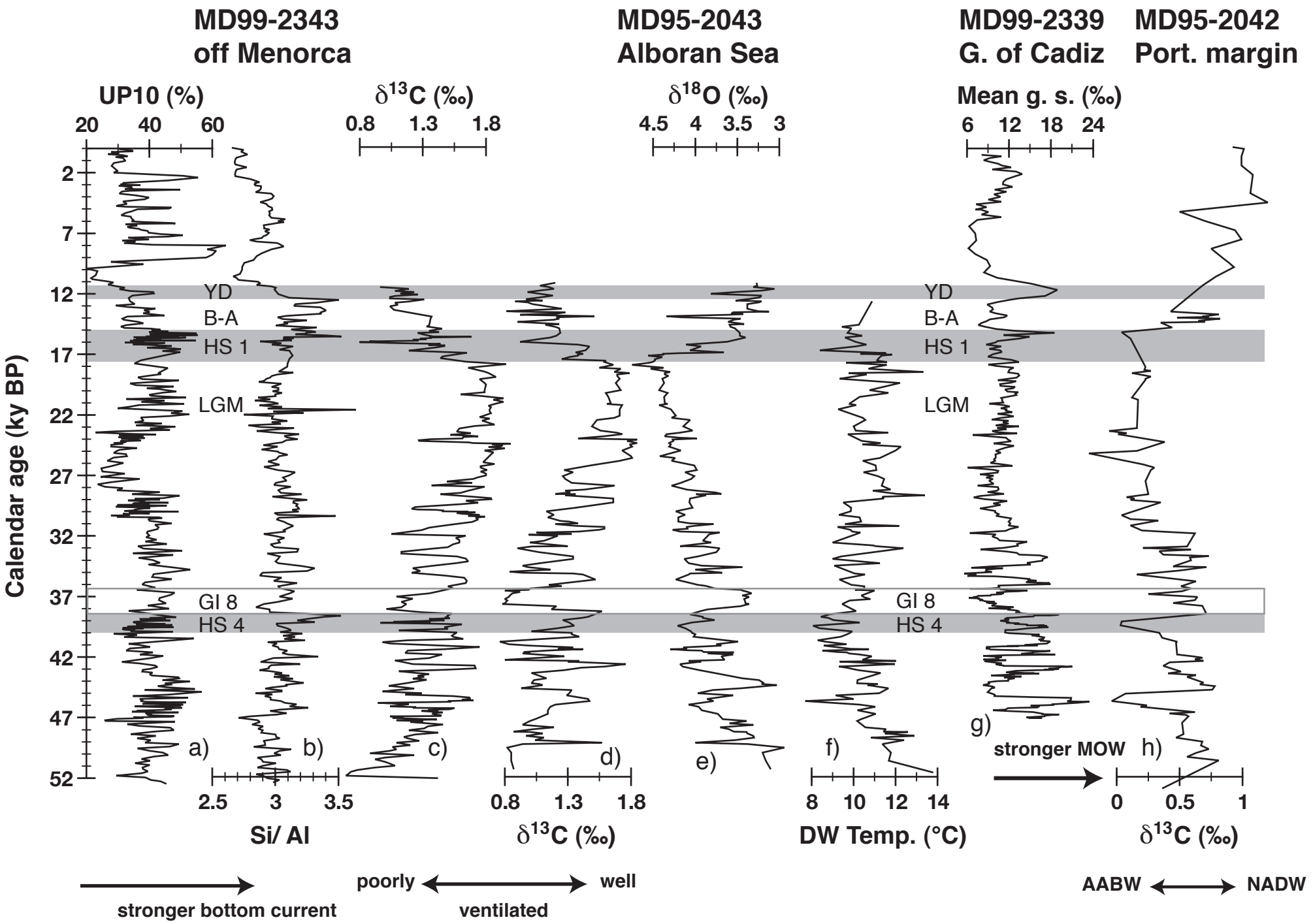
MD99-2343
off Menorca
MD95-2043
Alboran Sea
MD99-2339
G. of Cadiz
MD95-2042
Port. margin
UP10 (%)
20 40 60
δ13C (‰)
0.8 1.3 1.8
δ18O (‰)
4.5 4 3.5 3
Mean g. s. (‰)
6 12 18 24
Calendar age (ky BP)
2
7
12
17
22
27
32
37
42
47
52
YD
B-A
HS 1
LGM
GI 8
HS 4
a)
b)
c)
d)
e)
f)
g)
h)
2.5 3 3.5
Si/ Al
0.8 1.3 1.8
δ13C (‰)
8 10 12 14
DW Temp. (°C)
stronger MOW
0 0.5 1
δ13C (‰)
stronger bottom current
poorly
well
ventilated
AABW
NADW

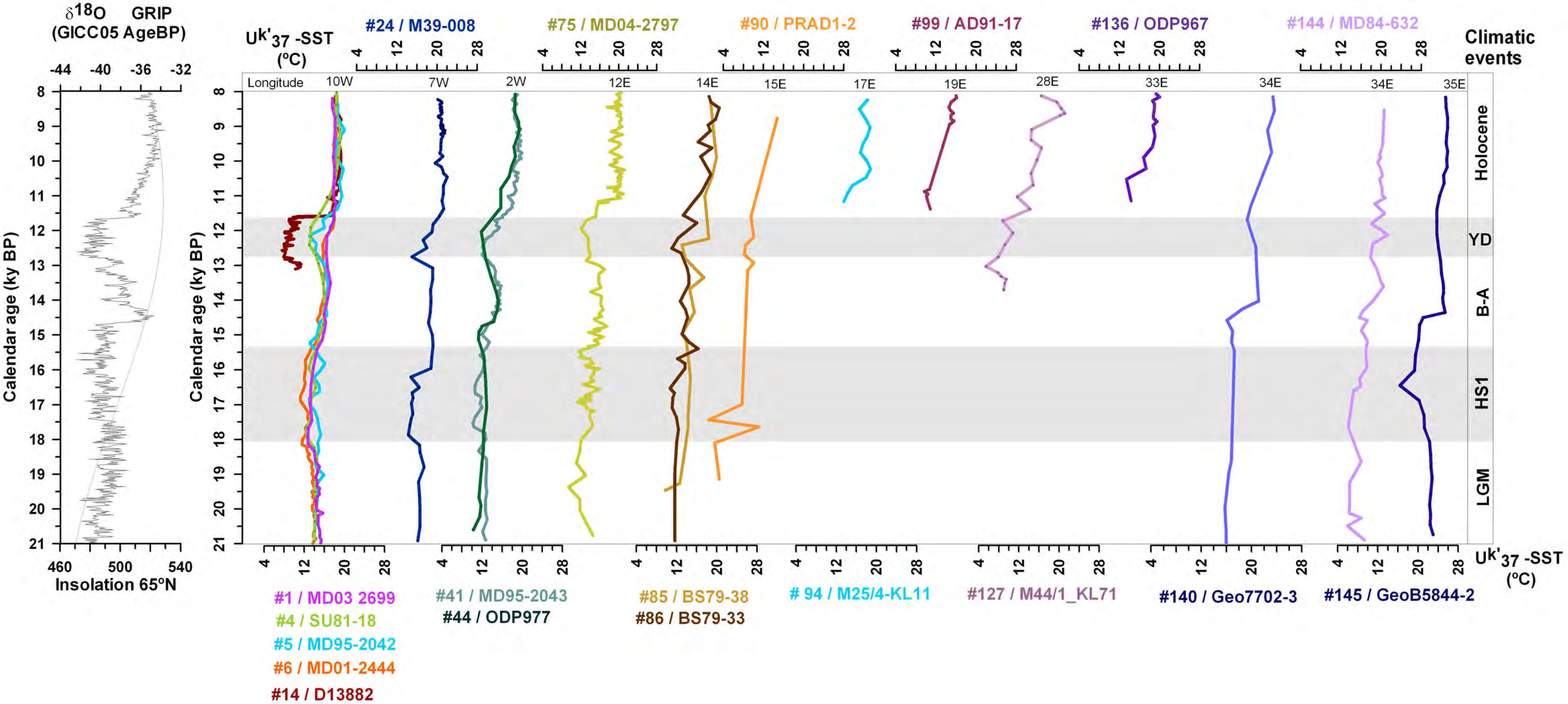
δ18O GRIP (GICC05 AgeBP)
-44 -40 -36 -32
Calendar age (ky BP)
460 500 540
Insolation 65°N
Uk'37 -SST (°C)
#24 / M39-008
#75 / MD04-2797
#90 / PRAD1-2
#99 / AD91-17
#136 / ODP967
#144 / MD84-632
Climatic events
Longitude
10W 7W 2W 12E 14E 15E 17E 19E 28E 33E 34E 34E 35E
Holocene
YD
B-A
HS1
LGM
#1 / MD03 2699
#4 / SU81-18
#5 / MD95-2043
#6 / MD01-2444
#14 / D13882
#41 / MD95-2043
#44 / ODP977
#85 / BS79-38
#86 / BS79-33
94 / M25/4-KL11
#127 / M44/1_KL71
#140 / Geo7702-3
#145 / GeoB5844-2

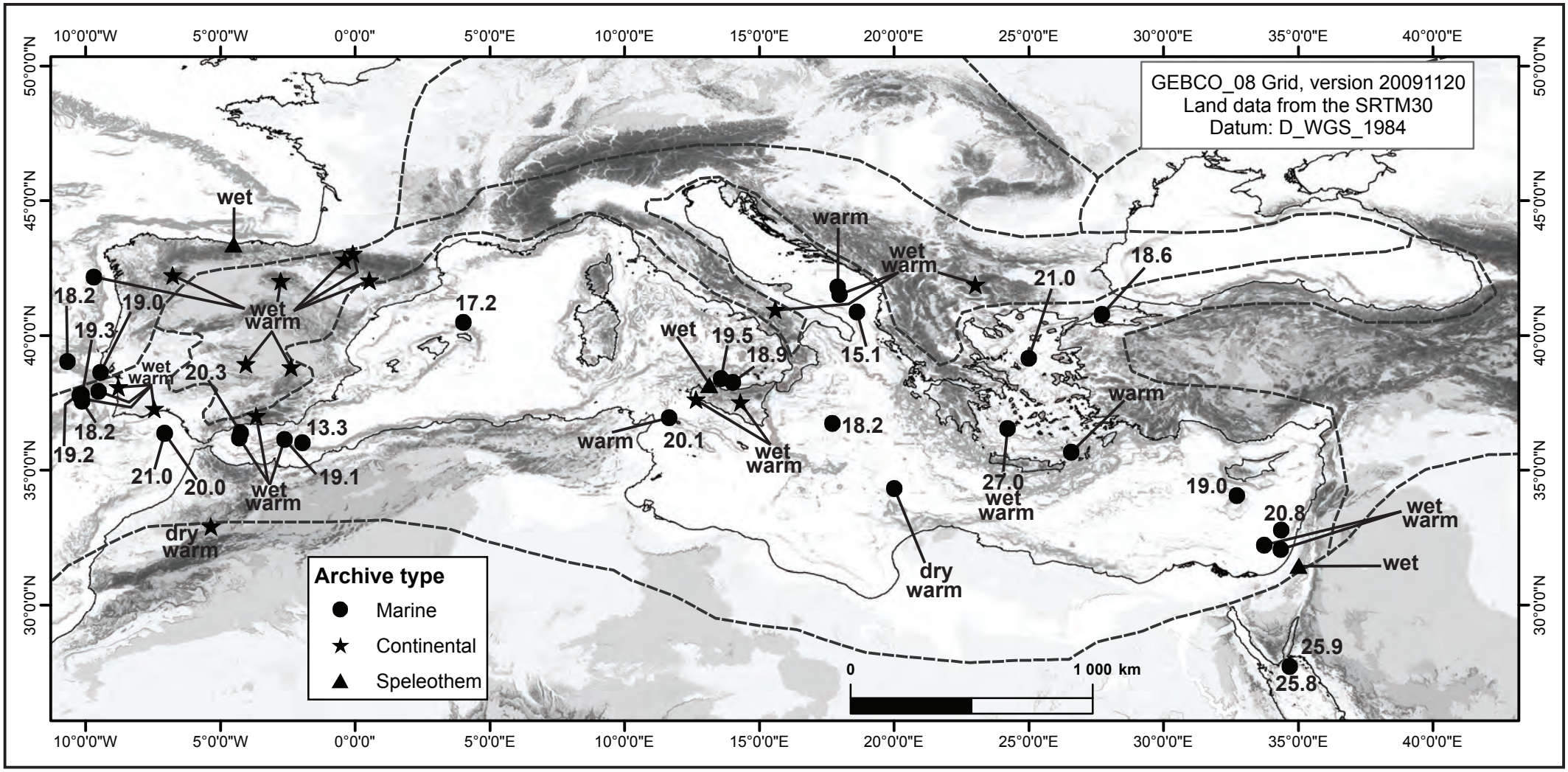
GEBCO_08 Grid, version 20091120
Land data from the SRTM30
Datum: D_WGS_1984
Archive type
Marine
Continental
Speleothem
0
1 000 km
10°0'0"W
5°0'0"W
0°0'0"
5°0'0"E
10°0'0"E
15°0'0"E
20°0'0"E
25°0'0"E
30°0'0"E
35°0'0"E
40°0'0"E
50°0'0"N
45°0'0"N
40°0'0"N
35°0'0"N
30°0'0"N
wet
18.2
19.0
19.3
wet warm
18.2
19.2
20.3
21.0
20.0
wet warm
13.3
19.1
dry warm
17.2
warm
wet warm
wet
19.5
18.9
15.1
warm
20.1
wet warm
18.2
dry warm
21.0
18.6
warm
27.0 wet warm
19.0
20.8
wet warm
wet
25.9
25.8

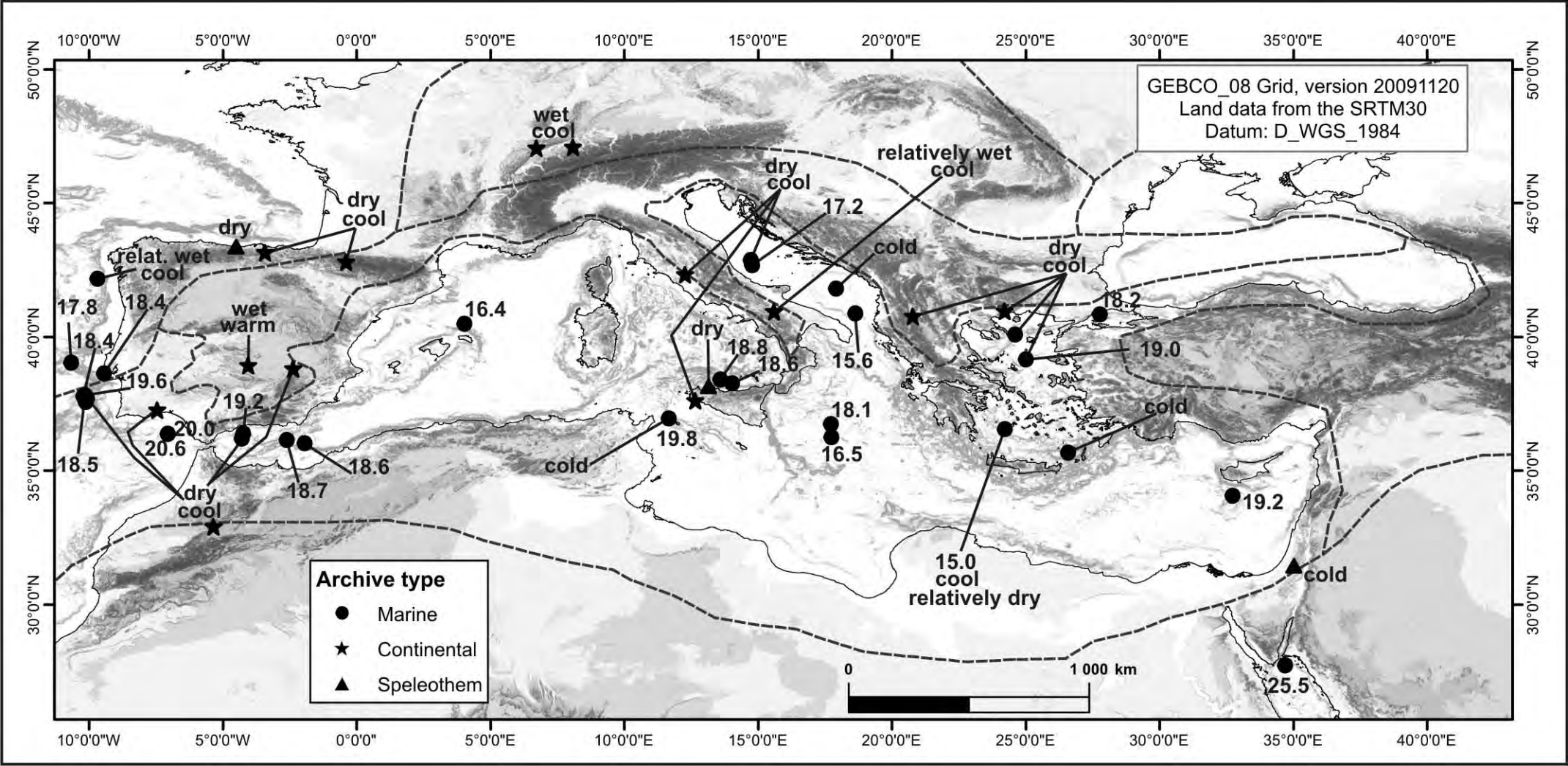
GEBCO_08 Grid, version 20091120
Land data from the SRTM30
Datum: D_WGS_1984
Archive type
Marine
Continental
Speleothem
0
1 000 km
wet cool
dry cool
dry
relat. wet cool
wet warm
relatively wet cool
cold
17.2
16.4
15.6
18.8
18.6
18.1
16.5
19.8
18.7
18.6
19.2
20.0
20.6
19.6
18.4
17.8
18.5
18.2
19.0
15.0 cool relatively dry
25.5

Site_ID	Site name	Latitude	Longitude	Elevation/ Water depth	Archive Map	Archive type	Time-slice	SST mean ± 1σ (°C)	SST min. (°C)	SST max. (°C)	Averaged interval (ky)	References
2	M16004-1	29.83	-10.65	-1512	Marine	Marine core	MIS 5e; MIS 3					Hooghiemstra et al., (1992)
5	MD95-2042	37.81	-10.15	-3146	Marine	Marine core	MIS 5e; MIS 3; LGIT; HO; 8.2ka	a: 19.1 ±2.1 f: 19.7 ±1.1	a: 14.3 f: 17.7	a: 21.9 f: 21.2	116-128	Sanchez Goñi et al., (1999; 2000; 2002; 2005); Pailler and Bard, (2002); Shackleton et al., (2000); Salgueiro et al., (2010)
6	MD01-2444	37.57	-10.13	-2656	Marine	Marine core	MIS 5e; MIS 3; LGIT; HO; 8.2ka	a: 19.5 ±1.4	a:13.9	a: 20.8	116-128	Martrat et al., (2007); Vautravers et al., (2006); Skinner et al., (2007); Margari et al., (2010);
7	SU92-03	43.20	-10.11	-3005	Marine	Marine core	MIS 5e; MIS 3	f: 17.5 ±0.6	f: 16.5	f: 18.0	116-128	Salgueiro et al., (2010)
9	MD95-2040	40.58	-9.86	-2465	Marine	Marine core	MIS 5e; MIS 3	a:18.9±1.2 f: 18.4 ± 0.6	a: 17.4 f: 17.7	a: 20.2 f: 19.6		Salgueiro et al., (2010)
11	MD99-2331	42.15	-9.69	-2110	Marine	Marine core	MIS 5e; MIS 3; LGIT					Naughton et al., (2007; 2009); Sanchez Goñi et al., (2005; 2008; 2009)
30	MD04-2845	45.35	-5.22	-4100	Marine	Marine core	MIS 5e; MIS 3	f:16.1±5.1	f: 3.3	f: 19.7	116-128	Sanchez Goñi et al., (2008)
44	ODP Site 977A	36.03	-1.96	-1984	Marine	Marine core	MIS 5e; MIS 3; LGIT; HO; 8.2ka	a: 20.6 ±1.8	a: 15.0	a: 23.5	116-128	Martrat et al., (2004)
56	Lac du Bouchet	44.92	3.78	1200	Continental	Lake core	MIS 5e; MIS 3; LGIT					de Beaulieu et al., (1984); Reille and de Beaulieu., (1988a,b); Reille and de Beaulieu, (1990); Reille et al., (1998)
57	Ribains/Landos/Velay 1	44.84	3.82	1080	Continental	Lake core	MIS 5e; LGIT					de Beaulieu et al., (1984); Reille and de Beaulieu., (1985; 1989); de Beaulieu and Reille., (1992)
58	borehole PRGL1	42.69	3.84	-300	Marine	Marine core	MIS 5e; MIS 3					Sierro et al., (2009)
60	M40/4-87SL	38.99	4.02	-1900	Marine	Marine core	MIS 5e	a: 21.2			122-127	Emeis et al., (2003); Weldeab et al., (2003)
64	ODP Site 975B	38.90	4.51	-2416	Marine	Marine core	MIS 5e; HO; 8.2ka	a: 20.2 ±3.3	a: 13.8	a: 22.6	120.9-123.5	Jimenez-Espejo et al., (2007: 2008); Doose et al., (1999)
65	les Echets	45.81	4.92	267	Continental	Lake core	MIS 5e; MIS 3					de Beaulieu and Reille., (1984); de Beaulieu and Reille., (1989); Ampel et al., (2008)
73	LC07	38.15	10.08	-488	Marine	Marine core	MIS 5e					Incarbona et al., (2008)
74	Antro del Corchia	43.98	10.13	840	Speleothem	Speleothem	MIS 5e					Drysdale et al. (2004; 2005; 2009)
82	Valle di Castiglione	41.89	12.76	44	Continental	Lake core	MIS 5e; MIS 3; LGIT					Folieri et al., (1989; 1993; 1998); Magri, (1994)
84	ODP Site 963A + 963D	37.03	13.18	-470	Marine	Marine core	MIS 5e; HO; 8.2ka					Incarbona.et al.,(2003); Sprovieri et al., (2006)
90	PRAD1-2	42.68	14.77	-185.5	Marine	Marine core	MIS 5e; LGIT; HO; 8.2ka	a: 18.6 ±2.4	a: 15.3	a: 21.6	116-128	Piva et al., (2008)
91	Lago Grande di Monticchio	40.94	15.61	656	Continental	Lake core	MIS 5e; MIS 3; HO; 8.2ka					Allen et al, (1999; 2000; 2002); Watts et al., (2000); Allen and Huntley, (2009)
95	KC01	36.25	17.74	-3640	Marine	Marine core	MIS 5e; HO; 8.2ka	a: 19.4 ±1.2	a: 18.3	a: 21.8	117.7-119	Doose, (1999)
98	KS205	38.20	18.14	-2384	Marine	Marine core	MIS 5e	a: 21.2 ±1.6	a: 17.8	a: 23.0	≈ 116-125	Rohling et al., (2002)
104	Ioannina 284	39.75	20.85	319	Continental	Lake core	MIS 5e; MIS 3; LGIT				≈ 117-126	Frogley et al., (1999); Tzedakis et al., (2002); Lawson et al., (2004)
105	Ioannina 249	39.65	20.92	470	Continental	Lake core	MIS 5e					Tzedakis et al., (1994)
108	Kopais	38.43	23.05	95	Continental	Lake core	MIS 5e; MIS 3;					Tzedakis, (1999)
109	M40/ 4-71SL	34.81	23.19	-2827	Continental	Lake core	MIS 5e	a: 21.2			117.7-119	Emeis et al., (2003); Weldeab et al., (2003)
116	Tenaghi Philippon 1	41.17	24.33	40	Continental	Lake core	MIS 5e; MIS 3; LGIT					Wijmstra. 1969; Wijmstra and Smit. 1976; Tzedakis et al.. 1997; 2003
119	ODP Site 971A	33.72	24.68	-2026	Marine	Marine core	MIS 5e	a: 19.9 ±1.6	a: 15.7	a: 21.4	117.8-126.4	Marino et al., (2007); Rohling et al., (2002; 2006); Osbourne et al., (2010)
121	ODP Site 969E	33.84	24.88	-2212	Marine	Marine core	MIS 5e					Emeis et al., (2003); Weldeab et al., (2003); Gallego-Torres et al., (2010)
124	LC21	35.67	26.58	-1522	Marine	Marine core	MIS 5e; HO; 8.2ka	a: 20.1 ±1.6	a: 15.4	a: 23.4	≈ 116-128	Rijk et al., (1999); Marino et al., (2007);van der Meer et al., (2007); Osborne et al., (2010)
125	M40/4-67SL	34.81	27.30	-2158	Marine	Marine core	MIS 5e	a: 22.8				Emeis et al., (2003); Weldeab et al., (2003); Schmiedl et al., (2003)
134	MD84642	32.67	32.57	-1260	Marine	Marine core	MIS 5e					Cheddadi and Rossignol-Strick, (1997)
135	KC20B	33.68	32.71	-882	Marine	Marine core	MIS 5e	a: 21.2 ±1.5	a: 17.9	a: 23.1	117.8-126.4	Doose, (1999)
136	ODP Site 967C	34.07	32.73	-2550	Marine	Marine core	MIS 5e; LGIT; HO; 8.2ka	a: 20.6 ±1.9	a: 16.1	a: 22.9	117.8-126.4	Emeis et al., (1998; 2000; 2003); Rohling et al., (2002; 2006); Scrivner et al., (2004)
141	GeoTü KL83	32.62	34.15	-1433	Marine	Marine core	MIS 5e					Schmiedl et al., (2003); Weldeab et al., (2003)
146	Soreq Cave	31.45	35.03	400	Speleothem	Speleothem	MIS 5e; MIS 3; HO; 8.2ka					Vaks et al., (2006), Affek et al., (2008); Bar-Matthews et al., (2003)
147	Jerusalem West Cave	31.78	35.15	700	Speleothem	Speleothem	MIS 5e					Frumkin et al., (1999; 2000)
148	Peqiin Cave	32.58	35.19	650	Speleothem	Speleothem	MIS 5e; MIS 3					Bar-Matthews et al., (2003)

a: alkenone based/ annual mean; f: planktonic foraminifer based/ summer

Site_ID	Site name	Latitude	Longitude	Elevation/ Water depth	Archive Map	Archive type	Time-slice	HS4 mean SST ±1σ (°C)	HS4 SST min. (°C)	HS4 SST max. (°C)	HS4 continental climate	References
2	M16004-1	29.83	-10.65	-1512	Marine	Marine core	MIS 5e; MIS 3				cold & dry	Hooghiemstra et al., (1992)
3	MD95-2039	40.57	-10.33	-3381	Marine	Marine core	MIS 3; LGIT				cold & dry	Roucoux et al., (2001; 2005)
								a: 11.7 ±1.3	a:10.3	a: 13.2		
5	MD95-2042	37.81	-10.15	-3146	Marine	Marine core	MIS 5e; MIS 3; LGIT; HO; 8.2ka	f: 9.7 ±0.6	f: 8.7	f: 10.2	3 phases: cold & wet/ cool & dry/ cold & wet	Sanchez Goñi et al., (1999; 2000; 2002; 2005); Pailler and Bard, (2002); Shackleton et al., (2000); Salgueiro et al., (2010)
								a: 10.8 ±0.4	a: 10.8	a: 11.3		
6	MD01-2444	37.57	-10.13	-2656	Marine	Marine core	MIS 5e; MIS 3; LGIT; HO; 8.2ka	f: 11.2 ±4.3	f: 5.3	f: 20	cold & dry	Martrat et al., (2007); Vautravers et al., (2006); Skinner et al., (2007); Margari et al., (2010);
7	SU92-03	43.20	-10.11	-3005	Marine	Marine core	MIS 5e; MIS 3	f: 7.2 ±1.9	f: 4.6	f: 9.1		Salgueiro et al., (2010)
								a: 10.3 ±1.1	a: 8.5	a: 11.4		
9	MD95-2040	40.58	-9.86	-2465	Marine	Marine core	MIS 5e; MIS 3	f: 7.4 ±0.5	f: 6.5	f: 8.1		Salgueiro et al., (2010)
11	MD99-2331	42.15	-9.69	-2110	Marine	Marine core	MIS 5e; MIS 3; LGIT	f: 5.8 ±1.9	f: 3.3	f: 7.9	2 phases: cold & wet/ cool & dry	Naughton et al., (2007; 2009); Sanchez Goñi et al., (2005; 2008; 2009)
12	MD95-2041	37.83	-9.52	-1123	Marine	Marine core	MIS 3	f: 9.1 ±1.6	f: 7.9	f: 11.9		Voelker and de Abreu, submitted
17	M15669-1	34.88	-7.82	-2030	Marine	Marine core	MIS 3				cold & dry	Hooghiemstra et al., (1992)
18	MD99-2339	35.88	-7.53	-1170	Marine	Marine core	MIS 3	f: 15.8 ±3.1	f: 9.8	f: 20.6		Voelker et al., (2006)
20	Area longa	43.60	-7.30	0	Continental	Terrestrial core	MIS 3				cold & dry	Gómez-Orellana et al., (2007)
30	MD04-2845	45.35	-5.22	-4100	Marine	Marine core	MIS 5e; MIS 3	f: 2.7 ±1.2	f: 0.4	f: 5.8	cold & dry	Sanchez Goñi et al., (2008)
32	ODP Site 976	36.20	-4.30	-1108	Marine	Marine core	MIS 3; LGIT; HO; 8.2ka				cold & dry	Combourieu-Nebout et al.. (1998; 2002; 2009);
								a: 10.5 ±0.6	a: 9.5	a: 11.4		
41	MD95-2043	36.14	-2.62	-1841	Marine	Marine core	MIS 3; LGIT; HO; 8.2ka	DWT: 8.8 ±0.7	DWT: 8.4	DWT: 10.3	3 phases: cold & wet/ cool & dry/ cold & wet	Cacho et al., (1999; 2000; 2001; 2006); Sanchez Goñi et al., (2002; 2009); Fletcher et al., (2008; 2010); Moreno et al. (2002; 2004)
44	ODP Site 977A	36.03	-1.96	-1984	Marine	Marine core	MIS 5e; MIS 3; LGIT; HO; 8.2ka	a: 10.6 ±1.0	a: 9.8	a: 12.3		Martrat et al., (2004)
61	MD99-2343	40.50	4.03	-2391	Marine	Marine core	MIS 3; HO; 8.2ka	f: 8.7 ±1.3	f: 7.2	f: 10.3		Sierro et al., (2005); Frigola et al., (2007; 2008)
65	les Echets	45.81	4.92	267	Continental	Lake core	MIS 5e; MIS 3				dry	de Beaulieu and Reille., (1984); de Beaulieu and Reille., (1989); Ampel et al., (2008)
76	Lagaccione	42.57	11.85	355	Continental	Lake core	MIS 3; LGIT				cold & dry	Magri, (1999)
78	Lagoon of Venice	45.52	12.53	-2	Continental	Lagoon	MIS 3; LGIT				cold & dry	Canali et al., (2007)
79	Azzano Decimo core	45.88	12.65	9.9	Continental	Terrestrial	MIS 3				cold & dry	Pini et al., (2009)
82	Valle di Castiglione	41.89	12.76	44	Continental	Lake core	MIS 5e; MIS 3; LGIT				cold & dry	Folieri et al., (1989; 1993; 1998); Magri, (1994)
88	KET80-03	38.82	14.48	-1900	Marine	Marine core	MIS 3; LGIT				cold & dry	Paterne et al.,(1999) Rossignol-Strick and Planchais, (1989); Rossignol Strick, (1995)
91	Lago Grande di Monticchio	40.94	15.61	656	Continental	Lake core	MIS 5e; MIS 3; HO; 8.2ka				cold & dry	Allen et al, (1999; 2000; 2002); Watts et al., (2000); Allen and Huntley, (2009)
114	C69	36.55	24.21	-632	Marine	Marine core	MIS 3; LGIT; HO; 8.2ka	f: 11.9 ±1.5	f: 10.3	f: 13.3	cold & dry	Geraga et al., (2005)
116	Tenaghi Philippon 1	41.17	24.33	40	Continental	Lake core	MIS 5e; MIS 3; LGIT				cold & dry	Wijmstra. 1969; Wijmstra and Smit. 1976; Tzedakis et al.. 1997; 2003
123	Megali Limni basin	39.10	26.33	323	Continental	Lake core	MIS 3				cold & dry	Margari et al.. 2009
132	Sofular Cave	41.42	31.93	700	Speleothem	Speleothem	MIS 3; HO				C4 plants	Fleitmann et al., (2009)
146	Soreq Cave	31.45	35.03	400	Speleothem	Speleothem	MIS 5e; MIS 3; HO; 8.2ka				cold & dry; C3 plants present	Vaks et al., (2006), Affek et al., (2008); Bar-Matthews et al., (2003)
148	Peqiin Cave	32.58	35.19	650	Speleothem	Speleothem	MIS 5e; MIS 3				C3 plants present	Bar-Matthews et al., (2003)
149	Lake Lisan	31.21	35.31	410	Continental	Lake core	MIS 3; HO				low lake level (dry)	Schramm et al., (2000); Stein et al., (2010); Bartov et al., (2003); Waldmann et al., (2009; 2010)
150	Ma' ale Efrayim cave, Israel	32.00	35.50	250	Speleothem	Speleothem	MIS 3				C3 plants present	Vaks et al., (2003)
153	Ghab	35.68	36.30	300	Continental	Lake core	LGIT; MIS 3				cold & dry	Bottema, (1995); Niklewski and van Zeist, (1970)
154	Dziguta River	43.02	41.02	120	Continental	River core	MIS 3; LGIT				cold & dry	Arslanov et al., (2007)

a: alkenone based/ annual mean SST;
f: planktonic foraminifera fauna based SST for summer;
DWT: deep water temperature

Site_ID	Site name	Latitude	Longitude	Elevation/ Water depth	Archive Map	Archive type	Time-slice	GI8 mean SST ±1σ (°C)	GI8 SST min. (°C)	GI8 SST max. (°C)	GI8 continental climate	References
3	MD95-2039	40.57	-10.33	-3381	Marine	Marine core	MIS 3; LGIT	a:14.5 ±1.3	a:12.4	a: 15.3	relatively warm & wet	Roucoux et al., (2001; 2005)
5	MD95-2042	37.81	-10.15	-3146	Marine	Marine core	MIS 5e; MIS 3; LGIT; HO; 8.2ka	f: 16.2 ±3.5 a: 13.8 ±1.1	f: 9.8 a:10.8	f: 21.1 a: 14.8	moderately warm & wet	Sanchez Goñi et al., (1999; 2000; 2002; 2005); Pailler and Bard, (2002); Shackleton et al., (2000); Salgueiro et al., (2010)
6	MD01-2444	37.57	-10.13	-2656	Marine	Marine core	MIS 5e; MIS 3; LGIT; HO; 8.2ka	f: 17.1 ±2.3	f: 13.9	f: 20.2	moderately warm & wet	Martrat et al., (2007); Vautravers et al., (2006); Skinner et al., (2007); Margari et al., (2010);
7	SU92-03	43.20	-10.11	-3005	Marine	Marine core	MIS 5e; MIS 3	f: 10.1 ±0.5 a: 13.6 ±0.2	f: 9.6 a: 13.3	f: 10.5 a: 13.7		Salgueiro et al., (2010)
9	MD95-2040	40.58	-9.86	-2465	Marine	Marine core	MIS 5e; MIS 3	f: 12.0 ±2.2	f: 9.9	f: 16.1		Salgueiro et al., (2010)
11	MD99-2331	42.15	-9.69	-2110	Marine	Marine core	MIS 5e; MIS 3; LGIT	f: 11.0 ±2.5	f: 7.8	f: 15.6	relatively warm & wet	Naughton et al., (2007; 2009); Sanchez Goñi et al., (2005; 2008; 2009)
12	MD95-2041	37.83	-9.52	-1123	Marine	Marine core	MIS 3	f: 17.4 ±2.8	f: 12.9	f: 19.9		Voelker and de Abreu, submitted
18	MD99-2339	35.88	-7.53	-1170	Marine	Marine core	MIS 3	f: 19.1 ±1.2	f: 17.1	f: 20.8		Voelker et al., (2006)
20	Area longa	43.60	-7.30	0	Continental	Terrestrial core	MIS 3				relatively warm & wet	Gómez-Orellana et al., (2007)
30	MD04-2845	45.35	-5.22	-4100	Marine	Marine core	MIS 5e; MIS 3	f: 11.1 ±1.6	f: 8.4	f: 12.5	cool & wet	Sanchez Goñi et al., (2008)
32	ODP Site 976	36.20	-4.30	-1108	Marine	Marine core	MIS 3; LGIT; HO; 8.2ka	a: 14.4 ±0.5	a: 13.7	a: 15.3	warm & wet	Combourieu-Nebout et al.. (1998; 2002; 2009);
41	MD95-2043	36.14	-2.62	-1841	Marine	Marine core	MIS 3; LGIT; HO; 8.2ka	DWT: 10.3 ±0.5	DWT: 9.5	DWT: 11.0	warm & wet	Cacho et al., (1999; 2000; 2001; 2006); Sanchez Goñi et al., (2002; 2009); Fletcher et al., (2008; 2010); Moreno et al. (2002; 2004)
44	ODP Site 977A	36.03	-1.96	-1984	Marine	Marine core	MIS 5e; MIS 3; LGIT; HO; 8.2ka	a: 14.0 ±0.4	a: 13.2	a: 14.6		Martrat et al., (2004)
49	Villars Cave, France	45.30	0.50		Speleothem	Speleothem	MIS 3				relatively warm & wet	Genty et al., (2003, 2010)
54	Lago de Banyoles	42.12	2.75	173	Continental	Lake core	MIS 3; LGIT; HO; 8.2ka				relatively warm & wet	Pérez-Obiol and Julia, (1994); Valero-Garcés et al., (1998)
61	MD99-2343	40.50	4.03	-2391	Marine	Marine core	MIS 3; HO; 8.2ka	f: 10.5 ±0.4	f: 10.1	f: 11.0		Sierro et al., (2005); Frigola et al., (2007; 2008)
76	Lagaccione	42.57	11.85	355	Continental	Lake core	MIS 3; LGIT				relatively warm & wet	Magri, (1999)
77	Lago di Vico	42.33	12.27	507	Continental	Lake core	MIS 3; LGIT; 8.2ka				relatively warm & wet	Lerov et al., (1996); Magri and Sadori. (1999); Magri and Parra. (2002)
79	Azzano Decimo core	45.88	12.65	9.9	Continental	Terrestrial	MIS 3				relatively warm & wet	Pini et al., (2009)
82	Valle di Castiglione	41.89	12.76	44	Continental	Lake core	MIS 5e; MIS 3; LGIT				relatively warm & wet	Folieri et al., (1989; 1993; 1998); Magri, (1994)
88	KET80-03	38.82	14.48	-1900	Marine	Marine core	MIS 3; LGIT				relatively warm & wet	Paterne et al.,(1999) Rossignol-Strick and Planchais, (1989); Rossignol Strick, (1995)
91	Lago Grande di Monticchio	40.94	15.61	656	Continental	Lake core	MIS 5e; MIS 3; HO; 8.2ka				moderately warm & wet	Allen et al. (1999; 2000; 2002); Watts et al., (2000); Allen and Huntley. (2009)
104	Ioannina 284	39.75	20.85	319	Continental	Lake core	MIS 5e; MIS 3; LGIT				moderately warm & wet	Frogley et al., (1999); Tzedakis et al., (2002); Lawson et al., (2004)
108	Kopais	38.43	23.05	95	Continental	Lake core	MIS 3; MIS 5e				moderately warm & wet	Tzedakis, (1999)
106	Lake Xinias	39.05	22.27	500	Continental	Lake core	MIS 3				moderately warm & wet	Bottema, (1979)
114	C69	36.55	24.21	-632	Marine	Marine core	MIS 3; LGIT; HO; 8.2ka	f: 21.7 ±3.4	f: 18.2	f: 27.0	moderately warm & wet	Geraga et al., (2005)
116	Tenaghi Philippon 1	41.17	24.33	40	Continental	Lake core	MIS 5e; MIS 3; LGIT				relatively warm & wet	Wijmstra. 1969; Wijmstra and Smit. 1976; Tzedakis et al.. 1997; 2003
123	Megali Limni basin	39.10	26.33	323	Continental	Lake core	MIS 3				moderately warm & wet	Margari et al.. 2009
132	Sofular Cave	41.42	31.93	700	Speleothem	Speleothem	MIS 3; HO				C3 plants; warm & wet	Fleitmann et al., (2009)
142	9509	32.02	34.27	-884	Marine	Marine core	MIS 3	a: 14.2 ±1	a:13.2	a: 15.2		Almogi-Labin et al., (2009)
146	Soreq Cave	31.45	35.03	400	Speleothem	Speleothem	MIS 5e; MIS 3; HO; 8.2ka				warm & wet; C3 plants present	Vaks et al., (2006), Affek et al., (2008); Bar-Matthews et al., (2003)
148	Peqiin Cave	32.58	35.19	650	Speleothem	Speleothem	MIS 5e; MIS 3				C3 plants present	Bar-Matthews et al., (2003)
149	Lake Lisan	31.21	35.31	410	Continental	Lake core	MIS 3; HO				high lake level (wet)	Schramm et al., (2000); Stein et al., (2010); Bartov et al., (2003); Waldmann et al., (2009; 2010)
150	Ma' ale Efrayim cave, Israel	32.00	35.50	250	Speleothem	Speleothem	MIS 3				C3 plants present	Vaks et al., (2003)
154	Dziguta River	43.02	41.02	120	Continental	River core	MIS 3; LGIT				relatively warm & wet	Arslanov et al., (2007)

a: alkenone based/ annual mean SST;
f: planktonic foraminifera fauna based SST for summer;
DWT: deep water temperature

Site ID	Site name	Latitude	Longitude	Elevation/ Water depth	Archive Map	Archive type	Time-slice	Variable1 (FN)	Variable2 (FN)	Varible3 (FA) precip	Variable4 (FA)_ SST-Uk37 (°C)	Variable5 (FA)_SST -Forams (°C)	References
1	MD03-2699	39.04	-10.67	-1895	Marine	Marine core	LGIT; HO; 8.2ka				18.18		Rodrigues et al., (2010)
4	SU 81-18	37.77	-10.21	-3135	Marine	Marine core	LGIT; HO; 8.2 ka	warm	wet		19.15		Lézine et al., (1997); Turon et al., (2003); Bard et al., (2002)
5	MD95-2042	37.81	-10.15	-3146	Marine	Marine core	MIS 5e; MIS 3; LGIT; HO; 8.2ka				19.30		Sanchez Goñi et al., (1999; 2000; 2002; 2005); Pailler and Bard, (2002); Shackleton et al., (2000); Salgueiro et al., (2010)
6	MD01-2444	37.57	-10.13	-2656	Marine	Marine core	MIS 5e; MIS 3; LGIT; HO; 8.2ka				18.21		Martrat et al., (2007); Vautravers et al., (2006); Skinner et al., (2007); Margari et al., (2010);
10	MD03-2697	42.17	-9.70	-2164	Marine	Marine core	LGIT; HO; 8.2ka	warm	wet				Naughton et al., (2007); Naughton., (2007)
13	SO75-6KL	37.94	-9.51	-1281	Marine	Marine core	LGIT	warm	wet				Boessenkool et al., (2001)
14	D13882	38.63	-9.45	-88	Marine	Marine core	LGIT; HO; 8.2ka				19.01		Rodrigues et al., (2009)
15	Santo Andre lagoon	38.08	-8.78	2.7	Continental	Lagoon core	HO	warm	wet				Santos and Sanchez-Goñi, (2003)
19	Guadiana basin	37.27	-7.45	0	Continental	Estuary core	LGIT; HO; 8.2ka	warm	wet				Fletcher et al., (2007)
23	MD99-2341+ GeoB5901	36.38	-7.07	-574	Marine	Marine core	HO; 8.2ka				20.00		Kim et al., (2004)
24	M39008	36.37	-7.07	-576	Marine	Marine core	LGIT; HO; 8.2ka				21.04		Cacho et al., (1999; 2000)
27	Laguna de la Roya	42.22	-6.77	1608	Continental	Lake core	LGIT; HO	warm	wet				Allen et al., (1996)
29	Tigalmamine	32.90	-5.35	1626	Continental	Lake core	HO; 8.2ka	warm	dry				Lamb et al., (1989); Lamb et al., (1995); Lamb and van der Kaars., (1995); Cheddadi et al., (1998)
32	ODP Site 976	36.20	-4.30	-1108	Marine	Marine core	MIS 3; LGIT; HO; 8.2ka	warm	wet				Combourieu-Nebout et al.. (1998; 2002; 2009);
33	TG-5	36.38	-4.25	-626	Marine	Marine core	HO; 8.2ka				20.30		Barcena et al., (2001)
34	Enol	43.18	-4.15		Continental	Lake / Peatbog cor	HO; 8.2ka			wet			Moreno et al., in press.
35	Fuentillejo maar	38.93	-4.05		Continental	Lake core	HO; 8.2ka			warm, wet			Vegas et al., in press.
36	Padul	37.00	-3.67	785	Continental	Lake core	LGIT; HO	warm	wet				Florschütz et al., (1971); Pons and Reille., (1988)
40	Hoyos de Iregua	42.02	-2.75	1780	Continental	Lake core	LGIT; HO	warm	wet				Gil Garcia et al., (2002)
41	MD95-2043	36.14	-2.62	-1841	Marine	Marine core	MIS 3; LGIT; HO; 8.2ka	warm	wet		19.09		Cacho et al., (1999; 2000; 2001; 2006); Sanchez Goñi et al., (2002; 2009); Fletcher et al., (2008; 2010); Moreno et al. (2002; 2004)
43	Villaverde	38.80	-2.37	900	Continental	Lake core	HO; 8.2ka	warm	wet				Carrion et al., (2001); Carrion., (2003); Jalut., (2005); Jalut et al., (2008)
44	ODP Site 977A	36.03	-1.96	-1984	Marine	Marine core	MIS 5e; MIS 3; LGIT; HO; 8.2ka				19.32		Martrat et al., (2004)
47	El Portalet	42.80	-0.38	1802	Continental	Peatbog core	LGIT; HO; 8.2ka	warm	wet	wet			González-Sampériz et al., (2005; 2006; 2008; 2009)
48	Biscaye	43.03	-0.07	410	Continental	Lake core	LGIT	warm	wet				Reille and Andrieu, (1995)
50	Estanya	42.03	0.53		Continental	Lake core	HO; 8.2ka			warm, wet			Morellon et al., (2009)
61	MD99-2343	40.50	4.03	-2391	Marine	Marine core	MIS 3; HO; 8.2ka				17.23		Sierro et al., (2005); Frigola et al., (2007; 2008)
75	MD04-2797	36.95	11.67	-771	Marine	Marine core	LGIT; HO; 8.2ka				20.05	warm	Essallami et al., (2007); I. Rouis-Zargouni et al., (2010)
80	Lake Gorgo Basso	37.62	12.65	6	Continental	Lake core	HO; 8.2ka	warm	wet				Tinner et al., (2009)
83	Grotta di Carburangeli	38.17	13.16	22	Speleothem	Speleothem	HO; 8.2ka			wet			S. Frisia et al., (2006)
85	BS79-38	38.41	13.58	-1489	Marine	Marine core	LGIT; HO; 8.2ka				19.45		Cacho et al., (2001)
86	BS79-33	38.26	14.03	-1282	Marine	Marine core	LGIT; HO; 8.2ka				18.89		Cacho et al., (2001)
87	Lago di Pergusa	37.52	14.30	674	Continental	Lake core	LGIT; HO	warm	wet				Sadori et al., (2008)
91	Lago Grande di Monticchio	40.94	15.61	656	Continental	Lake core	MIS 5e; MIS 3; HO; 8.2ka	warm	wet	warm, wet			Allen et al, (1999; 2000; 2002); Watts et al., (2000); Allen and Huntley, (2009)
94	M25_4-KL11	36.75	17.72	-3376	Marine	Marine core	LGIT; HO; 8.2ka				18.20		Emeis et al., (2000)
96	IN68-9	41.80	17.92	-1234	Marine	Marine core	HO; 8.2ka					warm	Rijk et al., (1999)
97	KET 8216	41.52	17.98	-1166	Marine	Marine core	LGIT; HO	warm	wet				Rossignol Strick et al., (1992); Rossignol strick, (1995)
99	AD91-17	40.87	18.64	-844	Marine	Marine core	LGIT; HO; 8.2ka				15.10		Giunta et al., (2006); Sangiorgi et al., (2003); Sangiorgi et al., (2008)
101	BAN 84 09 GC	34.32	20.02	-3405	Marine	Marine core	LGIT; HO	warm	dry				Cheddadi et al., (1991); Rossignol strick. (1995)
107	Lake Sedmo Rilsko	41.88	23.02	2925	Continental	Lake core	LGIT; HO	warm	wet				Bozilova and Tonkov, (2000)
114	C69	36.55	24.21	-632	Marine	Marine core	MIS 3; LGIT; HO; 8.2ka	warm	wet			27.00	Geraga et al., (2005)
122	MNB3	39.15	25.00	-800	Marine	Marine core	LGIT; 8.2ka				21.00		Geraga et al.. 2010; Gogou et al., (2007)
124	LC21	35.67	26.58	-1522	Marine	Marine core	MIS 5e; HO; 8.2ka					warm	Rijk et al., (1999); Marino et al., (2007);van der Meer et al., (2007); Osborne et al., (2010)
127	M44-1-KL71	40.84	27.76	-566	Marine	Marine core	HO; 8.2ka				18.60		Sperling et al., (2003)
136	ODP Site 967C	34.07	32.73	-2550	Marine	Marine core	MIS 5e; LGIT; HO; 8.2ka				19.03		Emeis et al., (1998; 2000; 2003); Rohling et al., (2002; 2006); Scrivner et al., (2004)
138	MD84627	32.22	33.75	-1185	Marine	Marine core	8.2ka	warm	wet				Cheddadi and Rossignol-Strick., (1995)
143	MD84629	32.07	34.35	-745	Marine	Marine core	HO; 8.2ka	warm	wet				Cheddadi and Rossignol-Strick., (1995)
144	MD84632	32.78	34.37	-1425	Marine	Marine core	LGIT; HO; 8.2ka				20.75		Essallami, (2007)
145	GeoB5844-2	27.71	34.68	-963	Marine	Marine core	LGIT; HO; 8.2ka				25.90	25.83	Arz et al., (2003)
146	Soreq Cave	31.45	35.03	400	Speleothem	Speleothem	MIS 5e; MIS 3; HO; 8.2ka			wet			Vaks et al., (2006), Affek et al., (2008); Bar-Matthews et al., (2003)

Site ID	Site name	Latitude	Longitude	Elevation/ Water depth	Archive Map	Archive type	Time-slice	Variable1 (FN)	Variable2 (FN)	Varible3 (FA) precip	Variable4 (FA)_média ºC SST-Uk37	Variable5 (FA)_média ºC Forams	References
1	MD03-2699	39.04	-10.67	-1895	Marine	Marine core	LGIT; HO; 8.2ka				17.76		Rodrigues et al., (2010)
4	SU 81-18	37.77	-10.21	-3135	Marine	Marine core	LGIT; HO; 8.2 ka				18.39		Lézine et al., (1997); Turon et al., (2003); Bard et al., (2002)
5	MD95-2042	37.81	-10.15	-3146	Marine	Marine core	MIS 5e; MIS 3; LGIT; HO; 8.2ka				19.15		Sanchez Goñi et al., (1999; 2000; 2002; 2005); Pailler and Bard, (2002); Shackleton et al., (2000); Salgueiro et al., (2010)
6	MD01-2444	37.57	-10.13	-2656	Marine	Marine core	MIS 5e; MIS 3; LGIT; HO; 8.2ka				18.54		Martrat et al., (2007); Vautravers et al., (2006); Skinner et al., (2007); Margari et al., (2010);
8	8057B	37.68	-10.08	-2811	Marine	Marine core	LGIT, 8.2ka	cool	dry				Hooghiemstra et al., (1992)
10	MD03-2697	42.17	-9.70	-2164	Marine	Marine core	LGIT; HO; 8.2ka	cool	relatively wet				Naughton et al., (2007); Naughton., (2007)
14	D13882	38.63	-9.45	-88	Marine	Marine core	LGIT; HO; 8.2ka				18.35		Rodrigues et al., (2009)
19	Guadiana basin	37.27	-7.45	0	Continental	Estuary core	LGIT; HO; 8.2ka	cool	dry				Fletcher et al., (2007)
23	MD99-2341+ GeoB5901	36.38	-7.07	-574	Marine	Marine core	HO; 8.2ka				20.00		Kim et al., (2004)
24	M39008	36.37	-7.07	-576	Marine	Marine core	LGIT; HO; 8.2ka				20.58		Cacho et al., (1999; 2000)
29	Tigalmamine	32.90	-5.35	1626	Continental	Lake core	HO; 8.2ka	cool	dry				Lamb et al., (1989); Lamb et al., (1995); Lamb and van der Kaars., (1995); Cheddadi et al., (1998)
31	El Pindar	43.38	-4.50		Speleothem	Speleothem	HO; 8.2ka			dry			Moreno et al., (2010)
32	ODP Site 976	36.20	-4.30	-1108	Marine	Marine core	MIS 3; LGIT; HO; 8.2ka	cool	dry				Combourieu-Nebout et al.. (1998; 2002; 2009);
33	TG-5	36.38	-4.25	-626	Marine	Marine core	HO; 8.2ka				19.20		Barcena et al., (2001)
35	Fuentillejo maar	38.93	-4.05		Continental	Lake core	HO; 8.2ka			warm, wet			Vegas et al., in press.
37	Puerto de los tornos	43.15	-3.43	920	Continental	Peatbog core	8.2ka	cool	dry				Peñalba., (1994); Muñoz Sobrino et al., (2005)
41	MD95-2043	36.14	-2.62	-1841	Marine	Marine core	MIS 3; LGIT; HO; 8.2ka				18.65		Cacho et al., (1999; 2000; 2001; 2006); Sanchez Goñi et al., (2002; 2009); Fletcher et al., (2008; 2010); Moreno et al. (2002; 2004)
43	Villaverde	38.80	-2.37	900	Continental	Lake core	HO; 8.2ka	cool	dry				Carrion et al., (2001); Carrion., (2003); Jalut., (2005); Jalut et al., (2008)
44	ODP Site 977A	36.03	-1.96	-1984	Marine	Marine core	MIS 5e; MIS 3; LGIT; HO; 8.2ka				18.57		Martrat et al., (2004)
47	El Portalet	42.80	-0.38	1802	Continental	Peatbog core	LGIT; HO; 8.2ka	cool	dry	dry			González-Sampériz et al., (2005; 2006; 2008; 2009)
61	MD99-2343	40.50	4.03	-2391	Marine	Marine core	MIS 3; HO; 8.2ka				16.44		Sierro et al., (2005); Frigola et al., (2007; 2008)
69	Le Locle	47.05	6.72	915	Continental	Lake core	LGIT; 8.2ka	cool	wet				Magni et al., (2001)
70	Soppensee	47.09	8.08	596	Continental	Lake core	8.2ka	cool	wet				Tinner and Lotter, (2001)
75	MD04-2797	36.95	11.67	-771	Marine	Marine core	LGIT; HO; 8.2ka				19.82	cold	Essallami et al., (2007); I. Rouis-Zargouni et al., (2010)
77	Lago di Vico	42.33	12.27	507	Continental	Lake core	MIS 3; LGIT; 8.2ka	cool	dry				Leroy et al., (1996); Magri and Sadori, (1999); Magri and Parra, (2002)
80	Lake Gorgo Basso	37.62	12.65	6	Continental	Lake core	HO; 8.2ka	cool	dry				Tinner et al., (2009)
83	Grotta di Carburangeli	38.17	13.16	22	Speleothem	Speleothem	HO; 8.2ka			dry			S. Frisia et al., (2006)
85	BS79-38	38.41	13.58	-1489	Marine	Marine core	LGIT; HO; 8.2ka				18.79		Cacho et al., (2001)
86	BS79-33	38.26	14.03	-1282	Marine	Marine core	LGIT; HO; 8.2ka				18.64		Cacho et al., (2001)
89	CM92-43	42.88	14.72	-252	Marine	Marine core	8.2ka	cool	dry				Ariztegui et al., (2000); Asioli et al., (2001)
90	PRAD1-2	42.68	14.77	-185.5	Marine	Marine core	MIS 5e; LGIT; HO; 8.2ka				17.18		Piva et al., (2008)
91	Lago Grande di Monticchio	40.94	15.61	656	Continental	Lake core	MIS 5e; MIS 3; HO; 8.2ka	cool	relatively wet				Allen et al, (1999; 2000; 2002); Watts et al., (2000); Allen and Huntley, (2009)
94	M25_4-KL11	36.75	17.72	-3376	Marine	Marine core	LGIT; HO; 8.2ka				18.05		Emeis et al., (2000)
95	KC01	36.25	17.74	-3640	Marine	Marine core	MIS 5e; HO; 8.2ka				16.45		Doose, (1999)
96	IN68-9	41.80	17.92	-1234	Marine	Marine core	HO; 8.2ka					cold	Rijk et al., (1999)
99	AD91-17	40.87	18.64	-844	Marine	Marine core	LGIT; HO; 8.2ka				15.58		Giunta et al., (2006); Sangiorgi et al., (2003); Sangiorgi et al., (2008)
103	K6 lake maliq	40.77	20.78	-818	Continental	Lake core	LGIT; 8.2ka	cool	dry				Bordon et al., (2009)
114	C69	36.55	24.21	-632	Marine	Marine core	MIS 3; LGIT; HO; 8.2ka	cool	relatively dry			15.00	Geraga et al., (2005)
115	Tenaghi Philippon 2	40.97	24.22	40	Continental	Lake core	8.2ka	cool	dry				Pross et al., (2010
118	GeoTü SL152	40.09	24.61	-978	Marine	Marine core	LGIT; 8.2ka	cool	dry				Kotthoff et al.. 2008a; b
122	MNB3	39.15	25.00	-800	Marine	Marine core	LGIT; 8.2ka	cool	dry		19.00		Geraga et al.. 2010; Gogou et al., (2007)
124	LC21	35.67	26.58	-1522	Marine	Marine core	MIS 5e; HO; 8.2ka					cold	Rijk et al., (1999); Marino et al., (2007);van der Meer et al., (2007); Osborne et al., (2010)
127	M44-1-KL71	40.84	27.76	-566	Marine	Marine core	HO; 8.2ka				18.20		Sperling et al., (2003)
136	ODP Site 967C	34.07	32.73	-2550	Marine	Marine core	MIS 5e; LGIT; HO; 8.2ka				19.22		Emeis et al., (1998; 2000; 2003); Rohling et al., (2002; 2006); Scrivner et al., (2004)